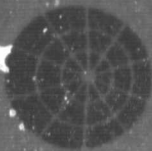


## **General Disclaimer**

### **One or more of the Following Statements may affect this Document**

- This document has been reproduced from the best copy furnished by the organizational source. It is being released in the interest of making available as much information as possible.
- This document may contain data, which exceeds the sheet parameters. It was furnished in this condition by the organizational source and is the best copy available.
- This document may contain tone-on-tone or color graphs, charts and/or pictures, which have been reproduced in black and white.
- This document is paginated as submitted by the original source.
- Portions of this document are not fully legible due to the historical nature of some of the material. However, it is the best reproduction available from the original submission.



**COMSAT**  
**Laboratories**

Final Report

(NASA-CR-168141) DEVELOPMENTS TOWARD AN 18%  
EFFICIENT SILICON SOLAR CELL Final Report  
(Communications Satellite Corp.) 142 p  
HC A07/MF A01 CSCI 10A

N83-25112

Unclass

H2/44 03722

## DEVELOPMENTS TOWARD AN 18% EFFICIENT SILICON SOLAR CELL

Submitted to

NASA Lewis Research Center  
21000 Brookpark Road  
Cleveland, Ohio 44135

Under Contract NAS-3-22217



April 1983

COMMUNICATIONS SATELLITE CORPORATION  
COMSAT Laboratories      Clarksburg, Maryland 20871

**Final Report**

**Developments Toward an 18% Efficient  
Silicon Solar Cell**

**by**

**A. Meulenberg, Jr.**

**Submitted to**

**NASA Lewis Research Center  
21000 Brookpark Road  
Cleveland, Ohio 44135**

**Under Contract NAS-3-22217**

**April 1983**

**ORIGINAL PAGE IS  
OF POOR QUALITY**

1. Report No. NASA CR 168141	2. Government Accession No.	3. Recipient's Catalog No.
4. Title and Subtitle Developments toward an 18% efficient silicon solar cell		5. Report Date April 1983
		6. Performing Organization Code
7. Author(s) A. Meulenberg, Jr.		8. Performing Organization Report No.
		10. Work Unit No.
9. Performing Organization Name and Address COMSAT Laboratories 22300 Comsat Drive Clarksburg, MD 20781		11. Contract or Grant No. NAS -3-22217
		13. Type of Report and Period Covered Final Report
12. Sponsoring Agency Name and Address National Aeronautics and Space Administration Lewis Research Center 21000 Brookpark Road Cleveland, Ohio 44135		14. Sponsoring Agency Code
15. Supplementary Notes		

**16. Abstract**

Limitations to increased open-circuit voltage have been identified and experimentally verified for 0.1  $\Omega$ -cm solar cells with heavily doped emitters. After major reduction in the dark current contribution from the metal-silicon interface of the grid contacts, the surface recombination velocity of the oxide-silicon interface of shallow junction solar cells is the limiting factor. In deep junction solar cells, where the junction field does not aid surface collection, the emitter bulk is the limiting factor. Singly-diffused, shallow junction cells have been fabricated with open circuit voltages in excess of 645 mV. Double-diffusion shallow and deep junctions cells have displayed voltages above 650 mV. MIS solar cells formed on 0.1  $\Omega$ -cm substrates have exhibited the lowest dark currents produced in the course of the contract work.

17. Key Words (Suggested by Author(s)) Solar cells                      Surface electric Diffusion lengths              fields Gettering                        MIS Surface effects                 Silicon Heavy doping effects Diffusion profiles		18. Distribution Statement  UNCLASSIFIED - UNLIMITED STAR Category 44	
19. Security Classif. (of this report) UNCLASSIFIED	20. Security Classif. (of this page) UNCLASSIFIED	21. No. of Pages 140	22. Price* -----

\* For sale by the National Technical Information Service, Springfield, Virginia 22161



SUMMARY

The primary objectives of this contract were to develop an 18-percent efficient 700-mV silicon solar cell in 0.1  $\Omega$ -cm p-type material and the experimental methods for realizing these goals. In the event these values were unattainable, the contract objectives were to determine the limitations that prevent their achievement and, through a thorough understanding of the device physics, explain the mechanisms of the limitations.

Based upon existing solar cell theory, experiments were designed to determine the relative impact of the various contributions to the solar cell dark current. Bandgap narrowing, as a result of heavy doping, has a deleterious effect on the dark current from both the surface and the bulk of the emitter. Even though heavy doping effects in the emitter (n-type silicon) were found to be less than predicted by many models, the magnitude of these effects is such as to have the greatest single impact on solar cell performance. Surface recombination velocity was also identified to be a limiting factor. After removal of the effects of high surface recombination from the metal-silicon interface of the grids, there remains significant recombination at the rest of the surface that dominates in cells with shallow junctions. Electric fields in the junction region were found to affect cell fill factors, and various emitter doping profiles were tried in an effort to improve fill factor and open circuit voltage.

Although the effects described above could not be altered enough to result in achieving either 18-percent efficiency or 700 mV, several improvements were realized. Reductions in the emitter and base dark diffusion currents were accomplished. Minority carrier lifetimes in the base were improved by low temperature gettering techniques to the point where 0.1  $\Omega$ -cm

ORIGINAL PAGE IS  
OF POOR QUALITY

lifetimes were comparable to those normally seen in 1  $\Omega$ -cm material. Induced n-type layers (created by applying surface charge, or forming MIS structures, for the purpose of studying the effects of heavy doping and surface recombination) in MIS cells were effective in achieving dark saturation current densities as low as  $2 \times 10^{-13}$  A/cm<sup>2</sup>. Electrostatic surface charge was found to alter open circuit voltage in cells with low doped emitters by as much as 100 mV.

The best cell, resulting from incorporating as many of these improvements as possible, achieved in the work of this contract was an n<sup>+</sup>-p, diffused junction cell which had an open circuit voltage of 654 mV under AM0 at 25°C. This is the highest open circuit voltage ever reported for this type of cell. The reasons for lack of improvement beyond this value of open circuit voltage are discussed.

ORIGINAL PAGE IS  
OF POOR QUALITY

Table of Contents

	<u>Page No.</u>
SUMMARY	
1. INTRODUCTION .....	1-1
2. BASE .....	2-1
2.1 P <sup>+</sup> Back Contacts .....	2-2
2.2 Base Diffusion Lengths, L <sub>n</sub> .....	2-6
2.3 Base Thickness, W .....	2-12
2.4 Base Doping Concentration, N <sub>A</sub> .....	2-14
2.5 Minority Carrier Diffusivity, D .....	2-15
3. EMITTER .....	3-1
3.1 Contacts .....	3-3
3.1.1 Contact Area .....	3-4
3.1.2 Grid Spacing .....	3-7
3.1.3 Low SRV Contacts .....	3-7
3.2 Oxide-Silicon Interface .....	3-11
3.2.1 Ta <sub>2</sub> O <sub>5</sub> .....	3-12
3.2.2 Other Oxides .....	3-15
3.3 Emitter Bulk .....	3-18
3.3.1 Emitter Profile .....	3-19
3.3.2 Arsenic Doped Emitters .....	3-21
3.3.3 Low Doped Emitters .....	3-24
3.4 Bandgap Narrowing from Heavy Doping .....	3-30
4. DOUBLE DIFFUSED CELLS .....	4-1
4.1 Processing .....	4-5
4.2 Development and Analysis .....	4-6
4.3 Hypothesis .....	4-9
4.4 Summary .....	4-14

ORIGINAL PAGE IS  
OF POOR QUALITY

Table of Contents (Continued)

	<u>Page No.</u>
5. I-V CHARACTERISTICS .....	5-1
5.1 Short Circuit Current .....	5-1
5.2 Fill Factor .....	5-3
5.3 Open Circuit Voltage .....	5-7
6. SPECIAL STRUCTURES .....	6-1
6.1 MIS Structures .....	6-1
6.2 MINP Structures .....	6-4
7. CONCLUSIONS AND REMARKS .....	7-1
APPENDIX A .....	A-1
APPENDIX B .....	B-1
APPENDIX C .....	C-1
C.1 Boron Gettering .....	C-1
C.2 Aluminum Gettering .....	C-4
C.3 Phosphorus and Arsenic Gettering .....	C-6
C.4 Other Process Dependent Influences on $I_{\gamma}$ .....	C-10
C.5 Summary .....	C-13
APPENDIX D .....	D-1
REFERENCES	

ORIGINAL PAGE IS  
OF POOR QUALITY

List of Illustrations

<u>Figure No.</u>	<u>Title</u>	<u>Page No.</u>
2-1	A Family of Curves Showing the Bracketed Term in Equation (2-1) as a Function of W/L and SL/D .....	2-3
2-2	A Family of Curves Showing the Diffusion Length Dependent Terms in Equation (2-1) as a Function of L/W and S/D .....	2-7
3-1	The IV Characteristic of a Cell with Low Doped Emitter and Dot Contacts .....	3-10
3-2	The IV Characteristic of the Same Cell as Figure 3-1, but with Dot Contact Grids Replaced by Full (5%) Contact Grids .....	3-10
4-1	IV Curves for Cell 1408-3, Bare (Dots) and Covered (Broken), Under Simulated AMO Conditions .....	4-2
4-2	Quantum Yield Results for Cell 1408-8 ( $x_j \approx 0.5 \mu\text{m}$ ) along with Shallow (1407-3) and Deep (1408-1) Junction Cells .....	4-3
4-3	IV Analysis of Cell 1408-8 Indicating the Junction Recombination (JR), Dark Diffusion (JD), and Leakage (V/RSR) Currents .....	4-4
4-4	Boron Concentration Profile in an Untreated 0.1 $\Omega\text{cm}$ Silicon Wafer .....	4-11
4-5	A 16-hr Prediffusion (N250C at 880°C) was Nearly Etched Off Prior to a 15 Minute Diffusion (N250°C at 820°C) .....	4-11

List of Illustrations (Continued)

<u>Figure No.</u>	<u>Title</u>	<u>Page No.</u>
5-1	The I-V Curve of a Shallow Junction Solar Cell with a "Flat" Spot Above the Knee .....	5-6
C-1	Profiles of P, As and Boron After a 15 Minute Diffusion (820°C) with N250 ....	C-11
C-2	Boron Concentration in an 0.1 $\Omega$ -cm Wafer, Thermally Oxidized (1050°C for 4 Hours) and Then Etched in Hf .....	C-11
D-1	Normalized Gamma-Cell Current vs Solar Cell Diffussion Length for $S = \infty$ and Different Cell Thicknesses W (for $S = 0$ use the curves corresponding to 2W) .....	D-4
D-2	Dark Current Components as a Function of Open Circuit Voltage at Various Levels of Irradiation. Electrical Characteristics of 0.2 $\Omega$ -cm cells: a) $S = 0$ ; b) $S = \infty$ .....	D-8
D-3	Dark Current Components as a Function of Open Circuit Voltage at Various Levels of Irradiation. Electrical Characteristics of 0.1 $\Omega$ -cm cells: a) $S = 0$ ; b) $S = \infty$ .....	D-9

ORIGINAL PAGE IS  
OF POOR QUALITY

List of Tables

<u>Table No.</u>	<u>Title</u>	<u>Page No.</u>
2-1	Influence of Heat Treatment and Aluminum or Boron on Solar Cell Parameters .....	2-10
2-2	Influence of Cell Thickness on Gamma Current .....	2-13
3-1	Influence of Grid contact Area on Different Resistivity Cells .....	3-5
3-2	Influence of Grid Contact Area on Different Junction Depth Cells .....	3-6
3-3	Various Emitter Profiles on 1 $\Omega$ -cm Substrates .....	3-26
3-4	The Influence of Surface Charge on Low Doped Emitters .....	3-29
4-1	Uncovered Characteristic of a Set of Single Diffused Cells (1407) and of a Set of Double Diffused Cells (1408) .....	4-8
C-1	Fabrication Steps in Boron Diffused Cells and the Resultant Gamma Currents $I_\gamma$ .....	C-2
C-2	Gamma Currents of 1 $\Omega$ cm Cells That Have Been Fabricated with Different Emitter Dopants and Schedules .....	C-8

## 1. INTRODUCTION

Over the past few years evidence [1] has been accumulating for mechanisms which limit the efficiency of silicon solar cells to significantly less than the idealized theoretical maximum [2] of about 24 percent AM0. Once recognized, these limiting mechanisms can be removed, bypassed, or at least reduced in their influence [3].

Bandgap narrowing, resulting from heavy doping, is one mechanism that limits cell open-circuit voltages. Recent efforts have sought to provide a consistent theoretical and experimental basis for predicting the extent of this limitation [4-8]. Other efforts have sought to reduce the consequences of bandgap narrowing by use of ion implantation to control junction profiles [9]; by use of high-low emitters to isolate the heavily doped regions [10]; and by use of charged oxides or metal-insulator semiconductor (MIS) structures to induce a high carrier concentration without the need for high doping concentrations [11]. Other voltage-limiting mechanisms such as surface recombination velocities [12] and junction recombination currents [1] have been identified.

The purpose of this contract was to develop a 0.1  $\Omega$ -cm silicon solar cell that under AM0 illumination and at 25°C would have an efficiency of 18 percent and an open circuit voltage of 700 mV. In the event these values were unattainable, the secondary objective was to determine and explain the mechanisms of the limitations that prevent their being achieved. To fulfill these goals, a major effort was made to confirm the limiting factors and overcome them, where possible. Results of this contract will pertain to all solar cell work in that simple theory is supported to explain limitations in cell open circuit voltages. In addition, experimental techniques were developed which have improved



terrestrial and space silicon solar cells and which might also improve characteristics of cells made from other materials.

The theoretical and experimental bases for this effort are described in Appendix A [1]. A discussion of the cell limitations and the technical approach to reducing these limitations was presented at the Third High Efficiency Solar Cell and Radiation Damage Conference in 1979 [3]. Parts of the proposal for this contract (Appendix B) cover the material presented at that time.

The theoretical limits for short circuit current in silicon solar cells have been approached by use of nonreflective surfaces, wrap around contacts, and sawtooth coverslides (see for example reference 13). The fill factor should increase with increased open-circuit voltage,  $V_{OC}$ . To achieve the 18-percent efficiency at AM0 and 25°C, one must obtain open circuit voltages in excess of 680 mV. Since the current limits were already reached, new technology would be needed only in the voltage study. In concurrence with the NASA technical monitor, the plan of attack was directed toward the 700-mV goal. The open circuit voltage depends primarily upon the dark diffusion current contributions from the emitter and base of the cell. This report is divided along these two lines with an additional chapter on special structures included to delineate promising devices that do not necessarily fit the theory and practice of diffused n<sup>+</sup>p solar cells. Another chapter is included to address the impact of processing, to improve voltage, on the other cell characteristics.

## 2. BASE

In material with resistivity,  $\rho$ , on the order of 1  $\Omega$ -cm, the dark diffusion current ( $\sim 2 \times 10^{-12}$  A/cm<sup>2</sup>) from the base dominates the open circuit voltage.\* When the resistivity is reduced to  $\rho \approx 0.1$   $\Omega$ -cm, the computed value of this dark current,  $J_{dp}$ , from a 0.02-cm thick base is lowered to  $J_{dp} \approx 1.0 \pm 0.6 \times 10^{-13}$  A/cm<sup>2</sup>.

The contribution to the dark current from the base can be written as

$$J_{dp} = \frac{qn_i^2 D}{N_A L_n} \left[ \frac{(SL_n/D) \cosh(W/L_n) + \sinh(W/L_n)}{(SL_n/D) \sinh(W/L_n) + \cosh(W/L_n)} \right] \quad (2-1)$$

where

$q \equiv$  electronic charge =  $1.6 \times 10^{-19}$  C

$D \equiv$  minority carrier diffusivity =  $10^{-15}$  cm<sup>2</sup>/s

$N_A \equiv$  acceptor doping level =  $1.5-4.5 \times 10^{17}$ /cm<sup>3</sup> ( $\rho = 0.1$   $\Omega$ -cm)

$L_n \equiv$  minority carrier diffusion length  $\geq 0.02$  cm

$n_i \equiv$  intrinsic carrier concentration =  $1.2-1.5 \times 10^{10}$ /cm<sup>3</sup>

$W \equiv$  base length  $\approx 0.02$  cm

$S \equiv$  back surface recombination velocity =  $10^4-10^6$  cm/s

The range limits indicate the possible choices for  $N_A$ ,  $n_i$ , and  $D$  obtained from the literature; the value of  $L_n$  for the particular cell; whether or not bandgap narrowing in the base is assumed; and the influence, which is reflected in the value for surface recombination velocity,  $S$ , of the back surface. The value of the

\*See Appendix A for a review of the diode equations, etc.

bracketed term in equation (2-1) is shown in Figure 2-1 as a function of  $W/L_n$  and  $SL_n/D$ . The impact of cell thickness and surface recombination velocity on dark current are clearly exhibited in this figure.

From equation (2-1), it can be seen that reducing  $S$  and  $D$  or increasing  $N_A$  will lower  $J_{dp}$  and thereby increase the open circuit voltage. Since  $L$  appears in functionally different forms, an increase of  $L$  does not necessarily reduce  $J_{dp}$ . The following sections detail the reductions in  $J_{dp}$  that were anticipated, based upon theoretical grounds, and the positive results and limitations encountered during the contract.

## 2.1 P<sup>+</sup> BACK CONTACTS

A  $p^+$  layer should reduce recombination at the back surface, thereby decreasing  $J_{dp}$ , increasing the open circuit voltage, and increasing the collected photocurrent. If the  $p^+$  layer is very effective, then the value of  $S$  (surface recombination velocity or SRV) in equation (2-1) is very low and the terms containing  $S$  can be ignored. In this case,

$$J_{dp} \approx \frac{qn_i^2}{N_A L_n} \tanh \frac{W}{L_n} \quad (2-2a)$$

If  $L_n \geq 3W$ , then  $\tanh(W/L) \approx W/L$ , equation (2-2a) becomes

$$J_{dp} \approx \frac{qn_i^2 DW}{N_A L_n^2} \quad (2-2b)$$

and the dark current is minimized by reducing  $W$  or increasing  $L_n$  or  $N_A$ .

ORIGINAL PAGE IS  
OF POOR QUALITY

$$[A] \equiv \frac{(SL/D) \cosh (W/L) + \sinh (W/L)}{(SL/D) \sinh (W/L) + \cosh (W/L)}$$

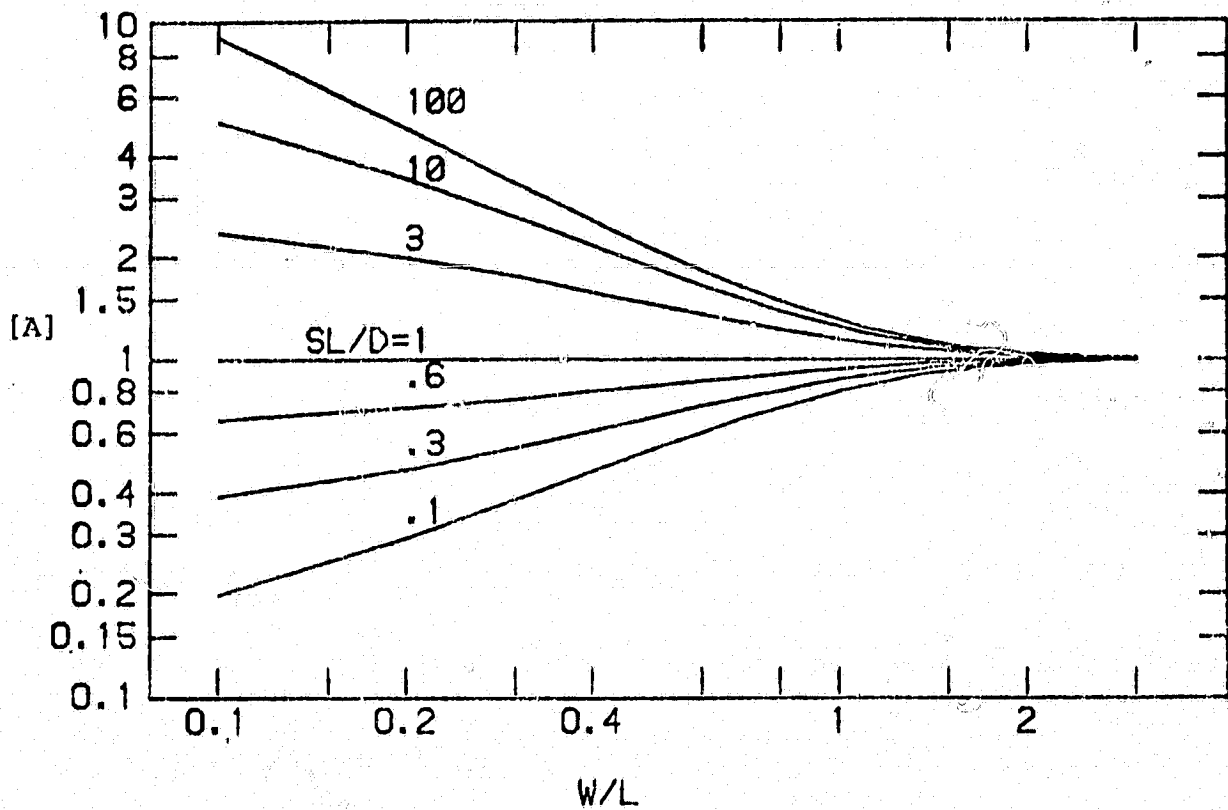


Figure 2-1. A Family of Curves Showing the Bracketed Term in Equation (2-1) as a Function of W/L and SL/D

ORIGINAL PAGE IS  
OF POOR QUALITY

If the  $p^+$  barrier is not very effective, then the situation is much more complicated. Reference 14 gives an excellent description of the means of calculating  $S$  and its impact on  $J_{dp}$ . ( $S$  of Reference 14 is our  $S$  times  $L_n/D_n$ .) In brief, the effectiveness of the  $p^+$  layer depends upon the height of the  $p$ - $p^+$  barrier expressed as the ratio of the doping concentrations in the two regions,  $N_A^+/N_A$ ; the greater the ratio, the higher the barrier and, therefore, the lower the value for  $S$ . In general, the SRV also depends inversely upon the rate of recombination in the  $p^+$  layer and, therefore, the better the diffusion length in this layer the lower the value for  $S$ . Unfortunately, heavy doping effects tend to keep the effective  $p^+$  doping from increasing as rapidly as the actual doping increases and the  $p$ - $p^+$  barrier to minority carriers is, thereby, reduced. This results in an increase of dark current generated in the  $p^+$  layer. Data exist indicating bandgap narrowing of 42 mV at  $10^{18}/\text{cm}^3$  boron doping [8] and 15 mV at  $2 \times 10^{17}/\text{cm}^3$ . The theoretical potential barrier resulting from a  $p$ -type doping level change from  $2 \times 10^{17}/\text{cm}^3$  to  $10^{18}/\text{cm}^3$  would be  $\sim 40$  mV so that with bandgap narrowing, the net barrier for electrons would be  $\sim 13$  mV\*, or less than  $kT/q$ . Likewise, at  $10^{19}/\text{cm}^3$  the bandgap narrowing is  $\sim 68$  mV compared to the theoretical  $p$ - $p^+$  barrier of  $\sim 100$  mV. Again, the net barrier to electrons is  $\approx kT/q$ . The referenced data extend only to  $N_A \approx 0.3 \times 10^{20}/\text{cm}^3$ . If the bandgap narrowing levels off somewhat at doping levels greater than  $10^{20}/\text{cm}^3$ , then an ionized acceptor concentration ( $p_0$ ) of  $3 \times 10^{20}/\text{cm}^3$  should improve the barrier beyond  $2kT/q$  with a corresponding improvement in collected photocurrent and a possible reduction in dark current. (However, Auger recombination may be

\* $40 - (42-15) = 13$  mV

be so high at this doping level that no decrease in dark current is observed.)

A  $p^+$  layer of  $1.5 \times 10^{20}/\text{cm}^3$  would have an effective doping of between  $3 \times 10^{17}$  and  $\sim 10^{19}/\text{cm}^3$  (as a result of bandgap narrowing),  $D \approx 1 - 3 \text{ cm}^2/\text{s}$ , and  $L_n \approx 1 - 10 \times 10^{-5} \text{ cm}$ . These large ranges of uncertainty in both effective doping and minority carrier diffusion length are obtained from the literature. If the most optimistic of these values are correct, a  $p^+$  contact with a low barrier ( $\sim 4 \text{ KT/q}$ ) would result [14]. Unfortunately, the generally accepted values (resulting from experiments to measure heavy doping effects [6],[8] and Auger recombination lifetimes [15]) indicate that such a heavily doped layer on  $0.1 \Omega\text{-cm}$  material would be little better than an ohmic contact (see Section 3.4).

Aluminum, when alloyed into the back surface, produces cells with good base diffusion lengths. However, on  $0.1 \Omega\text{-cm}$  material, no effective  $p^+$  layer has been observed from this process. Boron, which has a much higher solid solubility in silicon than does aluminum, could provide the high acceptor concentrations necessary to create an effective  $p^+$  layer. Emulsitone 0317D, which should provide surface concentrations on the order of  $10^{20}/\text{cm}^3$ , was used to form these layers (runs 1403, 1411, 1423, and 1433). Since the boron doping level does not reach the critical  $3 \times 10^{20}/\text{cm}^3$  level, the resulting values of  $I_{sc}$  and gamma cell\* currents should be, and are, comparable to those from the lower doped aluminum  $p^+$  backs. Some improvements of boron over aluminum [17] have been observed in higher resistivity

\*That current,  $I_y$ , resulting from the uniform carrier generation provided by a  $^{60}\text{Co}$  gamma cell, which is used to determine  $L$  [16] (large  $I_y$  implies large  $L$ ).

material (up to 1250  $\Omega$ -cm), but no attempts have yet been made to optimize the boron  $p^+$  layers as has been done for aluminum. (The boron  $p^+$  layer work is discussed in the next section and in Appendix C.) Of particular interest would be the use of laser annealing for very high concentrations of active boron ( $>3 \times 10^{20}/\text{cm}^3$ ) [18].

Alternatives to the laser annealing process for lowering the SRV would be the use of an MIS back contact [19] or a well passivated and/or charged oxide layer with very low area metal contacts distributed across the surface. Both procedures might benefit from a slightly increased doping at the back surface since boron tends to out-diffuse during growth of an oxide. The metal contact area must be very low ( $<1$  percent) in the second procedure or no benefit will be derived on 0.1  $\Omega$ -cm material.

## 2.2 BASE DIFFUSION LENGTHS, $L_n$

With the understanding that no significant improvement is likely from a  $p^+$  back on 0.1  $\Omega$ -cm material, equation (2-1) indicates that increasing the minority carrier diffusion length is the most likely candidate for reducing the dark current contribution from the base. Figure 2-2 explicitly displays the dependence of  $J_{dp}$  on  $L$  ( $W = 0.02$  cm). It is noted that with an ohmic or near ohmic contact ( $S/D > 1,000$ ), the bracketed term in equation (2-1) reduces to  $\coth(W/L)$ . No improvement in  $J_{dp}$  with  $L_n$  can be expected when  $L \geq 2W$  since  $\coth(W/L) \approx L/W$  and equation (2-1) reduces to

$$J_{dp} \approx \frac{qn_i^2 D}{N_{AW}} \quad (2-3)$$

ORIGINAL PAGE IS  
OF POOR QUALITY

$$[A] \equiv \frac{(SL/D) \cosh (W/L) + \sinh (W/L)}{(SL/D) \sinh (W/L) + \cosh (W/L)}$$

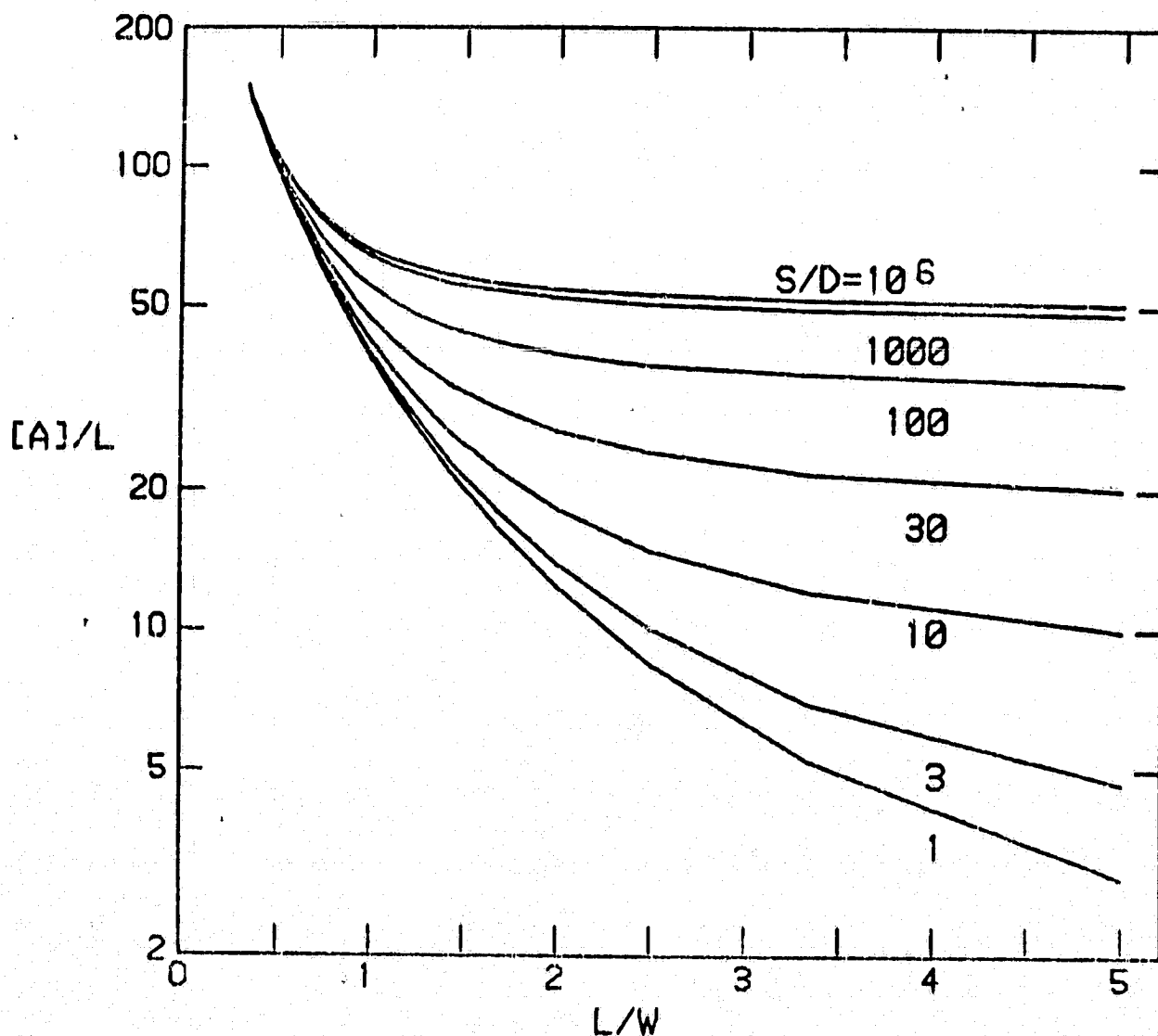


Figure 2-2. A Family of Curves Showing the Diffusion Length Dependent Terms in Equation (2-1) as a Function of  $L/W$  and  $S/D$



ORIGINAL PAGE IS  
OF POOR QUALITY

Given the present cell thickness of  $\sim 200 \mu\text{m}$ , and typical diffusion lengths in the range of  $200 < L_n < 400 \mu\text{m}$ , improvement from increasing  $L_n$  beyond  $400 \mu\text{m}$  is not expected (Figure 2-2). However, with an ohmic back contact and  $L_n \approx 400 \mu\text{m}$ , a factor of two decrease in  $J_{dp}$  could result from increasing  $W$  to  $800 \mu\text{m}$  (Figure 2-1).

In the low diffusion length regime ( $L < W/2$ ),  $\coth(W/L) \approx 1$  and equation (2-1) reduces to

$$J_{dp} \approx \frac{qn_i^2 D}{N_A L_n} \quad (2-4)$$

Diffusion length is obviously important in this case.

Most of the solar cells fabricated during the contract ( $W = 200 \mu\text{m}$ ) exhibited diffusion lengths with  $W/2 < L < 2W$ . If, in addition, the  $p^+$  back layer is effective enough to have the ohmic contact condition break down, the dependence of  $J_{dp}$  is closer to that of equation (2-3). For  $630^+$  mV cells from this contract, a large drop in  $L_n$  (e.g., as a result of irradiation) must be experienced before any significant effect on  $V_{oc}$  is observed. (A reduction of  $L$  to  $L/2$  results in less than 5 mV drop in  $V_{oc}$ .) This would indicate that  $L_n$  is in a range such that  $J_{dp}$  is not sensitive to large reductions in  $L$  (the right side of the  $S/D \geq 1000$  curve of Figure 2-2) and/or the total dark current is strongly dominated by the emitter or some other source. In the first case,  $L_n$  must exceed  $500 \mu\text{m}$ ; this is possible, but the second case is more probable. In the case of 650-mV cells,  $J_d$  is lower by a factor of 2. If we assume that the emitter current has been reduced to achieve this  $V_{oc}$ , then  $J_{dN}$  must be reduced by more than 2X and  $J_{dp}$  may dominate the dark current in such a case. Irradiation of 0.1 and 0.2  $\Omega\text{-cm}$  cells was carried out to

alter the base diffusion length and to distinguish the  $J_{dp}$  and  $J_{dN}$  contributions (Appendix D and Reference 31).

A large body of diffusion length data was obtained during this contract and several trends can be observed in Table 2-1. The results of a series of experiments in which the heat treatment and the  $p^+$  layer dopant were varied (Table 2-1) point to a weak dependence of  $V_{oc}$  with respect to  $L$  when  $I_Y \gtrsim 6.0$  mA. With a few exceptions, the gamma current of the cells increases with increasing time and temperature of heat treatment. Several cells are displayed that have low voltages, but with  $I_Y \gtrsim 6 \mu A$ , indicating a dominant failure mechanism other than the bulk diffusion length. In several cases the dark diffusion current,  $J_d$ , is included for comparison with  $I_Y$  and  $V_{oc}$ . It will be noticed that the cells of set 1441 (all with  $I_Y < 6 \mu A$ ) display a strong inverse relationship between  $I_Y$  and  $J_d$ . The high values of  $I_Y$  would correlate with a reduction in  $J_d$  only if the base were contributing to the dark current. However, set 1440, which exhibits some of the best values of  $I_Y$  in Table 2-1, has higher average values of  $J_d$  than does set 1441. The implication is that while the base diffusion length and the quality of the back contact (both together represented by  $I_Y$ ) can influence the dark current in these cells, some other source of dark current has a greater effect. The most probable source is the emitter (see Section 3). If this is the case, the emitter appears to be influenced by heat treatment and/or the nature of the back surface during such treatment. The cell voltage can also be influenced by junction recombination currents,  $J_r$ , as well as by the diffusion currents. Cells 1441-1 through 4 are examples of this. Their low values of  $J_d$  should provide about 5 mV greater  $V_{oc}$  than that of the other cells in the set if  $J_r$  were ignored. However, the junction recombination currents of

ORIGINAL PAGE IS  
OF POOR QUALITY

Table 2-1. Influence of Heat Treatment and Aluminum  
or Boron on Solar Cell parameters

Treatment	Cell No.	$I_Y$ ( $\mu$ A)*	$I_{SC}$ (mA)	$I_B$	$V_{OC}$ (mV)	$J_d$ (pA)
Al + 400°C/60 min.	1441-10	3.8	133	42	628	
Al + 525°C/10 min.	1426-4	6.4	141	38	611	
	-5	6.3	142	38	627	
	-6	3.7	131	38	587	
Al + 525°C/15 min.	1437-7	5.9	139	42	614	
	-8	5.2	138	41	631	
Al + 525°C/15 min. + 400°C/60 min.	1436-1	5.9	138	41	624	
	-2	5.9	138	42	611	
	-3	5.5	136	41	592	
Al + 750°C/30 min. + 400°C/60	1441-6+8	5.4	142	42	636 $\pm$ 2	0.51 $\pm$ 0.2
Al + 525°C/15 min. + 700°C/30 min.	1436-4	6.2	140	41	607	
	-5	6.2	144	42	623	
	-6	6.3	143	40	621	
	1439-4	6.8	140	40	631	
750°C/30 min. + Al + 525°C/15 min.	1437-4	6.1	141	42	639	
	-5	6.1	142	42	637	
	-6	5.6	141	42	632	

\*Gamma currents corrected for decay of  $^{60}\text{Co}$  source.

Table 2-1. Influence of Heat Treatment and Aluminum  
or Boron on Solar Cell Parameters (Continued)

Treatment	Cell No.	$I_Y$ ( $\mu$ A) *	$I_{SC}$ (mA)	$I_B$	$V_{OC}$ (mV)	$J_d$ (pA)
750°C/30 min. + Al + 525°C/15 min. + 400°C/60 min.	1437-1	6.7	142	42	643	
	-2	6.2	141	42	643	
	-3	6.1	137	41	640	
Al + 820°C/20 min.	1440-1+8	6.7±0.2	140±1	42	634±2	0.53±0.02
	1426-1	6.7	143	39	643	
	-2	6.7	143	39	631	
	-3	6.5	140	38	613	
Al + 820°C/20 min. + 400°C/60 min.	1441-5	5.4	140	43	637	0.49
Al + 820°C/20 min. + 750°C/30 min. + 400°C/60 min.	1441-1+4	5.9	141±1	42	638±2	0.41±0.02
B + 950°C/30 min. + 820°C/15 min. + 450°C/16 hrs.	1423-3	6.3	138	37	600	
	-4	6.4	137	36	602	
	-5	6.1	140	37	625	
	-6	6.1	140	37	631	
	-7	6.2	139	38	632	
	-8	6.0	140	37	632	
	-9	5.7	138	37	607	

\*Gamma currents corrected for decay of  $^{60}\text{Co}$  source.

the former are about twice those of the latter cells and this reduces both the fill factors and the open circuit voltages.\*

Cells with boron diffused  $p^+$  back contacts (set 1423 for example) can achieve values of  $I_{\gamma}$  (given long anneal times) comparable to cells with aluminum  $p^+$  backs but their voltages and base diffusion lengths are not consistently as high as those of cells fabricated more simply and quickly with high temperature aluminum. Appendix C describes a self-consistent model of gettering that compares the action of various diffusants and processes on bulk lifetime in silicon.

### 2.3 BASE THICKNESS, W

A means of reducing base dark current contribution in high resistivity material is the reduction in base thickness  $W$  if a good  $p^+$  back layer can be achieved (Figure 2.1 and eq. 2-2b). However, as mentioned in Section 2.1, a good  $p^+$  back cannot be achieved with 0.1  $\Omega$ -cm substrate material and so the best to be expected is a relative independence of bulk dark current on cell thickness once  $W$  becomes greater than  $\sim 2L$ . On the other hand, if a very thin layer of higher resistivity  $p$ -type silicon were used between the emitter and a  $p^+$  substrate, an effective  $p$ - $p^+$  barrier results and equation (2-2b) pertains (since  $\tau = L^2/D$ ,  $J_{dp} = qn_i^2 W/N_A \tau$ ). If the  $p$  layer were 2  $\Omega$ -cm and 10  $\mu$ m thick instead of 0.1  $\Omega$ -cm and 200  $\mu$ m thick ( $n^+pp^+$  vs  $n^+p^+$ ), if the lifetimes  $\tau$  were comparable, and if the  $p^+$  back contact were perfect ( $S \approx 0$ ), the base dark current would be lower in the 2  $\Omega$ -cm

\*The junction recombination current is deduced from the I-V curves by a computer fit to the diode equation which contains a term in  $\exp(qV/nkT)$ , where  $n \approx 2$  (see Section 4.1).

case. As a means of evaluating such thin base structures, epitaxial layers on  $\sim 0.01 \Omega\text{-cm}$  substrates have been made into solar cells. Initial attempts have been carried out with commercially available material ( $2\text{-}9 \Omega\text{-cm}$ ,  $11\text{--}30\text{-}\mu\text{m}$  thick epi layers on  $0.01 \Omega\text{-cm}$  substrates) to determine feasibility of using this type structure. The short circuit currents were low, as expected from such thin active layer devices, and correlated well with epi layer thickness. The voltages were lower than those from  $n^+p^+$  control cells or those predicted by simple theory. That the voltages are less than simple theory is not unexpected since perfect  $p^+$  backs cannot be obtained even on higher resistivity material. If the epi layer is good, this technique provides a means of determining bandgap narrowing in heavily doped p-type silicon. However, the cell fill factors were low and so indicate a problem with the epi material. Work in this area was, therefore, not pursued.

On several occasions solar cells of basically the same material but different thicknesses were fabricated. The strong dependence of gamma current on cell thickness (Table 2-2) points to long diffusion lengths ( $L_n \geq 200 \mu\text{m}$ ) and ohmic or near ohmic back contacts. The maximum  $I_\gamma$  values indicate non-ohmic back contacts and/or extremely high values for  $L_n$ .

Table 2-2. Influence of Cell  
Thickness on Gamma Current

Material	$I_\gamma (\mu\text{A})$	
	Avg.	Max.
COMSAT $0.1 \Omega\text{cm}$		
8 mil	6	6.8
10-11 mil	7.2	8.4
NASA $0.1 \Omega\text{cm}$		
9 mil	6	
25 mil	12	

As another means of determining the relative contribution of the base dark current, 0.2  $\Omega$ -cm cells were fabricated in parallel with 0.1  $\Omega$ -cm material. Use of equation (2-1) indicates the influence of this change.  $D$  is slightly larger for the 0.2  $\Omega$ -cm material; therefore,  $N_A$  should decrease by a factor of  $>2$  and  $L$  should increase somewhat. The increase in  $L$  should not change  $J_{dp}$  much (as discussed in Section 2.2), but the reduction in base doping will increase the effectiveness of the  $p$ - $p^+$  barrier. The improved barrier will increase  $I_\gamma$  and  $I_{sc}$  but will have little or no effect on  $J_{dp}$  since the dark current contribution from the  $p^+$  layer is unchanged. The net result is that, if the cell is base-dominated,  $(J_d)_{0.2} \gtrsim 2 \times (J_d)_{0.1}$  and  $V_{oc}$  of the 0.2  $\Omega$ -cm cell should be  $\gtrsim 18$  mV less than that of the 0.1  $\Omega$ -cm cell. In actuality, the results (set 1402) confirm the increase in  $I_\gamma$  but reveal only a 9 mV lower  $V_{oc}$  relative to the 0.1  $\Omega$ -cm values. The small difference indicates that contributions to the dark current from the  $p^+$  layer and/or the emitter dominate that from the bulk.

Irradiation, sufficient to lower the diffusion length of both 0.1 and 0.2  $\Omega$ -cm cells to approximately 40  $\mu m$ , was used to establish the relative contributions from the base and emitter of these cells. If we assume that the contribution from the junction is small compared to that from the emitter and bulk, calculation for an unirradiated 635 mV, 200  $\mu m$ , 0.1  $\Omega$ -cm cell indicates that the base dark current is less than 30 percent of the total dark current. If the  $p^+$  layer is a perfect reflector ( $S = 0$ ), the contribution from the base is about 28 percent of the total dark current for the unirradiated cell. If the  $p^+$  layer is ineffective and acts as an ohmic contact, then the

contribution from the base is negligible. The real case is somewhere in between. Similar calculation from the data for a 0.2  $\Omega$ -cm cell indicates the base contribution to the total dark current to be less than 50 percent prior to irradiation.

A later experiment, comparing 1  $\Omega$ -cm and 0.1  $\Omega$ -cm cells (set 1455), proves that excellent diffusion lengths can be maintained for material below 1  $\Omega$ -cm. Assuming that the 1  $\Omega$ -cm cells are voltage limited by the base, an increase in base doping by an order of magnitude would increase  $V_{OC}$  from 605 to 665 mV, if  $n = 1$  and no contribution from the emitter were experienced in the 0.1  $\Omega$ -cm cells. On this basis, 650 mV, 0.1  $\Omega$ -cm cells (with the same diffusion length) have about equal dark current contributions from the base and the emitter.

Heavy doping effects could influence the base bulk contribution to the dark current [8] even at a resistivity as low as  $\rho = 0.1 \Omega$ -cm ( $2 - 4 \times 10^{17}/\text{cm}^3$ ). If these effects are not strong, if the diffusion length does not change rapidly with  $\rho$ , and if the contribution from the  $p^+$  layer is small (or the cell is made thick enough), then lowering the bulk resistivity could be an important means of reducing the total dark current for 660 mV cells.

## 2.5 MINORITY CARRIER DIFFUSIVITY, D

The last variable to be discussed in equation (2-1) is the diffusivity,  $D$ . Normally, this term is assumed constant for a given doping concentration; however, two earlier observations might indicate a source of variability. We have commented on the apparent insensitivity of  $V_{OC}$  to variations in  $L$  for unirradiated 630-mV solar cells (Section 2.2) and attributed this to a



dominant emitter dark diffusion current. Another explanation is that stress generated by the cooling of a silicon-aluminum alloy on the back of a cell might lower  $D$  throughout the cell and, thereby, result in a lower  $J_{pp}$  compared to an unstressed cell with the same measured diffusion length. In addition, unexpectedly low quantum yield results (Section 4) in cells fabricated with a double diffusion process [20] could support such a hypothesis for the emitter region and front portion of the cell.

In recent work at NASA/Lewis (private communication, Vic Weizer), the alloyed region was removed from the back and rediffused with boron. This process should remove stress arising from the Al alloy in the cell without disturbing the  $pp^+$  field created by the Al diffusion front. No change in  $I_{sc}$  or  $V_{oc}$  was noted, so a change in  $D$  from stress appears unlikely in the base as a result of the  $p^+$  back diffusion.

### 3. EMITTER

The previous section indicates severe limitations on the reduction of dark diffusion current from the base. However, significant data exist (e.g., Table 2-1 and Section 2.4) to indicate that base parameters may influence but do not dominate  $V_{oc}$  and, therefore, it is concluded that a major portion of the total dark current in most present cells (630-640 mV) must come from the emitter. Sources of the emitter dark current,  $J_{dN}$ , include the grid contacts, the oxide-silicon interface, and the bulk of the emitter. Each of these regions has been studied experimentally in an attempt to minimize  $J_{dN}$ . A simplified model [1] is used for shallow junction solar cells in order to facilitate discussion. The assumptions in this model are:

- a. The doping profile consists of a thin (depth  $W_s \approx 0.03 \mu m$ ) heavily doped layer near the surface followed by a lower doping concentration which grades down to the junction;
- b. Bandgap narrowing is intense in  $W_s$ ;
- c. Auger recombination dominates lifetime in  $W_s$ ;
- d. Dark current from the low-doped region of the emitter is negligible compared to that from  $W_s$ ;
- e. All photogenerated carriers transit the low doped region without loss; and
- f. The dark current from the surface can be obtained by a linear combination of contributions from the metal contact area and from the oxide-covered area. The emitter dark current ( $J_{dN}$ ) can, therefore, be written as

$$J_{dN} = (A_m/A_t)J_{dN}^m + (1 - A_m/A_t)J_{dN}^o \quad (3-1)$$

ORIGINAL PAGE IS  
OF POOR QUALITY

where  $A_m/A_t$  is the fraction of the total cell area contacted by metal.

In view of assumption d, the emitter dark current term can be written as:

$$J_{dN} \approx \frac{q p_0 D_p}{L_p} \frac{S_p + (D_p/L_p) \tanh (W_s/L_p)}{(D_p/L_p) + S_p \tanh (W_s/L_p)} \quad (3-2)$$

which can be simplified since (as seen below)  $W_s \ll L_p$ . Therefore,  $\tanh (W_s/L_p) \approx W_s/L_p$  and, with  $1/\tau \approx D/L^2$ ,

$$J_{dN} \approx q p_0 \frac{S_p + W_s/\tau_p}{1 + S_p W_s/D} \quad (3-3)$$

The dark current from the metal contact area ( $J_{dN}^m$ ) becomes

$$J_{dN}^m \approx q \frac{n_i^2}{N_D^*} \frac{D}{W_s} \quad (3-4)$$

since  $S_m$  (the SRV of the metal interface) has a very high value (for ohmic contacts  $\sim 10^6$  cm/s) and  $p_0 = n_i^2/N_D^*$ . The dark current from the oxide area ( $J_{dN}^o$ ) becomes

$$J_{dN}^o = q \frac{n_i^2}{N_D^*} \frac{S_o + W_s/\tau_A}{1 + S_o W_s/D} \quad (3-5)$$

where  $N_D^*$  is the effective doping level in  $W_s$ ,  $S_o$  is the SRV of the oxide interface,  $\tau_A$  is the Auger lifetime, and the other symbols have their usual meaning.

ORIGINAL PAGE IS  
OF POOR QUALITY

Some typical values for the surface layer are:

Donor density	$N_D \approx 2 \times 10^{20}/\text{cm}^3$
Effective donor density	$N_D^* \approx 10^{18}/\text{cm}^3$
Auger lifetime for $N_D$	$\tau_A \approx 0.3 - 1 \times 10^{-9} \text{ s}$
Diffusivity for $N_D$	$D \approx 1 \text{ cm}^2/\text{s}$
Surface Layer thickness	$W_S \approx 1 - 3 \times 10^{-6} \text{ cm}$
SRV	$S_O \approx 5 \times 10^3 \text{ cm/s}$
Intrinsic carrier concentration	$n_i \approx 1.2 \times 10^{10}/\text{cm}^3$
Diffusion Length in $W_S$	$L_A \approx 2-3 \times 10^{-5} \text{ cm}$

As can be seen from equations (3-1) and (3-4) the dark current from the metal contacts can be reduced by reducing the contact area or increasing the thickness of the heavily doped layer beneath the contacts (so that  $W_S \rightarrow L_A$ ). The dark current contribution from the oxide-silicon interface and emitter bulk [equation (3-5)] is reduced by lowering the surface recombination velocity  $S_O$  and the heavily doped surface layer ( $W_S/\tau_A$ ) term. (For our normal values of  $S_O$  and  $W_S$  the  $S_OW_S/D$  term in the denominator of equation (3-5) can be ignored.) It is apparent that heavy doping effects (which lower  $N_D^*$ ) increase the dark current from the emitter bulk, the contacts, and the surface.

### 3.1 CONTACTS

With a normal grid contact area of about 5 percent of the solar cell surface, the calculated dark current contribution from this area is 2-5 times greater than the contribution from a reasonable oxide-silicon interface. By restricting the contact

area to small holes through the oxide, the ohmic contact area can be reduced by nearly two orders of magnitude, to only 0.1 percent of the cell area, and thus its contribution to  $J_{DN}$  should be insignificant, or at least much less than that from the oxide [1].

Historically, COMSAT Laboratories has fabricated solar cell contacts by evaporating Ta metal over the cell surface and then Cr-Au grids on top. During the thermal oxidation of the Ta to  $Ta_2O_5$  (525°C), near ohmic contacts were made ( $S_m \approx 4 \times 10^5$  cm/s, [1]). The present low area contacts are made by: a. evaporating Ta over a photoresist grid pattern which is then lifted off; b. oxidation of the remaining Ta which provides an AR coating with narrow bands of bare silicon exposed; and c. deposition of Cr-Au grids and pads at right angles to the exposed silicon. The resulting cross-hatch pattern of grids across open lines in the AR coating provides point contacts that are approximately 1/4 mil x 1/2 mil rectangular "dots." An additional advantage of this process is that the contacts are not heated; and, therefore, the contacts have a lower SRV than would be expected from an ohmic contact. With  $S_m < 3 \times 10^5$  cm/s,  $J_{DN}^m$  would no longer be accurately described by equation (3-4) and the contribution to  $J_{DN}$  is less than that from ohmic "dot" contacts.

### 3.1.1 CONTACT AREA

A set of 2- and 0.12- $\Omega$  cm cells [1], processed identically except for the grid contact area is compared in Table 3-1. The low contact area is seen to have an effect even for the 2- $\Omega$  cm cells. In the 0.12  $\Omega$ -cm cells, where dark current from

the emitter dominates, the impact of the contact area is quite strong.

Table 3-1. Influence of Grid Contact Area on Different Resistivity Cells

Substrate Resistivity ( $\Omega$ -cm)	Grid Metal to Silicon Contact (%)	$J_d$ , Total Dark Diffusion Current ( $\text{pA}/\text{cm}^2$ )	Open Circuit Voltage (mV)
2	5	2.8	598
2	0.14	2.4	601
0.12	5	1.8	606
0.12	0.14	0.8	616

A set of cells (1410) was fabricated to test the effect of reducing the area of present contacts by comparing the open circuit voltage of medium and shallow junction ( $X_j = 0.3 - 0.4$  and  $0.1 \mu\text{m}$ ) solar cells with 5-percent and 0.1-percent contact area. The 5-percent contacts were laid "in," not "across" the open spaces in the AR coating, but still were never heated. Table 3-2 displays the results and indicates that even medium junction-depth cells are slightly influenced by the present metal contact area if the heavily doped layer ( $W_S$ ) is not too deep. The difference in  $V_{OC}$  between the 5-percent and 0.1-percent area contacts is only about 7 mV on the shallow junction 637-mV cells as compared to 10 mV on 616-mV cells in Table 3-1. This indicates that the SRV of the present metal contacts, which are never heated, is significantly less than the  $7 \times 10^5 \text{ cm/s}$  reported earlier [1] (and in Table 3-1) for Cr contracts heated to above  $300^\circ\text{C}$ . The fact that the change in  $V_{OC}$  is greater for the shallow junction cells than for the medium junction cells when  $A_m/A_t$  varies (Table 3-2) indicates that minority carrier transport

between the surface and the junction is not as good in the case of the thicker emitter. This conclusion is strengthened by the higher blue current ( $I_b$ ) seen in the shallow-junction low contact area cells. It should be noted that the relatively constant value of fill factor verifies that no increase in series resistance has resulted from the reduced, or dot, contact area.

A comparison (in Table 3-2) of cells 1 and 2 with cells 5 and 6 shows the slight average increase in blue response expected from shallow junction cells; however, a significant drop ( $\sim 5$  mV) in  $V_{oc}$  is also observed. The loss in  $V_{oc}$  for the 5-percent contact cells with shallow junctions points to the qualitative agreement of data with equation 3-4 and the dominance of the contacts in equation 3-1. The  $V_{oc}$  of the shallow-junction low contact area cells (7 and 8) is not greater than that of the deeper junction cell 3. This points to the SRV of the oxide-silicon interface as the limiting factor in the emitter of these cells (which were designed to minimize the dark current contribution from the bulk of the emitter, see Sections 3.3.1 and 4.1).

Table 3-2. Influence of Grid Contact Area on Different Junction Depth Cells

Junction Depth*	Contact Area	$V_{oc}$	$I_b$	Fill Factor
1410-1 0.3-0.4 $\mu m$	5 %	635 mV	39	0.79
1410-2 0.3-0.4 $\mu m$	5 %	635 mV	38	0.79
1410-3 0.3-0.4 $\mu m$	0.1 %	638 mV	38	0.79
1410-5 0.1 $\mu m$	5 %	628	40	0.79
1410-6 0.1 $\mu m$	5 %	632	39	0.80
1410-7 0.1 $\mu m$	0.1 %	636	41	0.79
1410-8 0.1 $\mu m$	0.1 %	637	42	0.76

\*Estimated junction depths based on measurements made on silicon wafers treated in a like manner.

### 3.1.2 GRID SPACING

An experiment (set 1420) was carried out to check the effect of the grid structure on shallow-junction solar cells because it was noticed that 2 x 2-cm, 0.1  $\Omega$ -cm cells made with 45 line patterns consistently displayed lower  $V_{OC}$  than like cells with 60 line patterns. Line densities were varied (45/cell, 60/cell, 89/cell, and 178/cell) and it was observed that  $V_{OC}$  increased with increasing density up to 60/cell and then leveled off. It has been suggested that increased line density would reduce the excursions in surface potential at  $V_{OC}$  that are revealed in a 2-dimensional analysis of a distributed resistance model [21]. This explanation has not been confirmed for the contact geometry and sheet resistivities typical of our cells.

### 3.1.3 LOW SRV CONTACTS

The processing to form ohmic contacts typically either severely disturbs or heavily dopes the contacted surface. A sufficiently disturbed surface under the contact is a strong source or sink of both type of carriers. An adequately doped surface results in a Debye length that is short compared to an easy tunneling distance. An aluminum alloy step is probably a combination of the two cases, although the dominant nature is process dependent.

If the material to be contacted is already heavily doped, most contacts will be ohmic in the current density range of interest without processing beyond the evaporation step. The surface recombination velocity of such a contact would be low, but could be increased by heating; however, for most purposes



this is unnecessary. To put this in perspective, consider an ohmic contact with an SRV of  $10^6$  cm/s on a material actively doped to  $10^{20}/\text{cm}^3$ . The charge flow, that would introduce a 0.1-mV voltage drop in the contacted material, will create at the surface a deficit of majority carriers (in the limit of small V)  $\Delta n \approx qVn_0/KT \approx 4 \times 10^{-3}n_0$ . The current density through the contact will be

$$J = \Delta n \cdot q \cdot S = 4 \times 10^{-3} \cdot 10^{20} \cdot 1.6 \times 10^{-19} \\ \cdot 10^6 \approx 6 \times 10^4 \text{ A/cm}^2.$$

Our "dot" contacts (6,000-9,000 per  $2 \times 2$  cm cell,  $5 \times 10 \mu\text{m}$ ), if ohmic, could carry 30 mA/dot (3 orders of magnitude more than required). Therefore, even if the SRV were  $10^4$  cm/s no resistive losses would be expected at the contacts. If, however, the doping in the material is lowered, the current capacity of the contacts decreases markedly as  $n$  decreases, since the tunneling distance becomes longer and, therefore, the barrier is less likely to be penetrated ( $s$  decreases). Another problem is the voltage loss associated with the reduced current capacity of the less heavily doped emitter layer and the current concentration about the dot contacts (Section 3.1.2).

When the material doping becomes too low, unheated contacts become resistive and high current densities result in voltage drops at the contacts. Under these circumstances, dot contacts become detrimental to solar cell characteristics. Larger area contacts, with their lower current density, would not have such an effect. Large area contacts are also more likely to have localized regions of high conductivity in the interface. (The density of these small regions is assumed to be the same regardless of contact area.)

Small local regions of high conductivity in a large area rectifying contact become like dot contacts on a heavily doped emitter structure. However, such region in dot contacts may be far enough apart that severe surface resistance limitations are encountered, especially since the sheet resistivity ( $\rho_s$ ) of even a thick, low-doped emitter is generally higher than that of a heavily-doped, very thin emitter. (An emitter doped to  $10^{19}/\text{cm}^3$  would have to be  $\sim 2 \mu\text{m}$  deep to be comparable in  $\rho_s$  to a  $0.2 \mu\text{m}$  emitter doped to  $10^{20}/\text{cm}^3$ .) Figure 3-1 displays the I-V characteristics of a low doped emitter with dot contacts. The central curve is the AMO response with no surface charge added. The cell, when forward biased to voltages beyond the ankle near  $V_{oc}$ , will result in a flattened curve between 0.5 and 0.7 V. Beyond this region, a second knee is observed and the curve turns down again. The total curve is identical to an illuminated diode in series with a dark diode. The upper curve indicates the influence of positive charge on the surface of this cell (see Section 3.2.1). Even though the SRV of the cell is reduced (as seen in the increased current and voltage), and the sheet resistivity is lowered by accumulation of majority carriers in the emitter, the curve shape does not lose the ankle near  $V_{oc}$ . The reason is that the charge cannot influence the region below the grids and, therefore, cannot alter the tunneling barrier. The lower curve is the blue response characteristic (with positive charge) and confirms that sheet resistivity is not the cause of the unusual curve shape since reduction in current does not alter the shape. If the contacts and AR coating are removed and replaced with full grid contacts (Figure 3-2), the curve shape is returned to a more normal solar cell characteristic. (No change in surface doping or contact material was made.) This identifies

ORIGINAL PAGE IS  
OF POOR QUALITY

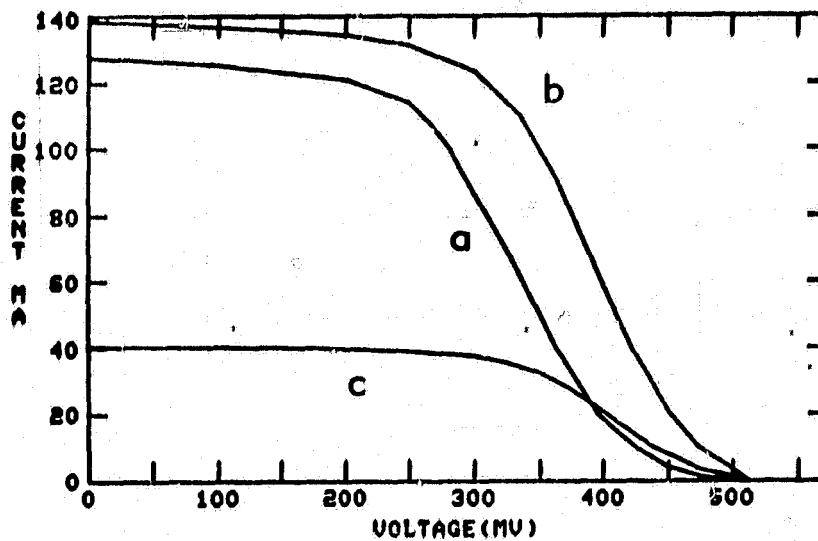


Figure 3-1. The IV Characteristic of a Cell with Low Doped Emitter and Dot Contacts: a) No Surface Charge AM0; b) Positive Surface Charge AM0; c) Positive Surface Charge, Blue Filter

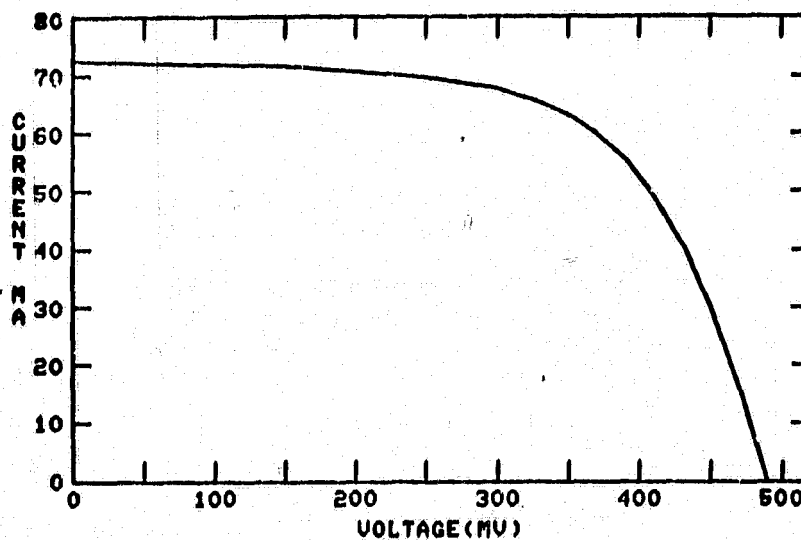


Figure 3-2. The IV Characteristic of the Same Cell as in Figure 3-1, but with Dot Contact Grids Replaced by Full (5%) Contact Grids

the curve shape problem as due to rectifying contacts and not contact spacing.

MIS contacts (which have an insulator deliberately placed between the metal and silicon) would not have the same problem on low-doped substrates because: 1) they are generally larger area, and 2) they accumulate charge under the contact and thereby reduce the tunneling distances to near that of the thin oxide. Therefore, good MIS contacts display low resistance and low SRV regardless of the substrate doping (Section 6.1). (For low doped emitters, use of dot contacts may not be necessary for low net SRV, but it is unlikely that full area contacts could be used if they are heated.) The metal used on the MIS contacts should have a work function low enough to induce a field in the emitter to prevent depletion of the subcontact layer and to assist charge transport through the oxide.

### 3.2 OXIDE-SILICON INTERFACE

The antireflective (AR) coating on all cells fabricated under this contract is thermally oxidized tantalum. The surface recombination velocity (SRV) has been determined to be  $5 - 7 \times 10^3$  cm/s for Ta<sub>2</sub>O<sub>5</sub> on heavily doped n-type silicon [1]. Several experiments (sets 1434, 1436, 1437, 1438, 1439) were performed in an attempt to lower this value by annealing of the Ta<sub>2</sub>O<sub>5</sub>-silicon interface in forming gas (450 and 700°C) and by growth of dry or wet silicon dioxide (at 750°C) layers between the Ta<sub>2</sub>O<sub>5</sub> and the silicon. Success in this endeavor has been only marginal in that no improvement was observed from single step anneal processes and a maximum reduction in SRV of only 20 percent was inferred from V<sub>oc</sub> values after use of a dry

oxidation process for 30 minutes at 750°C. The inability to significantly reduce the SRV is not unexpected since lower values reported in the literature for the oxide-silicon interface are almost always measured on undiffused and much less heavily doped material. In addition, surface state density has been shown [22] to increase markedly with dopant concentration. With the "dot" contact pattern used on all shallow junction cells at present, the SRV under the AR coating appears to be the limiting factor.

### 3.2.1 $\text{Ta}_2\text{O}_5$

The emitter dark current contribution from SRV depends upon both  $S_p$  and  $p_0$  [equation (3-3)] where  $S_p$  is the recombination velocity of holes at the surface and  $p_0$  is the hole concentration. Passivation techniques are used to reduce  $S_p$ . Other techniques (such as ion implantation, material modification, or electrostatic charging) can alter the oxide to reduce  $p_0$  at the silicon surface (Section 3.2.2) by producing strong electric fields with positive charge trapped in or on the oxide. Thermal annealing in forming gas is expected to inject  $\text{H}_2$  through the AR coating to tie up loose silicon bonds that would act as recombination centers at the interface. The failure of this treatment on thermally oxidized Ta could imply that the silicon bonds are all tied up or that other recombination centers dominate the interface.

Electrostatic charge applied to the surface of the AR coating should generate an intense field within the dielectric and for a very short distance into the heavily-doped emitter. This field can shift the carrier concentrations (and, therefore, Fermi level) near the surface and thereby alter  $p_0$ , the SRV, and the resultant dark current contribution. When such charge is applied to cells with only thermally oxidized  $Ta_2O_5$  coatings, no change is observed.\* There are four possible explanations for this negative result.

a. The defect density at the oxide-silicon interface is so high that the charge trapped there prevents any field from entering the silicon. High SRV and low blue response would result if this were the case. We have fabricated cells with a quantum yield approaching unity at  $0.3 \mu m$ , which would argue against such high defect densities. However, these cells had very shallow junction structures with doping gradients which could provide electric fields which extend to the surface. Under these circumstances, the recombination rate at the surface could still be moderately high, but the photogenerated minority carriers are swept out of the thin surface region ( $W_S$ ) before recombination can occur. The high recombination rate could, therefore, contribute to the emitter dark current and lower the open circuit voltage without hurting the blue response. Another argument against a high  $Ta_2O_5$ -silicon interface defect density can be inferred from the results from other oxides which provided poorer  $V_{oc}$  and/or blue response.

\*A Zerostat® anti-static pistol, normally used to neutralize static charge on phonograph records, was the method of depositing charge upon the surface.

b. The charge trapped in the  $Ta_2O_5$  exceeds the charge deposited on the surface, and, therefore, little change in field is observed at the interface. It is known [23] that thermally oxidized Ta contains negative charge when processed on p-type silicon. If similar charge results in n-type diffused layers, it will raise the SRV and lower the blue response of our cells. Nevertheless, the amount of charge trapped in the  $Ta_2O_5$  on p-type silicon is not adequate to allow a null effect for the charge applied to the surface.

c. Migration or tunneling of charge through the interface into the dielectric could be adequate to compensate the surface charge and, therefore, reduce the electric field at the interface. Only minor hysteresis is observed in C-V measurements of MOS structures with this oxide on p-type silicon [23]. If the results are similar for heavily doped n-type material, charge transfer is inadequate to compensate the surface charge.

d. The inability of surface charge to alter  $V_{OC}$  would also result if the change in minority carrier concentration ( $p_0$ ) is offset by a change in SRV as the Fermi level at the interface is shifted by the external field. This explanation has much to recommend it, since a shift in Fermi level ( $E_F$ ) will change the population of the different charge states of a defect (with  $E_d \approx E_F$ ) so as to increase the recombination probability as  $p_0$  goes down and decrease it as  $p_0$  is increased. Also field enhanced recombination can compensate for changes in minority carrier population. The argument against this explanation is based on the improbability of two or three effects interacting in such a manner as to cancel out so well.

None of these explanations can be rejected or accepted completely, as yet. It is likely that some combination of these effects takes place at the  $Ta_2O_5$ -silicon interface.

The scope of this contract did not permit detailed investigation of this type of side issue that often surfaced. A very useful but difficult [24] test would involve C-V measurements of MOS structures on heavily doped (preferably diffused) n-type silicon with the thermally oxidized Ta applied as in our solar cells. However, further tests of the nature of the Ta<sub>2</sub>O<sub>5</sub> and interface with n-type silicon were carried out by comparison with other oxide structures.

### 3.2.2 OTHER OXIDES

Removal of trapped negative charge\* from the Ta<sub>2</sub>O<sub>5</sub> should lower the SRV and reduce the requirements for an extremely shallow junction. In an attempt to replace the negatively charged Ta<sub>2</sub>O<sub>5</sub> with neutral or positively charged oxides, Nb<sub>2</sub>O<sub>5</sub>, evaporated SiO and thermally grown oxides were used in various combinations. The Ta<sub>2</sub>O<sub>5</sub> was the best, by far, which points to the fact that surface state density and nature (energy levels, capture cross section, etc.) may be more important than charge alone. (Passivation of these other oxide-silicon interfaces by annealing in forming gas or other ambients was not attempted for all combinations.)

The most successful modification to the COMSAT process was an addition of a 30 min. 750°C dry oxidation step after the thermal oxidation of Ta at 525°C. An average (but not consistent) increase in V<sub>OC</sub> of ~5 mV was observed in cells with this modification. However, the most interesting change was an onset

---

\*Negative charge in the Ta<sub>2</sub>O<sub>5</sub> is verified by the greater impact of positive surface charge than negative charge on the structures described below.



of sensitivity to surface charge. Cells with  $V_{oc} \approx 635$  mV could be raised to nearly 650 mV by the addition of positive charge to the surface of the AR coating. Negative charge could lower  $V_{oc}$  by a smaller amount. Unfortunately, cells initially near the 650 mV mark did not show similar gains. Addition of this thin silicon oxide between the  $Ta_2O_5$  and the silicon could: a. alter the density of defects at the oxide-silicon interface; b. reduce the negative charge in the  $Ta_2O_5$  and/or compensate it by a positive charge in the  $SiO_2$  layer; c. block migration of charge from the silicon into the  $Ta_2O_5$  when a field is applied; and/or d. alter the interface defect energy levels and/or nature so that a change in Fermi level would not alter the recombination rates of the defects.

Part of a single set of cells (set 1441, Table 2-1) exposed to the 750°C oxidation step was further annealed in forming gas. A slight improvement was noted in  $V_{oc}$  as was a slightly greater sensitivity to surface charging. The hydrogen attachment to dangling silicon bonds appears useful at a  $SiO_2$ -Si interface but not at a  $Ta_2O_5$  interface. (However, a forming gas anneal of p-type  $Ta_2O_5$  structures was observed to lower negative trapped charge [23]).

A probable explanation of the success of  $Ta_2O_5$ , in spite of some major limitations, involves the presence of impurities at the surface of a heavily diffused layer. As is noted in Appendix C, the phosphorus diffusion getters material to the silicon surface. These impurities, and the phosphorus itself, can form major interface defect sites during the oxidation of such a surface. If these impurities are trapped in or on the  $Ta_2O_5$  during the early oxidation stage then the Si surface is much cleaner by the time the  $SiO_2$  begins to grow. The  $SiO_2$  under

Ta<sub>2</sub>O<sub>5</sub> is, therefore, a much better surface passivator than silicon oxides thermally grown on bare silicon with similar doping concentrations. C-V measurements were made on MOS structures where the oxides were formed on p-type silicon by: a. growing SiO<sub>2</sub> underneath a thermally oxidized layer of Ta (continuing the oxidation process after all of the Ta is oxidized); and b. growing a dry oxide on silicon then thermally oxidizing a layer of Ta deposited on top. The result of the first oxide structure had opposite trapped charge compared to the second structure. The SiO<sub>2</sub> in the first case was probably grown at a much lower rate. Since no impurities were drawn to the surface by a diffusion step in these test structures, oxide growth rate may be more important than surface impurity concentration.

Cursory attempts at anodic oxidation and acid etching of the silicon surfaces prior to application of the AR coating produced low voltage cells. The idea in these attempts was to remove surface contaminants and a small portion of W<sub>g</sub>. The method and/or technique that we tried introduced more problems than were solved; nevertheless, this concept is sound and should be pursued.

The use of surface charge to increase V<sub>OC</sub> is a useful tool. However, it does not provide a permanent improvement. Section 4.3 discusses a more permanent structure with great promise in the use of SiO which has a large positive trapped charge density. Work at NBS has involved implantation of Na into an oxide for similar purposes [25]. Later sections will describe other results of tests involving surface charging as a tool.

## 3.3

EMITTER BULK

Use of the "dot" contacts gives a value of  $A_m/A_t = 10^{-3}$  in equation (3-1). Therefore, the contribution from the contact regions is small relative to that from the rest of the emitter and  $J_{dN} \approx J_{dN}^0$ . Since  $SW_S/D \ll 1$  for the oxide used, equation (3-5) reduces to  $J_{dN}^0 = qn_i^2(S + W_S/\tau_A)/N_D^*$ ; i.e., a simple sum of the surface and heavily doped layer components.

In the previous section, the surface-related term was discussed; in this section the surface layer and bulk of the emitter will be discussed. To differentiate the two terms more clearly, equations (3-5) and (3-3) are combined with the  $SW_S/D \ll 1$  assumption to give:

$$J_{dN}^0 = qp_0S + qn_i^2W_S/\tau_A N_D^* \quad (3-6)$$

where:  $p_0$  is the hole concentration at the surface and use of this form rather than  $n_i^2/N_D^*$  (which terms are not affected by field) more clearly indicates the influence of surface fields on the dark current contribution from the surface;  $n_i^2/N_D^*$  gives the hole contribution in the emitter region where fields are too weak to modify the hole concentration; and the implicit dependence of doping concentration and heavy doping effects are displayed in  $N_D^*$ .


Chronologically, the first efforts at reducing  $J_{dN}^0$  involved the lowering of  $W_S$ . Since this heavily doped surface layer grows linearly with time ( $t$ ) and the remainder of the emitter ( $x_j - W_S$ ) grows as  $\sqrt{t}$ , short diffusion time is the best means of reducing  $W_S$  without lowering  $x_j$  too much. (If  $x_j$  gets too small, problems with cell fill factor become severe as a result of strong junction fields and interaction with surface

defects.) Diffusion times as short as 5 minutes at 820°C have produced successful cells (f.f. > 0.79). However, the majority of these cells displayed lower fill factors. Moreover,  $V_{OC}$  did not improve for diffusion times below 15 minutes at 820°C. A slight reduction in  $J_{DN}$  could be observed with decreasing time, but an increase in the  $n \approx 2$  component of dark current (from the junction region) kept  $V_{OC}$  from rising. A number of variations in emitter dopant and doping profile were attempted in an attempt to reduce both the  $n \approx 1$  and  $n \approx 2$  components and improve the yield of high quality cells.

### 3.3.1 EMITTER PROFILE

The major goal of emitter modification was to provide a very thin, heavily doped surface layer ( $W_S$ ) with an abrupt drop in doping adjacent and a more gradual gradient in the junction region to spread out the space charge region and reduce the electric fields in the junction. This variation on the high-low emitter [10] must not increase the size (and, therefore, the recombination volume) of the space charge region too much, or there will be an increase in dark current from the junction [1]. (A minimum in junction dark current is to be found between the high-field, narrow-space-charge regime, and the high-recombination, broad-space-charge regime.) Several processes were tried in the attempt to obtain the "ideal" profile.

a. Arsenic is capable of creating a high concentration surface layer with a very abrupt drop in doping beyond. Therefore,



- (1) a shallow arsenic diffusion followed by a low concentration phosphorus diffusion to form a deep junction; or
- (2) a phosphorus diffusion followed by a shallow arsenic diffusion which would lower the P concentration and drive in the P to form a deep junction would provide near ideal shape.

b. A shallow P diffusion followed by a cleaning step to remove the spin-on dopant, a 16-hour drive-in step, and then a second shallow diffusion would provide near ideal shape. (This process of diffusion-clean-drive-diffusion will be referred to as the dddd process. Other processes, such as long diffusion-clean-diffusion, ldcd; and diffusion-clean-drive, dcd, are minor variations.)

c. Anodic oxidation and etching is a means of reducing  $W_s$  on a medium junction cell to provide an "improved" but not ideal profile.

d. A shallow diffusion on a thin, lightly boron-doped, epitaxial layer would provide a long space charge region while maintaining strong gradients in the emitter. The size of the space charge layer is controlled by the doping in the epi-layer.

e. Variations in the composition of N250C might allow the codiffusion of P and As to provide the ideal profile in a single step.

None of the above processes produced cells with better  $V_{oc}$  than a single diffusion with N250C and most resulted in significantly poorer cells for one reason or another.

- a. Results poor -  $V_{oc}$  and  $I_{sc}$  were low. See Sections 3.3.2 and C.3.

- b. Results good -  $V_{OC}$  was comparable with single diffusion results, the fill factor was improved (0.80-0.81, vs 0.79-0.80), but the blue response was down as expected. See Section 3.3.4.
- c. Results poor -  $V_{OC}$  and fill factor were down. See Section 3.2.2.
- d. Results mixed - base diffusion length  $L_n$  was very poor, but  $V_{OC}$  was better than would be expected for such low  $L_n$ . See Sections 2.3 and 3.3.6.
- e. Results poor - both voltage and fill factor were down. See Sections 3.3.3 and C.3.

The inability of the modified profiles to raise  $V_{OC}$  is attributed to the limitation created by the SRV (Section 3.2). The improvement in fill factor for the dcdd process is a positive step which predicts that if the SRV limitation can be overcome, cells with both high  $V_{OC}$  and high fill factor can be fabricated.

### 3.3.2 Arsenic Doped Emitters

During the contract, periodic attempts were made to use arsenic as a means of a. increasing the surface donor concentration ( $4 \times 10^{20}/\text{cm}^3$  vs  $2 \times 10^{20}/\text{cm}^3$  for phosphorus); b. altering the junction profile (to provide a high-low emitter); and c. reducing the lattice stress which could propagate damage into the junction. Hope was raised in this endeavor since use of Emulsi-tone N250C spin-on dopant has been so successful. This material contains four times as much arsenic as phosphorus and its use has resulted in reproducibly better cells than use of gaseous phosphorus sources.

Attempts at arsenic doping alone (with Emulsitone spin-on sources, sets 1421 and 1435) resulted in poorer cell performance characteristics than those resulting from use of N250C. Use of N250C, either prior to (sets 1428 and 1430) or subsequent to (set 1422) arsenic doping improved the situation, but not to a point comparable to N250C alone (see Section C.3). Doping concentration profiles from secondary ion mass spectroscopy (SIMS) data (Figure C-1) indicate that despite the higher arsenic concentration in N250C, the arsenic concentration in an N250C diffused surface will be two orders of magnitude less than the phosphorus concentration. However, sheet resistivity measurements on arsenic diffusions alone indicate doping concentrations in excess of  $10^{20}/\text{cm}^3$ . The conclusion that the presence of phosphorus reduces arsenic diffusion is inescapable.

Since arsenic diffusions alone do not give good results, but arsenic with phosphorus (as N250C) does, an attempt was made to vary the ratio of arsenic to phosphorus in a single mixture. Two variations from the basic N250C formulation were tried (Appendix C.3). One had a reduced phosphorus concentration (LoP/RA) and the other had a reduced phosphorus and arsenic concentration (LoP/LoA). A series of diffusion schedules (sets 1448 and 1449) were carried out with the new formulations on 1  $\Omega$ -cm material. Sheet resistance and junction depth measurements have indicated that the interaction between the diffusing dopants is more complicated than expected. It appears that only a high concentration of phosphorus suppresses arsenic diffusion, but a high concentration of arsenic strongly enhances phosphorus diffusion. The use of the LoP/RA mixture, therefore, provides a good donor profile for a high-low emitter by driving a low concentration of phosphorus in front of a shallow heavily doped arsenic layer.

Other results from these experiments include confirmation that both blue response and open circuit voltage are reduced when arsenic is used (alone or with phosphorus in concentrations below that in N250C) and that minority carrier lifetime in the bulk is degraded for high concentration arsenic diffusions above 850°C. Three hypotheses are proposed to explain the data:

- a. The surface recombination velocity (SRV) of arsenic-doped silicon is higher than for phosphorus-doped silicon.
- b. The arsenic doping relieves stress in the heavily diffused region and thereby increases the mobility over a region heavily doped with phosphorus (therefore, the junction fields have less opportunity to draw carriers away from the surface before recombination occurs).
- c. The active doping in heavily arsenic-diffused layers may exceed that of phosphorus-diffused layers. If this were the case, the majority carrier concentration would increase and therefore the Auger recombination would also increase and the blue response would decrease. The effective doping which could raise  $V_{OC}$  would probably not increase much; but this prediction depends upon which bandgap narrowing model is used.

A high SRV (as in a.) would not reduce the open circuit voltage on deep arsenic-diffused cells, but such devices have not been fabricated because of the time required for low temperature diffusions. A higher mobility in arsenic-doped material (as in b.) would not alter  $V_{OC}$  [see equation (3-6)], but in deep junction cells, would reduce the minority carrier gradient toward the junction and thereby reduce the blue response. When compared to phosphorus-doped material, a high mobility in As-diffused silicon could show up in experiments comparing the two dopants in deep



junction cells where D becomes important [equation (3-2)]. If Auger recombination is higher in the As-doped emitters ( $\tau_A$  is smaller), these cells (as in c.) would be dominated by the heavily-doped layer rather than SRV, and the emitter dark currents should be more sensitive to variations in  $W_S$  than our N250C diffused cells.

The present status of arsenic-doped solar cells is that solar cell characteristics are degraded by use of this dopant, either alone or in conjunction with phosphorus, when it is the dominant source of donors. Therefore, in spite of our ability to diffuse nearly ideal emitter profiles\* by combined use of As and P, this technique does not appear useful in solar cell processing. However, a comparison of As- and P-doped emitters might provide data and insight on surface recombination velocities and/or stress effects on mobility.

### 3.3.3 LOW-DOPED EMITTERS

This section describes the effort to raise  $V_{OC}$  by reducing the heavy-doping effects [6] and, thereby, raise  $N_D^*$  in equation (3-5). A comparison of cells with low-doped emitters, with and without shallow heavily-doped surfaces, provides important information as to the effectiveness of doping profiles, doping concentration, and surface passivation.

Theoretical calculations, based on several of the bandgap-narrowing models [5]-[7] predict an optimum effective emitter concentration ( $N_D^*$ ) at an actual doping level near

\*Profiles were deduced from sheet resistivity and junction depth measurements.

$10^{19}$  phosphorus atoms/cm<sup>3</sup>. We have obtained these surface concentrations by diffusion from low concentration sources and by diffusing a thin layer of heavily-doped silicon, removing the spin-on source, and driving the remaining dopant into the silicon over a long period of time. The first process provides a lightly doped ( $\sim 5 \times 10^{19}$ /cm<sup>3</sup>) shallow layer and the second process (dcd) provides a lightly doped ( $\sim 10^{19}$ /cm<sup>3</sup>) deeper layer. In both cases, the Auger recombination will be much lower than in the heavily doped surfaces and the effective doping should be higher. Therefore,  $J_{DN}$  should be lower (because of  $N_D^*$ ) and dominated by  $S$  [see equation (3-5)]. Since the surface doping is lower than that of regular cells,  $S$  should be lower also. The cell should also be more responsive to surface charge, since the Debye length is longer in the less heavily-doped surface material, and  $p_0$  at the surface will be more easily altered by externally applied fields.

Table 3-3 gives the results of a series of experiments to identify the impact of low emitter concentrations on cell characteristics. A more lightly-doped base (1  $\Omega$ -cm) was chosen to reduce the probability of excess acceptor buildup at the emitter surface (see Figure C-1) which would have a particularly harmful effect on cells with low donor concentrations in the emitter. The dark current contribution from the bulk is higher for 1  $\Omega$ -cm cells but the influence of emitter structure is still apparent. Dot contacts were used to assure contributions to  $J_{DN}$  only from the oxide interface and the emitter bulk. Shallow (1451-4,5) and deep (1450-7,8) junction cells with heavily doped emitters are used to define the extreme conditions of cells dominated by SRV and emitter bulk, respectively. Addition of a low doped step ( $\sim 10^{19}$ /cm<sup>3</sup>) to separate the junction from the heavily doped surface (1453-1,2 vs. 1451-4,5) creates a drop in blue

Table 3-3. Various Emitter Profiles on 1  $\Omega$ -cm Substrates

Cell #	Emitter Structure	$X_j$ ( $\mu$ m)	$V_{oc}$ (mV)	$I_{sc}$ (mA)	$I_b$ (mA)	$I_T$ ( $\mu$ A)
1451-4,5	shallow, heavy doped	~.15	$603 \pm 1$	$147 \pm 2$	41	8.7
1453-1,2	deep, low doped + heavy doped	0.7	605	$145 \pm 1$	36	8.4
1453-6,7	deep, low doped + heavy doped	0.6	602	$146 \pm 2$	$36 \pm 1$	8.5
1450-5,6	deep, low doped	0.8	598	127	26.5	8.8
1453-3,4a	deep, low doped	0.7	593	132	27	8.3
1453-8a	deep, low doped	0.6	586	133	28	8.6
1453-9a	deep, low doped	0.6	583	130	28	7.8
1450-7,8	deep, heavy doped <sup>b</sup>	2.1	588	92	12	7.0

a positive surface charge raises these values to  $V_{oc} > 597$ ,  $I_{sc} \approx 140$ , and  $I_b \approx 33$ .  
<sup>b</sup>N250C diffused overnight.

current ( $I_b$ )\* but has no significant impact on  $V_{oc}$ . Addition of the heavily doped surface layer (1453-1,2,6,7) to a deep, low-doped emitter (1453-3,4,8,9) creates a major increase in  $I_b$  and a distinct rise in  $V_{oc}$ . The varied dependence of  $V_{oc}$  and  $I_b$  on junction depth ( $x_j$ ) and surface condition points to an emitter which (for  $x_j \approx 7 \mu m$ ): 1) allows transport of minority carriers through it; 2) captures some minority carriers generated by blue light within it; and 3) has a high enough SRV so that  $SL/D > 1$  (see Figure 2-1). The addition of a positive charge to the front surface of the AR coating reduces the SRV but is not as effective at this as is a heavily-doped surface layer (compare footnoted values in Table 3-3 with 1453-6,7). The cell data in the table provide evidence for strong statements about heavy doping effects and SRV.

a. An effective high-low barrier exists between regions doped at  $2 \times 10^{20}/cm^3$  and  $10^{19}/cm^3$ . Therefore, bandgap narrowing does not fit the models which predict a reduction in effective doping with an increase in actual doping [5]-[7] (Section 3-4).

b. Surface recombination velocity at the  $10^{19}/cm^3$  level appears to be comparable to that at the  $2 \times 10^{20}/cm^3$  level ( $\sim 5 \times 10^3$  cm/s). (Negative charge trapped in the  $Ta_2O_5$  would have a greater effect on the lower-doped emitter surface, thus preventing the expected decrease in SRV.)

c. Based on change in  $V_{oc}$  and expected contributions from the bulk (base and emitter), the dark current from the emitter surface, as a result of added surface charge, should decrease

\*A slight difference in AR coating thickness between batches 1451 and 1453 makes the change in  $I_b$  appear more drastic than it really is.

by more than a factor of 2. Since the heavily doped layer is even more effective, the effective doping at  $2 \times 10^{20}/\text{cm}^3$  could well be three to four times that at  $10^{19}/\text{cm}^3$ .

Some other low doped structures were examined in preparation for MINP\* work. These results, shown in Table 3-4, are from cells with relatively shallow, low-doped emitters and ultra-shallow moderately-doped emitters. Cell 1460-4 had an overnight drive-in (diffusion after a light deposition of N250, a short diffusion, and removal of excess). Cell 1460-2 was treated in a similar manner but a  $\text{Ta}_2\text{O}_5$  layer was thermally grown on the wafer surface prior to this drive-in step ( $\text{SiO}_2$  will grow under the  $\text{Ta}_2\text{O}_5$  during drive-in). Of particular interest here is the fact that negative charge can also increase the current collection in this case where a thick† thermal silicon-oxide is present on the surface. The  $V_{OC}$  changes in the expected manner, but only to a very small extent.

Cell 1460-4 acts in a more expected manner, and the lower response to a negative charge compared to a positive charge implies that the  $\text{Ta}_2\text{O}_5$  does in fact contain negative charge trapped within it. The near total collection of photocarriers generated in the surface region, when positive charge is applied to the AR coating, is different than that seen in Table 3-3 for deep, low-doped emitter cells. The very low voltage when recombination losses at the front surface are made near zero is hard to explain unless the effective donor concentration is two orders of magnitude less than that of heavily-doped emitters. If this were the case, a greater response to surface charge would be

\*A structure utilizing MIS contacts and charged oxides to accumulate an  $n^+$  surface in a lightly doped n layer on a p-type substrate.

†Thick relative to  $\text{SiO}_2$  grown under  $\text{Ta}_2\text{O}_5$  for 30 min. at  $750^\circ\text{C}$ .

Table 3-4. The Influence of Surface Charge on Low Doped Emitters

Cell #	Emitter Structure	$x_j$ ( $\mu\text{m}$ )	Charge	$V_{oc}$ (mV)	$I_{sc}$ (mA)	$I_b$ (mA)	$I_y$ ( $\mu\text{A}$ )
1460-2	Lightly doped $\text{TaO}_{2.5}$ mask	0.2	+	525	131	40	
			0	520	113	32	
			-	517	121	35	3.7
1460-4	Lightly doped	0.4	+	513	140	40.5	
			0	496	128	34.5	6.9
			-	480	127	33.5	
1460-6	Very shallow moderately doped ( $\sim 5 \times 10^{19}/\text{cm}^3$ )	$\sim 0.07$	+	390	125		
			0	328	57	27	5.1
			-	287	18		

expected. The possibility of heavy compensation by boron, from the 0.1  $\Omega$ -cm background and/or additionally accumulated during the diffusion (Figure C-1), would reduce charge effects and account for a poor effective donor concentration.

The very large impact of surface charge on the very shallow emitter of cell 1460-6 is in part due to the increase in surface conductivity resulting from accumulation of the n-type silicon in the diffused emitter. The propagation of field into the diffused emitter implies an increased junction barrier height and corresponding  $V_{OC}$ . Since the charge cannot reach beneath the contacts, full benefit of the increased junction potential cannot be realized but the influence on dark current is seen. MIS contacts could take full advantage of both effects (see Section 4.2). The very low voltages could alternatively be a result of leakage currents through or around the very thin junction; however, shunt resistance was measured to be in the 1 k $\Omega$  range and that is too high to cause any loss of  $V_{OC}$ . Tunneling through a portion of the very shallow high concentration gradient, emitter, would influence (shunt) the forward biased cell but not the unbiased cell.

### 3.4 BANDGAP NARROWING FROM HEAVY DOPING

We have seen in Section 2.1 that an effective  $p^+$  back on 0.1  $\Omega$ -cm material has not been achieved by diffusion processes. Recent work at NASA/Lewis (private communication, Vic Weizer) has confirmed these results for boron doped layers, diffused by laser heating, where the active doping should be significantly greater than that possible by diffusion. The band gap narrowing model of Slotboom and Degraaff [8] predicts an

improvement in the  $pp^+$  barrier characteristic above  $\sim 10^{20}/\text{cm}^3$  and this is observed in  $nn^+$  barriers (Section 3.3.3). Three explanations are possible:

a. There is a difference in bandgap narrowing with heavy doping above  $3 \times 10^{19}/\text{cm}^3$  in n- and p-type silicon. Theory [5] predicts that bandgap narrowing would be more severe in n-type silicon. However, this theory also predicts a functional dependence of bandgap narrowing with n and p doping concentration that is quite different from that experimentally observed in this work and in Reference 8.

b. The  $p^+$  layers had ohmic surfaces and their thicknesses were less than the diffusion lengths in the  $p^+$  material so that the surface, not the  $p^+$  bulk, dominated recombination in the  $p^+$  regions.

c. The measurement techniques were not sensitive enough to detect an improvement in  $pp^+$  barrier characteristics. Both gamma current,  $I_\gamma$ , and  $V_{OC}$  measurements should be sensitive to changes in the back surface for the cell parameters used. However, no distinction can be made between changes in the back surface and in the bulk diffusion length.

Studies of  $p^+pn$  cells (thin p layer) with light incident on the  $p^+$  surface should be a method of verifying the bandgap narrowing model for p-type silicon as was done for n-type silicon in Section 3.3.3.

For the present, we feel that the Slotboom and DeGraaff [8] model fits both n- and p-type silicon data for doping below  $2 \times 10^{19}/\text{cm}^3$ . Results in n-type silicon appear to show somewhat less bandgap narrowing than predicted above  $2 \times 10^{19}/\text{cm}^3$ . Results in p-type silicon appear to indicate greater bandgap narrowing than predicted above  $2 \times 10^{19}/\text{cm}^3$ .



#### 4. DOUBLE DIFFUSED CELLS

The best cell (1408-8) fabricated so far under this contract is characterized, with and without a coverslide, in Figure 4-1. It is seen that this cell is healthy in all respects prior to being covered; however, it appears that the cell has had its fill factor reduced as a result of being covered (0.80-0.78). Nevertheless, the expected increases in  $I_{SC}$  and  $V_{OC}$  are observed for the covered cell. The quantum-yield data are presented in Figure 4-2 along with data from a deeper junction cell ( $x_j \approx 1.6 \mu m$ ) from the same batch and a shallow junction ( $x_j \approx 0.1 \mu m$ ) single diffused cell (1407-3). A quantum yield in excess of 0.8 at 300 nm is very good, but shallower junctions should improve it further and raise  $I_{SC}$  by  $\geq 4$  mA.

Results of an analysis of the illuminated I-V characteristic of the bare cell 1408-8 are shown in Figure 4-3. The data are fitted with three components of the diode equation:

- a. The junction recombination ( $J_r$ ) term with an  $n \approx 2$  slope;
- b. The diffusion current ( $J_d$ ) term with an  $n = 1$  slope; and
- c. The current leakage term resulting from shunt resistance ( $R_{sh}$ ).

The series resistance ( $R_s$ ) is varied to get the best correlation of data to the diode equation. It is seen that neither  $R_s$  or  $R_{sh}$  contributes to the curve shape near  $P_{max}$  (at  $V \approx 560$  mV) but that the  $n = 1$  and  $n \approx 2$  terms are nearly identical at this point and  $J_r$  will, therefore, reduce  $P_{max}$ . The fill factor (FF) for this cell exceeds 0.80 despite the strong  $n = 2$  contribution, but will

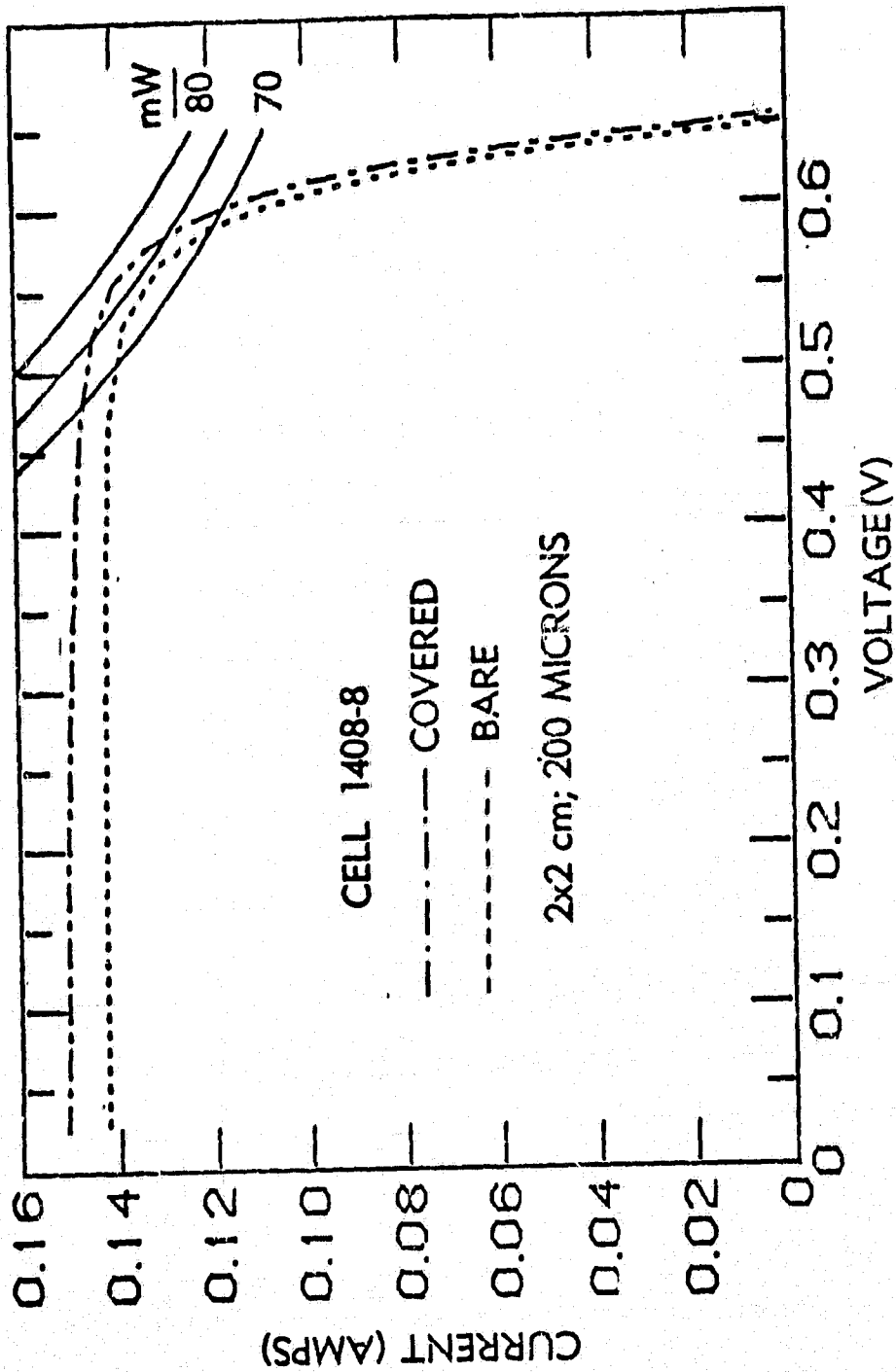


Figure 4-1. IV Curves for Cell 1408-3, Bare (Dots) and Covered, (Broken) Under Simulated AM0 Conditions

ORIGINAL PAGE IS  
OF POOR QUALITY

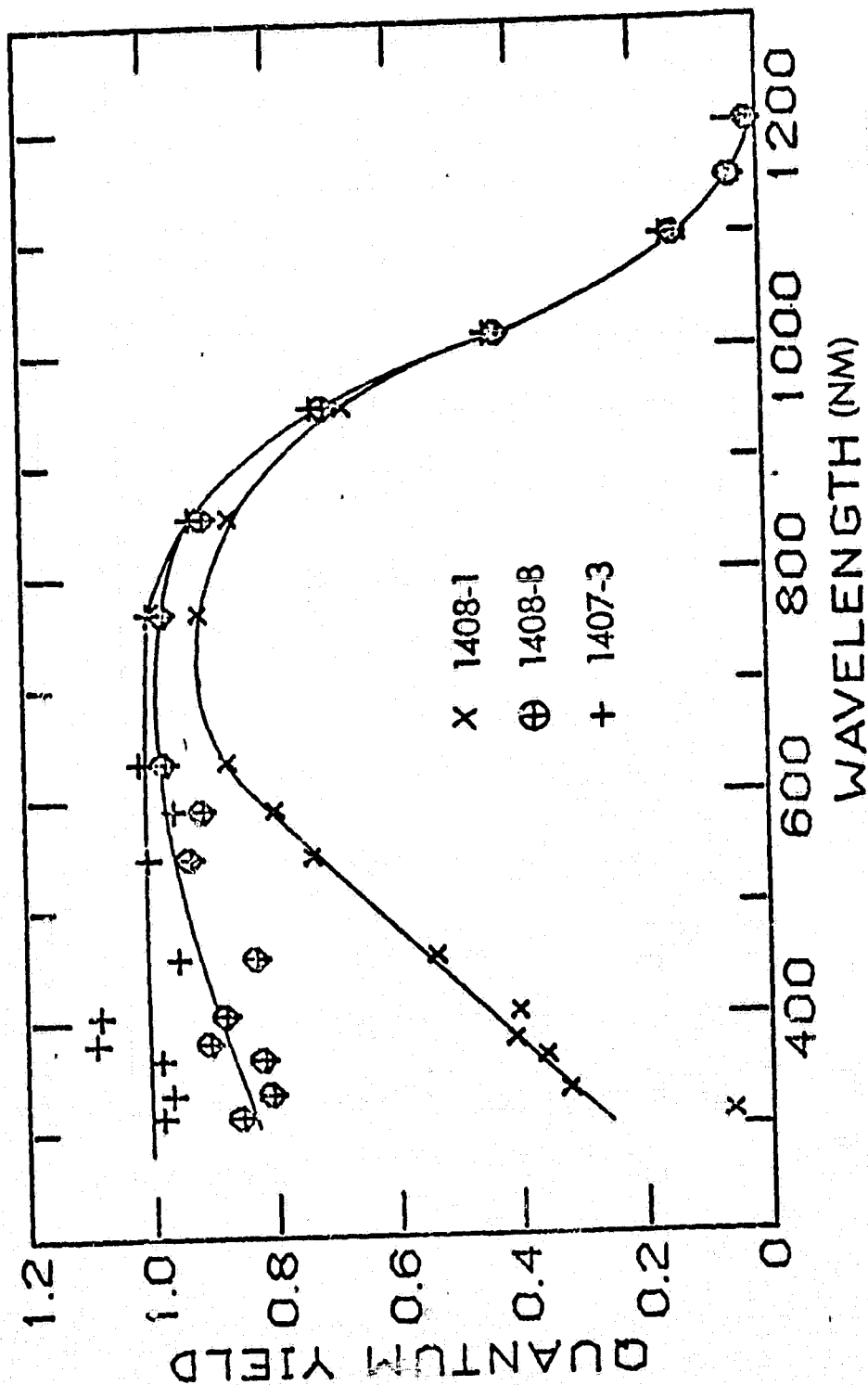


Figure 4-2. Quantum Yield Results for Cell 1408-8 ( $x_j \approx 0.5 \mu m$ )  
Along with Shallow (1407-3) and Deep (1408-1) Junction Cells

ORIGINAL PAGE IS  
OF POOR QUALITY

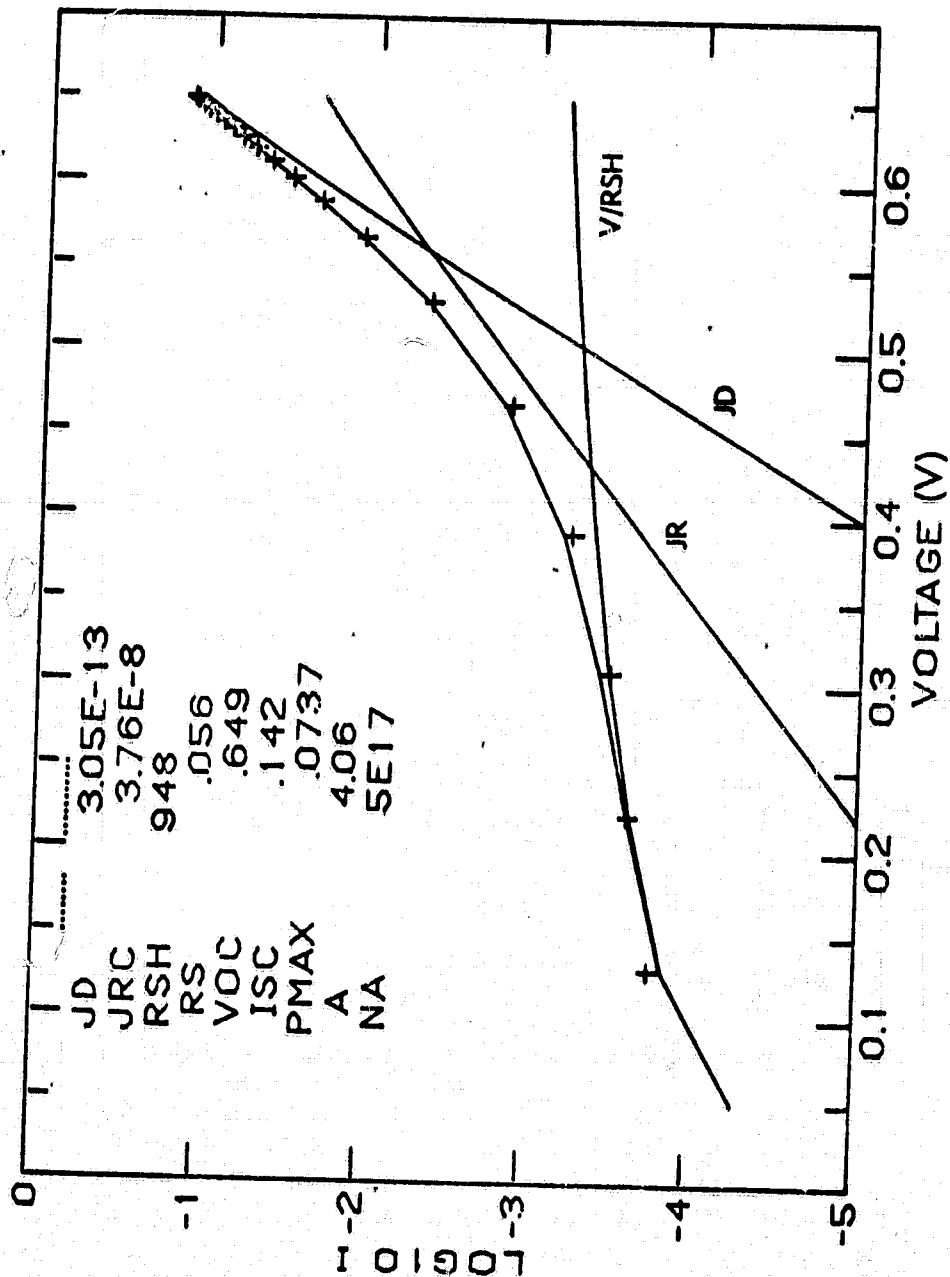


Figure 4-3. IV Analysis of Cell 1408-8 Indicating the Junction Recombination ( $J_R$ ), Dark Diffusion ( $J_D$ ), and Leakage ( $V/R_{SH}$ ) Currents

not increase as  $V_{OC}$  is increased unless  $J_r$  is reduced. Therefore, it is seen that to achieve cells with significantly higher maximum power, both  $J_d$  and  $J_r$  must be reduced.

#### 4.1 PROCESSING

Fabrication was a combination of COMSAT and NASA/Lewis developments. Critical factors include the dot contact [12] and the  $Ta_2O_5$  AR coating [23] which lower the effective surface recombination velocity and permit use of shallow junctions to achieve the resulting high blue response without loss of  $V_{OC}$ . In fact, the best values for  $V_{OC}$  were obtained for the cells with highest blue response. The NASA/Lewis development is the use of a two-step diffusion process with intervening etch step [20]. Without this two-step process, the best voltages obtained were nearly as good but not consistently as good. The specific steps used here are:

- a. An overnight (17 hr) drive-in at 880°C of an (Emulsitone) N250C spin-on, followed by
- b. An etch step that removes nearly all of the diffused layer, and then
- c. A 15-min. diffusion at 820°C, again with N250C.

The back surface has 1  $\mu m$  of evaporated aluminum applied prior to the second diffusion.

Tantalum metal is evaporated over a fine line grid (50 lines/cm) pattern of photoresist. The photoresist is removed and the remaining Ta oxidized at 525°C. Chrome-gold contacts are evaporated in a grid pattern at right angles to the pattern in

the  $\text{Ta}_2\text{O}_5$  on the cell front (resulting in  $5 \times 10 \text{ } \mu\text{m}$  "dot" contacts at the intersections) and over all the back surface. All metal is silver plated and a  $2 \times 2 \text{ cm}$  square cell is cut out of the round wafer and given a quick edge-etch to remove saw damage and other sources of shunt resistance. Standard solid-state fabrication practice is followed in cleaning the silicon slices prior to and during processing.

#### 4.2 DEVELOPMENT AND ANALYSIS

A major effort of this contract was directed toward improving  $V_{oc}$  by use of shallow, abrupt junctions to reduce the volume of heavily-doped (and, therefore, bandgap-narrowed) material which can contribute so strongly to the emitter dark current. Use of dot contacts reduced the recombination at the contacts and, thereby, permitted the reduction of junction depths to below  $0.1 \text{ } \mu\text{m}$  in  $0.1 \text{ } \Omega\text{-cm}$  material without the increase in  $J_d$  experienced with full contacts. Reduction of carrier losses in the emitter and its surface resulted in a quantum yield at  $300 \text{ nm}$  approaching unity. The use of shallow junctions was not entirely without cost as two problems were observed to correlate directly with reduced junction depth. Shunt current and junction recombination both became more significant as the junction was moved closer to the surface. The shunt currents could sometimes be reduced to insignificant levels by use of a longer edge etch; but often a residual, low shunt resistance was still present and the cell fill factor was reduced. The junction recombination current ( $J_r$ ) has been found to increase markedly with reduced junction depth and has been attributed to field-enhanced recombination [1]. Again, the fill factor is lowered as this  $n \approx 2$

component is increased. Use of the two-step diffusion process appears to have reduced both of these problems.

Typically, the front junction is created using N250C in a short, low-temperature process as a simple, reliable method of providing a high-quality  $n^+$  layer. Diffusion with the N250C spin-on dopant results in migration of impurities (gettering), including boron, into the diffused region (see Section C.3). These gettered impurities can shunt the junction and also lower the lifetime in the junction and emitter regions. As a consequence of etching off the results of a diffusion, the material with most of the impurities is removed. Therefore, the shunt resistance is higher and the  $J_r$  term is lower after a subsequent diffusion. Table 4-1 gives the pertinent characteristics of two sets of cells. Set 1407 is diffused with N250C at 820°C for 15 minutes, and set 1408 has had an overnight diffusion with N250C at 880°C followed by different etch times prior to the same N250C diffusion at 820°C for 15 minutes. Comparison of the two sets of data indicates several differences resulting from a prediffusion. Most important are a 10-mV increase in  $V_{OC}$  and an improved fill factor with more consistent results within a set. The penalty paid is a reduced  $I_{SC}$  and blue current  $I_b$ . The improved  $V_{OC}$  is explained by the lower  $J_d$ ; the better fill factor is due to the lower  $J_{RC}^*$  and higher  $R_{SH}$  (Table 4-1). Since the diffusion lengths (as indicated by  $I_\gamma$ ) are nearly the same,  $J_{dp}$  (that portion of  $J_d$  from the p-type base) will be the same unless the minority carrier diffusion coefficient,  $D$ , is changed [14]. If  $D$  changes, an opposite change in minority carrier lifetime  $\tau$  is required to maintain a constant value of  $L$  since  $L = \sqrt{D\tau}$ . If  $J_{dp}$

\* $J_{RC}$  is the junction recombination current extrapolated back from  $P_{max}$  to  $V = 0$  assuming  $n = 2$ .

Table 4-1. Uncovered Characteristics of a Set of Single  
Diffused Cells (1407) and of a Set of Double  
Diffused Cells (1408)

	Cell #	Process	I <sub>sc</sub> (mA)	V <sub>oc</sub> (mV)	I <sub>B</sub> (mA)	f.f.	a I <sub>Y</sub>	J <sub>D</sub> (pA)	J <sub>RC</sub> (nA)	R <sub>SH</sub> (Ω)
1408 Double Diffusion	1	N250	130.4	647	29.6	0.82	6.9	0.32	20	365
	2	1.6 μ	123.7	642	27.9	0.80	6.8	0.37	32	111
Variable etch depth	3	N250	133.9	640	33.3	0.80	6.6	0.44	32	1K
	4	~0.9 μ	136.7	646	33.5	0.80	6.7	0.35	31	540
	5	N250	142.8	644	37.3	0.80	6.5	0.40	36	1K
	6	~0.3 μ	143.1	646	37.2	0.80	6.6	0.35	43	1K
	7	N250	142.8	648	37.5	0.80	6.5	0.31	50	1K
	8	~0.15 μ	142.6	650	37.3	0.80	6.2 <sup>b</sup>	0.3	39	1K
1407	1		149.3	629	41	0.73	6.8	0.54	111	46
	2	N250	150.8	630	40.8	0.71	7.2	0.54	110	37
	3	0.1 μ	150.1	637	40.8	0.77	6.8	0.46	88	134
	4		149.2	634	41	0.73	6.4	0.47	974	49

<sup>a</sup>an I<sub>Y</sub> of 7.0 corresponds to a diffusion length of > 240 μm.

<sup>b</sup>Measured with coverslide which reduces I<sub>Y</sub> [16].



is unchanged by the prediffusion step, then the decrease in  $J_d$  must be a result of decreased  $J_{dN}$ . Material improvement in the emitter and junction regions appears to be the mechanism responsible for improvement of  $V_{oc}$  in the double-diffused cells fabricated under this contract.

#### 4.3 HYPOTHESES

The double diffusion process used to fabricate cells with  $V_{oc} > 650$  mV had an influence that does not easily fit present models. If only a deep junction cell showed such a high voltage, then a fit to the general model could be made by assuming that the mobility  $\mu$  (and thus  $D$  in equation 3-2) in the emitter were somehow reduced. This hypothesis is supported by the observed loss in blue current which would result from the increased emitter transit time, which increases the minority carrier concentration in the emitter and therefore allows a higher chance for carrier recombination in the bulk and at the surface of the emitter.

If only a shallow junction cell exhibited high voltage as a consequence of the double diffusion process, then the simple model would suggest a reduction in  $S$  rather than mobility since removal of the bulk contribution term [ $W_s/\tau_A$  in equation (3-5)] is probably not adequate to cause the observed voltage increase. However, in the case of reduced  $S$ , the blue response would increase rather than decrease as observed; therefore, this hypothesis will not stand alone.

Since 650-mV cells have been fabricated with junction depths of both 1.5 and  $\sim 0.15$   $\mu\text{m}$ , the possibility of other mechanisms must be examined. An increase of effective doping  $N_D^*$  in

equation (3-2) is one of the possibilities examined. It has been proposed [1] that the compensating acceptors in the emitter increase the bandgap narrowing in the  $n^+$  layer. In the process of studying the doping profile of diffused structures, some support for this hypothesis was provided. SIMS data of 0.1  $\Omega$ -cm silicon diffused with Emulsitone N250C spin-on dopant (Figure C-1) indicated a very high concentration of boron at the surface. A blank silicon wafer with no diffusion or heat treatment was similarly measured (Figure 4-4) and no excess surface boron concentration was observed. A hypothesis is proposed that the boron buildup during the first diffusion is removed in the subsequent etch step, and as a consequence, the buildup during the second diffusion is reduced. Figure 4-5 shows such a reduced build up and also hints that out-diffusion (perhaps with "emitter push") reduces the boron concentration slightly in the layer beneath the surface. The first effect (reduced buildup) should lower the bandgap narrowing in the emitter surface layer and the second effect (out-diffusion) could reduce the bandgap narrowing in the rest of the emitter. If the boron surface concentration is not electrically active, other effects such as changes in minority carrier lifetime and/or mobility must be considered.

In an attempt to simulate the undoping of boron from the wafer surface, high temperature oxidation was tried (Figure C-2). However, no improvement was observed when solar cells were fabricated from such oxidized material. (A degraded bulk lifetime points to damage introduced by the high temperature step.) A second attempt was made to reduce the boron surface concentration by using 2- $\mu$ m, 50-100  $\Omega$ -cm, p-type, commercially prepared, epitaxial layers on 0.1  $\Omega$ -cm substrates. The wafers were made into cells with the N250C diffused into the epi layer. The base diffusion lengths of the resultant cells were less than

ORIGINAL PAGE IS  
OF POOR QUALITY

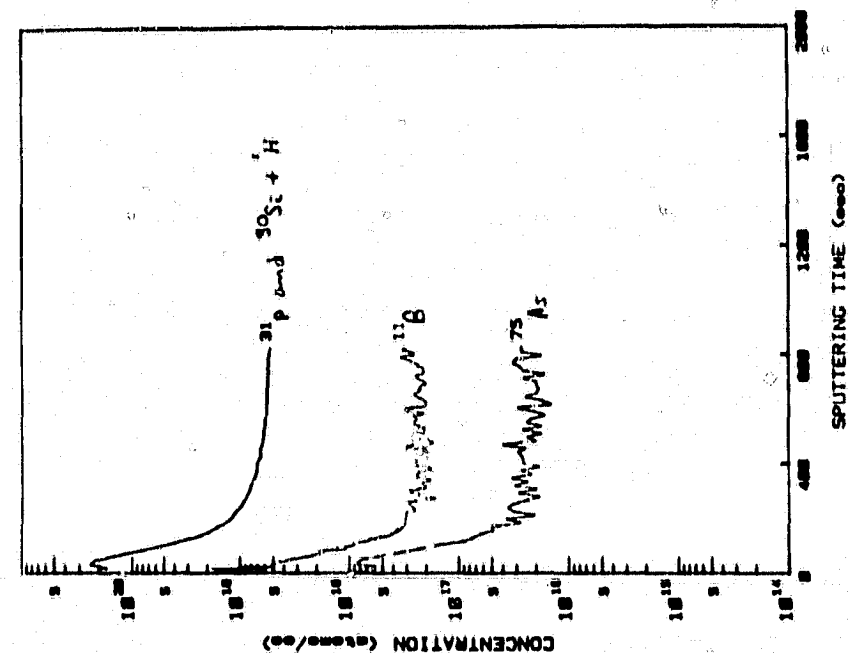


Figure 4-5. A 16-hr Prediffusion  
(N250C at 880°C) Was Nearly  
Etched Off Prior to a  
15-Minute Diffusion  
(N250C at 820°C)

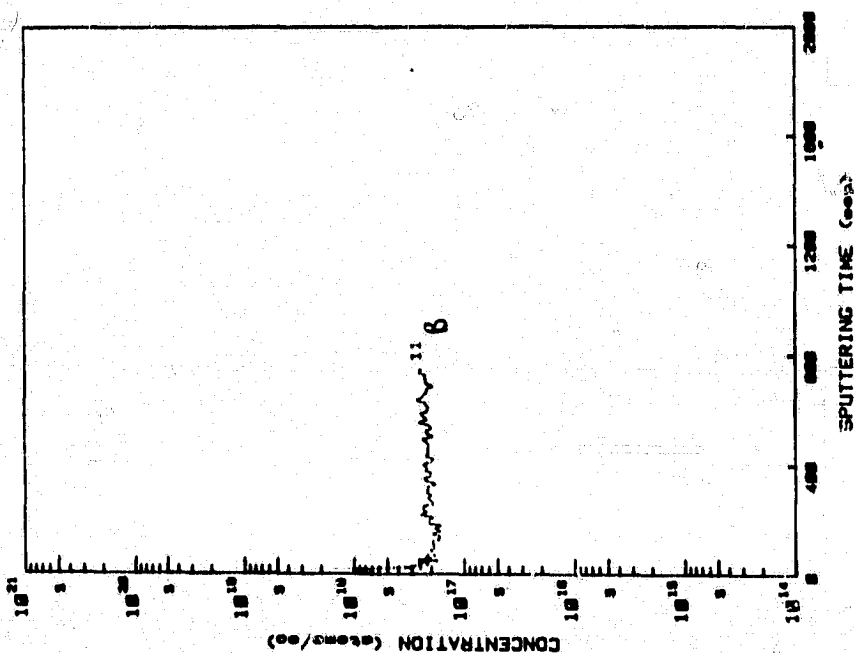


Figure 4-4. Boron Concentration  
Profile in an Untreated 0.1 ohm  
Silicon Wafer (SIMS Data by  
Charles Evans and Assoc.,  
San Mateo, CA)

50  $\mu\text{m}$ , or from 5-10 times lower than cells fabricated from the same material without an epitaxial layer. Since open-circuit voltages approaching 630 mV were obtained in spite of the low value for  $L_n$ , several attempts were made to getter and/or anneal the material prior to, during, and after the diffusion step. Only minor improvement was observed. Some samples were processed with the epi layer etched off, and diffusion lengths were still low. The problem was attributed to substrate poisoning during the epitaxial deposition.

The effort (as above) to provide verification of the influence of boron on the double diffused cells was not successful. Nevertheless, this hypothesis logically explains the data available.

One of the early difficulties with the double diffusion process was control of the etch rate in a diffused sample with the 100:1,  $\text{HNO}_3\text{:HF}$  acid used. A well-controlled hydrazine etch allowed us to etch off thick layers (1-2  $\mu\text{m}$ ) to within a few percent of desired thickness. The first double diffusion cells made using this process were almost exactly that expected from single diffused cells of the same structure; i.e., the voltages did not show the improvement and the blue current did not show losses expected from the new process. A possible explanation of this result [20] is that the long first diffusion of the double diffusion process stresses the material in such a manner as to significantly reduce the mobility in the emitter and perhaps beyond. There is evidence that differences exist in stress relief when using acid etches as opposed to basic etches [26].

#### 4.4

#### SUMMARY

High-quality shallow-junction solar cells have been fabricated on 0.1  $\Omega$ -cm float zone refined silicon using N250C. Use of a process similar to the NASA/Lewis double-diffusion process has reduced shunt leakage and junction recombination currents while adding 5-10 mV to the average open-circuit voltages obtained from our single-diffusion process. I-V analysis indicates that the junction recombination current has a small influence on open-circuit voltage and a more significant influence on the fill factor.

## 5. I-V CHARACTERISTICS

The primary effort in this contract was directed at increasing  $V_{OC}$ . It is desirable that the other I-V characteristics (which had been optimized previously) not be degraded in the process of improving  $V_{OC}$ . Such degradation could be innate to the structure or process or a result of non-optimized conditions. In only a few instances were the voltages enhanced if the other characteristics were not near optimum.

### 5.1 SHORT CIRCUIT CURRENT

Several structures which were designed to increase  $V_{OC}$  resulted in lower  $I_{SC}$ .

a. In Section 3.1.2, it was noted that grid spacing has an influence on  $V_{OC}$ . The finer grid spacing (required for maximum  $V_{OC}$ ) increases the grid shadowing and, therefore, lowers  $I_{SC}$ .

b. MIS structures require a metallic layer over the whole surface, thereby introducing an optically absorbent layer which also increases the surface reflectance. (The actual  $V_{OC}$  at AM0 was lower than the best diffused cells because the metalization was not optimized for optical transmission and no AR coating was applied, Section 6.1.)

c. Double diffused cells with the best voltages also had reduced blue response (Section 4).

d. Decreased base resistivity (to  $0.1 \Omega\text{-cm}$ ) was expected to reduce  $I_{SC}$  as well as the base dark current by lowering both  $L_n$  and increasing  $N_d$  (Section 2.4). However, we have maintained diffusion lengths of  $0.1 \Omega\text{-cm}$  material at the values

typical of 1- $\Omega$  cm material (set 1455). Therefore, further reduction in resistivity is expected to result in only a small decrease in  $L_n$  and  $I_{SC}$ , a decrease in  $J_{dp}$ , and an increase in  $V_{OC}$ . The limitation in base doping will be reached when  $L_n$  is dominated by Auger recombination and/or when heavy doping effects prevent any further increase in effective doping, Section 2.4.

Some structures optimized for  $I_{SC}$  would reduce  $V_{OC}$ .

a. A textured, (or nonreflective) surface [27] improves light collection, but it also increases the emitter surface area and volume, and therefore lowers  $V_{OC}$ .

b. Choice of different metals or use of transparent conductors in MIS structures can result in increased  $I_{SC}$  but the work functions are likely to be less appropriate for high  $V_{OC}$ .

c. The use of  $Ta_2O_5$  (thermally oxidized Ta) as an AR coating provides the best optical coupling (when a coverslide is used) and also the best voltages obtained on diffused cells; however, the negative charge trapped within the layer lowers  $V_{OC}$  to some extent. Use of slowly evaporated  $SiO$  (to provide a positive trapped charge) on a thermally oxidized surface has been reported to provide superior voltages in an MINP structure [11]. Unfortunately,  $SiO$  absorbs in the ultraviolet and does not have the optimum index of refraction for covered cells; therefore, lower  $I_{SC}$  results.

Some improvements in current collection can be made without incurring  $V_{OC}$  degradation.

a. Use of sawtooth coverslides [13] can increase the cell current by refracting light between the grids. This allows a

small grid spacing to be maintained without the penalty of increased grid coverage. (In permitting thicker grids, it also allows light concentration without series resistance and, therefore, permits improved efficiency.)

b. If MIS back contacts are effective enough to lower SRV in this region, then the cells can be made thinner (with possible increase in  $V_{OC}$ ) and back surface reflection, inherent in this structure, would increase cell red response.

Means of improving  $I_{SC}$  in high voltage solar cells which do not hurt  $V_{OC}$ , therefore, include:

- a. Sawtooth coverslides,
- b. Back surface reflectors,
- c. Shallow junctions,
- d. Wrap around contacts,
- e. MIS or low contact back layers, if lower SRV can be attained thereby,
- f. Charged oxides (front and back), if lower SRV can be attained thereby, and
- g. Nonreflective front surfaces, only if the resultant percentage increase of emitter dark current is not greater than that of the increased  $I_{SC}$ .

## 5.2 FILL FACTOR

Solar cell fill factor depends on:

- a. series resistance (primarily grids and  $n^+$  layer),



- b. shunt resistance (leakage currents), and
- c. junction recombination.

When using shallow-junction, low-contact-area structures, all of these effects must be addressed.

Series resistance shows up in several ways. A simple ohmic loss in the grids is the easiest to model. However, it is not a likely problem with the high grid density used in this contract (Section 3.1.2). An expected problem might be the spreading resistance in the shallow emitter layer since carriers have to travel further to reach the dot contacts than they would to reach bar contacts. The dot contacts are spaced at  $\sim 0.2$ -mm intervals so that the maximum distance a carrier need travel is  $\sim 0.14$  mm. This corresponds to a grid density of 33/cm which is more than adequate for almost any emitter with a surface concentration of  $10^{20}/\text{cm}^3$ .

In low-doped emitters, the sheet resistivity is kept at reasonable levels by increasing the emitter thickness. However, a more serious problem is encountered with the low area, low SRV contacts used here. These contacts are non-ohmic, Schottky barriers and, therefore, are severely affected by lowered emitter doping which increases the barrier width through which carriers must tunnel (Section 3.3.3). Use of MIS or larger area contacts solve this problem.

The change in illuminated I-V curve shape is different for each of the above cases. In the simple series resistance case, the absolute value of the slope  $dI/dV$  at the voltage intercept is reduced. In the high spreading resistance case, the curve shape at the intercepts is generally unaltered and the "knee" is just "softened," almost as if an increased  $n = 2$  component were present [21]. The Schottky barrier case provides

a soft knee and an "ankle" near the voltage intercept (Figure 3-1). This shape is more often seen in cases where the back contact is improperly made on the moderately doped substrate.

Shunt resistances are associated with edge effects and/or surface defects (leakage-current paths). In shallow junction, heavily doped cells, the electric fields in the junction region are very high because the Debye lengths are so low. Under these conditions, leakage would be especially high and extreme care must be exercised in fabrication to prevent damage to surfaces or edges of the cells. Damage associated with the contacts (attributed to thermally activated dissolution of silicon into the metal contacts) has been reported [28]. Our use of unheated, dot contacts removes this as a problem. We did find it necessary to edge-etch the wafers (after slicing) more than 1 mil to solve the problem of defects at the cell edges. The double diffusion and high-low emitter structures deepen the junction and reduce the junction fields; therefore reducing the leakage currents also.

The leakage currents are not likely to be truly linear in voltage for any of these defects; but if they were, the effect on the I-V characteristic would be an increase in  $dI/dV$  at the current intercept and a reduction in  $V_{OC}$ . Most of the leakage currents are linear enough to display these traits. In a non-linear case, a "flat" spot above the knee of the curve (beginning at the break at about 170 mV in Figure 5-1) has been observed from edge damage and other point defects in the emitter of the cell.

Junction recombination is a potential problem in shallow junction solar cells because of the close proximity of the junction to the heavily doped and damaged surface and because of the field enhanced recombination which increases with the higher junction fields of such structures [1]. Contaminants getterred

ORIGINAL PAGE IS  
OF POOR QUALITY

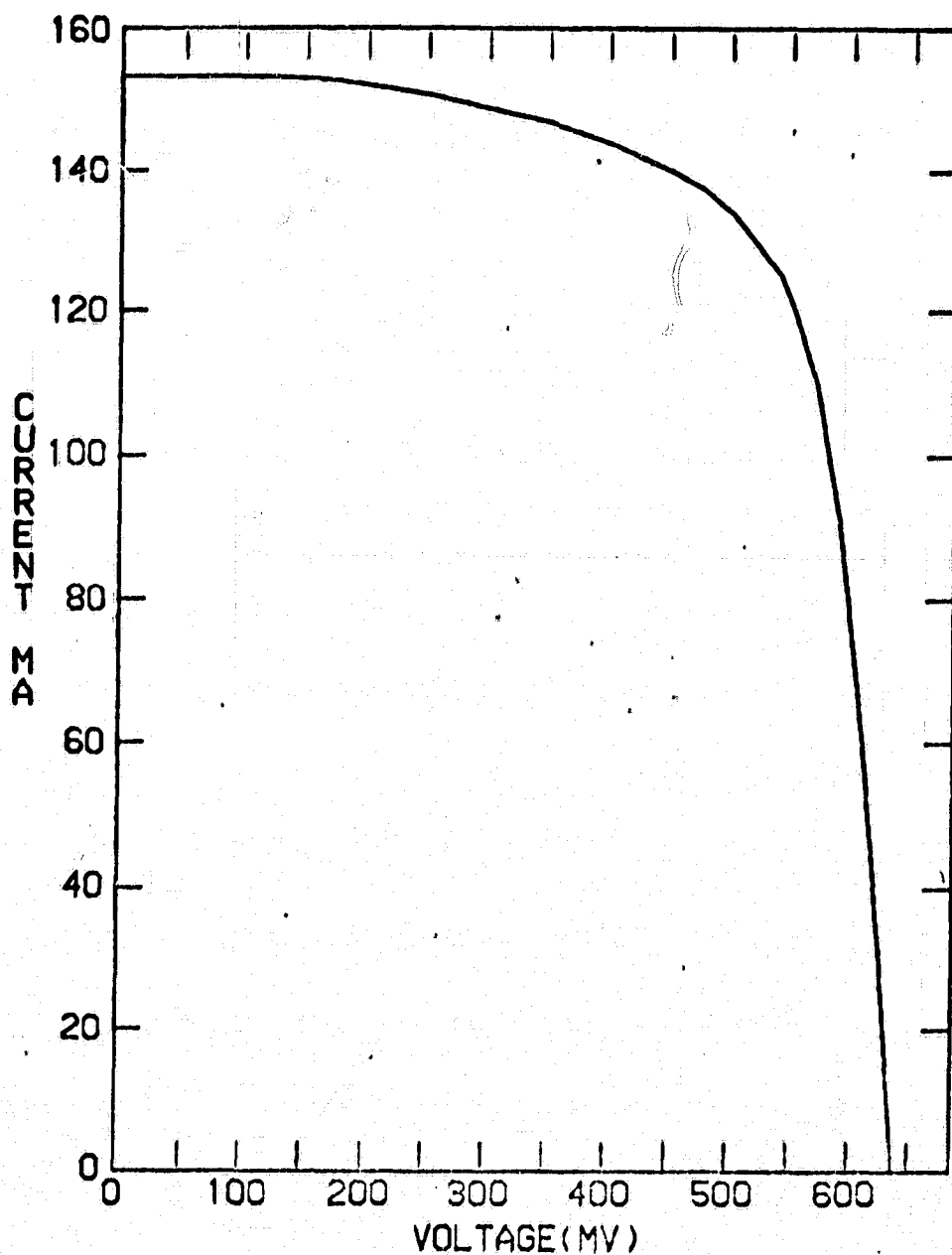


Figure 5-1. The I-V Curve of a Shallow Junction Solar Cell  
with a "Flat" Spot Above the Knee.  
This is Characteristic of  
Localized Defects

toward the surface or driven in from the surface during the diffusion step can contribute to recombination in the space charge region. It was observed that double diffused cells had improved fill factors (Section 4.1) even if all of the initial diffusion were etched off. Anodic oxidation and wet thermal oxidation of the emitter surface were both found to reduce the fill factor on shallow junction cells. This reduction is attributed to stress-induced defects propagated through the junction region, which increased both  $J_r$  and cell leakage currents.

The effect of  $J_r$  on cell I-V characteristics is that of softening the knee. When severe, this  $n = 2$  term will dominate the curve and may significantly lower  $V_{oc}$ .

The means of maintaining or improving cell fill factor without degrading  $I_{sc}$  or  $V_{oc}$  include:

- a. use fine grid patterns;
- b. minimize surface and edge defects;
- c. reduce junction electric field (careful tradeoffs may be necessary here);
- d. keep junction clear of defects and contaminants from a heavily-diffused surface layer.

### 5.3 OPEN CIRCUIT VOLTAGE

The majority of this report is devoted to improvements in  $V_{oc}$ , so only areas of future potential are mentioned here.

Use of thin epitaxial layers, to reduce the boron doping in the emitter did not provide expected results because of poor material (Section 4.1.3). Nevertheless, this structure

should be beneficial for diffused  $n^+p$ , MIS, and MINP cells. With the present limitations to  $V_{oc}$  of bandgap narrowing and high surface recombination velocity, some alternative approaches might be considered in future work. Instead of using heavily doped emitters, metal layers in MIS structures, or induced emitters in MINP structures to conduct current to collection grids, one might consider a different structure. A heterojunction might be as easy to fabricate as any of these earlier structures. The top layer (a wider bandgap material than silicon) could be extremely thin since, if it were very heavily doped for high conductivity, bandgap narrowing would only make it a better match to lightly-doped silicon. Exact lattice matching might be unnecessary because a thin oxide layer, as in the MIS structure, could tie up loose bonds. This new SIS structure could well be optimized in an SINP structure similar to that of the MINP cell. Attempts along the SIS lines have been made with amorphous materials such as doped  $SnO_2$  [29]; but semicrystalline or polycrystalline material might be more successful, particularly if it could be, at least partially, lattice-matched with the silicon. If the doping in this nonsilicon layer is graded properly, the only bandgap narrowing will be in this layer and the remaining source of dark current should depend primarily on recombination at the oxide interfaces.

The SINP structure would in many respects be like the GaAlAs "window" on a GaAs cell in that the effective surface recombination velocity would be reduced by the presence of a wider bandgap semiconductor. The wider bandgap assures a lower minority carrier concentration and therefore lower dark current, even if electrical contact is made to the silicon rather than the non-silicon layer. Similar structures on the back surface could provide excellent  $p^+$  layer characteristics.

Means (present and future) of improving  $V_{oc}$  include:

- a. Reduce SRV (front and back)
  - (1) dot contacts
  - (2) MIS contacts
  - (3) reduce interface surface state density
  - (4) charged oxides
- b. Reduce bandgap narrowing from heavy doping
  - (1) remove boron from emitter region
  - (2) provide heterojunction for highly conductive regions.
- c. If very low SRV is possible (from a and/or b)
  - (1) reduce emitter thickness
  - (2) reduce base thickness

## 6. SPECIAL STRUCTURES

### 6.1 MIS STRUCTURES

MIS structures in which the surface of a p-type base is inverted to form an induced n-type layer are innately interesting and useful tools with which to study the oxide-silicon interface and, by comparison, diffused n<sup>+</sup>p structures. The dark current equations should apply to a good MIS structure as well as to the diffused junction structures. Deviations from these equations can be predicted in certain cases and can also be useful in diagnostics. The base components should be unchanged and we will ignore them here by assuming that the contribution from 0.1  $\Omega$ -cm substrates do not contribute to our results. Equations (3-4) and (3-5) contain an effective doping term  $N_D^*$  which has no meaning in an induced n layer. However, bandgap narrowing in the emitter is considered to result primarily from electron-electron interaction [6] and an inverted layer has the same number of electrons as a comparable diffused layer. An associated problem is Auger recombination which depends on the square of the electron concentration. Therefore, the major dark current contributions in MIS cells and diffused junction cells will have the same basic limitations ( $n_i^2/N_D^*$  must be explicitly written as  $p_0 e^{\Delta E_g/kT}$  for the influence of bandgap narrowing from heavy doping effects).

Some differences can be readily considered in the two structures. The diffusion profile provides a region of little or no field at the surface whereas the field in the silicon is strongest at the oxide-silicon interface in the MIS structure. This means that the electron concentration will be decreasing rapidly from this interface; and therefore, the emitter bulk term

[represented by  $W_s/\tau_A$ , in equation (3-5)] will be negligible. The Auger recombination term would not appear explicitly in the dark current equations in this case, but defect-assisted Auger recombination would probably be the dominant term in defining SRV. In addition to the other recombination mechanisms at the surface, field enhanced recombination [1] will now have a maximum at the surface rather than at the junction.

The  $n = 1$  value normally associated with the emitter term may be greater than 1 if a potential drop exists through the oxide. This drop could result from trapped charge within the oxide and/ or leakage currents through defects in the oxide. Such a situation would reduce the electron concentration and field at the interface, thereby reducing the SRV (if Auger and/or field dominated) but the negative impact on the cell fill factor and voltage is increased by the higher value of  $n$ . An example of this is an MIS cell that when illuminated at 1, 2, and 4 AMO produced  $V_{oc}$ 's of 629, 654, and 674 mV (cell 1455-15). The  $n$  value starts out near 1.5 and drops closer to 1 at higher intensity as the leakage current is reduced by lowered internal junction potential at  $V_{oc}$  or the trap population is shifted by increased illumination. Alternatively, local defects act in parallel with the remainder of the cell. At higher voltages, the  $n > 1$  characteristic of the defect regions is decreased relative to the  $n = 1$  characteristic of the undamaged region.

Other differences between the MIS and diffused junction cells are the relatively stress-free inverted layer compared to a diffused layer; the lower impurity and dopant concentrations at the oxide-silicon interface; the low fabrication temperatures; the lack of metal-silicon contacts; and the requirement for an adequately conductive layer and proper work function metal for the MIS structure. All but the last item are generally plusses



for the MIS structure. However, the lower temperature and lack of diffused layer can reduce the gettering generally observed in diffused cells; therefore, the base lifetime may become a limiting factor in MIS cells with high  $V_{oc}$ .

MIS cells were fabricated under this contract to compare, where possible, the differences resulting from diffusion process steps. Erbium metal ( $\sim 100 \text{ \AA}$ ) was used because it has a very low work function,  $\phi = 3.1 \text{ eV}$  [30]. Chromium ( $\sim 50 \text{ \AA}$ ) was evaporated over the Er surface to prevent oxidation which would otherwise ruin the MIS structure. No attempt was made to optimize the cells by altering the thickness or composition of the metal layers or by adding an AR coating.

The highest voltage obtained on an MIS cell was 647 mV for a cell with  $I_{sc} = 75 \text{ mA}$  (AM0 at  $25^\circ\text{C}$ ). The saturation dark current for this cell was  $\sim 2 \times 10^{-13} \text{ A/cm}^2$  which is two-thirds of the value for our best  $n^+p$  cell of  $\sim 3 \times 10^{-13} \text{ A/cm}^2$ . Since the cell base is unchanged, the emitter current is seen to be an important factor, at least in this dark current range. Addition of a lightly doped n-layer to the MIS structure will reduce the field at the interface and lower the maximum field intensities at any point in the emitter region. At the same time, it may allow a higher hole concentration at the surface itself and increase the recombination in subsurface regions of the emitter.

Optimization of the MIS fabrication processing should provide an improvement over the results obtained here. However, preliminary use of light phosphorus diffusion of the MIS surface layer did not produce any improvement. Further work in these areas is recommended, specifically:

- a. Gettering of the wafer by P and Al with subsequent removal of impurities by silicon etch prior to MIS formation;

b. Improved surface conditions by repeated oxidation and oxide etch steps; and

c. combination of steps a and b in a device that has a lightly doped layer beneath the metal-oxide layers but with low surface impurity concentrations and good bulk lifetimes.

## 6.2 MINP STRUCTURES

The MIS structure has shown improvement in dark current over the diffused  $n^+p$  junction device. However, a heavily-doped cap region on a lightly-doped emitter is seen to be more effective in reducing  $J_d$  than an induced layer (Section 3.3.3) on the same lightly-doped emitter. If the induced layer beneath a charged oxide and an MIS structures are considered to be the same, these results appear to be inconsistent. However, if the hole concentration at the MIS structure interface is much lower than that at the induced layer interface previously described, then the results are reasonable. This would occur if the interface field resulting from the work function difference between Er and Si is greater than that resulting from an external positive charge on a  $Ta_2O_5$  AR coating. These interface fields can be increased by reduction of the AR coating thickness and/or negative charge. Green et al. [11] have accomplished this by use of oxides (e.g., SiO) which have positive charge incorporated during the evaporation process. The resulting charge is much closer to the interface and more charge can be stably contained in a layer than can be achieved by external charge deposited on a surface. (However, the surface must now be protected so that negative charge does not accumulate and reduce the interface fields). If the positive charge sites are thermally stable and high enough

above the Fermi level in the silicon, they will not migrate nor be compensated by electrons from the emitter. With their configuration [11], a low work function metal is no longer required to induce an emitter and, therefore, can be replaced by an AR coating to improve the optical coupling of light into the semiconductor. The contacts must still be MIS structures to maintain the  $n^+p$  junction.

A limitation of this MIS gridded, induced-junction structure is surface conductivity, since carriers must now flow beneath the surface to the collection grids rather than tunneling through an oxide to the metal contact. The inverted layer, on a heavily-doped p-type substrate, is very shallow, and charge transported along this thin layer will probably encounter severe surface scattering and other effects which reduce the conductivity of the layer. Lightly counter doping the surface layer will increase the number of electrons available for transport to the grids (a small effect), but more importantly, it will reduce the intensity of the electric fields which force the current to interact so strongly with the surface.

Green et al. have found that doping the surface layer also increases  $V_{OC}$ ; but doping it too heavily lowers the  $V_{OC}$  of this "MINP" structure. They optimized the doping level at a value which minimized the surface recombination velocity; but in the theoretical analysis of this level, they assumed bandgap narrowing models for heavy doping effects which our work indicates are incorrect (Section 3.3.3).  $V_{OC}$  should, therefore, be greater at emitter doping levels beyond those experimentally found to be optimal by Green, et al. Why is there a discrepancy? We believe that heavy diffusions contaminate the surfaces and, therefore, raise the SRV; reduction of the surface fields below a certain level may increase the capture cross section of surface states,

and/or the Debye length in the heavily-doped surface layer is so short that holes can tunnel through the field barrier to the surface states.

The importance of the MINP structure (beyond the fact that the highest values of  $V_{OC}$  reported have resulted from it) is that it provides a low SRV contact (an MIS structure) and a low oxide-silicon interface SRV. Improvements in this technology are expected along the lines set for MIS cells (at the end of Section 4.2). However, dot contact cells with the same oxide-silicon structure should be equivalent since the critical factor is the SRV of this oxide interface and is, therefore, independent of the contacts. Additional improvements might be possible by the use of appropriate ion implantation into the oxide [25]. If the radiation damage from implantation can be annealed from the oxide and the net positive charge increased beyond that possible from the evaporated oxides of Green, et al., then the SRV should decrease and/or a higher doped  $n^+$  layer may be optimum.

Success of the MINP cell has verified our model (which indicated that SRV was the critical limitation in high  $V_{OC}$  cells) and pointed to a means of removing a major limitation. However, before significant improvements in solar cell voltage can be made beyond that obtained in MINP structures, it is likely that similar improvements must be made on the back of the solar cells to provide a low SRV back contact [19]. Based on MINP success in the emitter, there is hope that negatively charged oxides ( $Ta_2O_5$ ) with dot or MIS contacts might be successful in providing a  $p^+$  back layer that is effective on  $0.1 \Omega\text{-cm}$  substrates. If such is the case, 700-mV silicon solar cells may still be attainable. However, if bandgap narrowing in heavily doped ( $> 10^{20}/\text{cm}^3$ ) p-type is greater than that in n-type silicon (Section 3.4) these structures may be no more successful than those already tried.

## 7. CONCLUSION AND REMARKS

Gettering (Appendix C) and low temperature processing techniques have provided 0.1  $\Omega$ -cm solar cells with diffusion lengths comparable to those in 1-2  $\Omega$ -cm material. The possibility of maintaining these results on lower resistivity material ( $\rho < 0.1$ - $\Omega$ -cm) is worth investigating (Section 2.4).

Attempts at achieving effective  $p^+$  back contacts on 0.1  $\Omega$ -cm material were not successful (Section 2.1). Bandgap narrowing as a result of heavy doping effects appears to be the major cause of this failure.

The emitter dark current appears to be the major limitation in present 0.1  $\Omega$ -cm solar cells (Section 3.2). Bandgap narrowing from heavy doping and surface recombination are the main sources of this current.

Use of low area "dot" contacts removes the metal-silicon interface as the major contributor to surface recombination (Section 3.1.1). MIS contacts would have a similar effect (Section 3.1.3).

Surface recombination at the oxide-silicon interface has been reduced by use of static charge on the anti-reflecting coating (Section 3.2.1) and by use of electric fields created by an MIS structure (Section 6.1). Charged oxides, as used in MINP structures, would have a similar effect.

Bandgap narrowing in heavily doped n-type silicon is found to be less than predicted by the more pessimistic of the present models (Section 3.3.3). The results for both n- and p-type silicon are in agreement with the data of Slotboom and DeGraaff [8] (Section 3.4).

The highest  $V_{OC}$  obtained for diffused  $n^+p$  0.1  $\Omega$ -cm cells was 654 mV at 25°C under AMO illumination (Section 4). The saturation dark current for this cell (fabricated using the double diffusion technique) is  $J_d = 3 \times 10^{-13}$  A/cm<sup>2</sup>.

MIS cells, fabricated with erbium metal have displayed lower dark currents than those obtained on the best diffused cells. The best saturation current computed was  $J_d = 2 \times 10^{-13}$  nA/cm<sup>2</sup>.

## Dependence of Efficiency of Shallow Junction Silicon Solar Cells on Substrate Doping

E.S. Rittner,\* A. Meulenbergt and J.F. Allison‡  
COMSAT Laboratories, Clarksburg, Md.

Experimental evidence is provided to support a modification of solar cell theory to include the field-enhanced junction recombination dark current. This term is shown to become more important in limiting shallow junction solar cell efficiency as base resistivity is decreased. The anomalously high-diffusion dark current in the *n*-region is also significant in limiting open-circuit voltage. This excess dark current is shown to result from high-surface recombination at the metallic contacts on the front surface ( $S_{1p} = 4 \times 10^3$  cm/s,  $S_{1n} = 7 \times 10^3$  cm/s) along with bandgap narrowing and high Auger volume recombination in the diffused *n*-region caused by high donor density. It is also pointed out that the effective thickness of the *n*-region is substantially less than the junction depth. Methods are proposed for reducing the magnitude of both dark currents to improve overall cell performance.

### Introduction

CLASSICAL theory of the *p-n* junction solar cell predicts a monotonic increase in open-circuit voltage and conversion efficiency with substrate doping up to the saturation solubility limit.<sup>1</sup> However, attempts to improve the output of cells intended for terrestrial use by increasing the substrate doping density have not been successful. According to Iles and Soclof,<sup>2</sup> the open-circuit voltage displays a maximum as a function of substrate doping density in the range of  $10^{17}$ – $10^{18}$ /cm<sup>3</sup>, and the conversion efficiency peaks at a doping density slightly less than  $10^{17}$ /cm<sup>3</sup>.

Two different suggestions have been advanced to explain the fall-off in open-circuit voltage and efficiency with increased substrate doping. Rittner<sup>3,4</sup> has proposed that the recombination dark current in the junction enhanced by the thermal counterpart of the Franz-Keldysh effect is responsible. On the other hand, Lauwers et al.<sup>5</sup> and Lindholm et al.<sup>6</sup> have found experimental evidence for an anomalously large *n*-region diffusion current component in solar cells with a substrate resistivity of 0.1 Ω-cm (equivalent to a doping density of about  $4 \times 10^{17}$ /cm<sup>3</sup>). More recently, Redfield<sup>7</sup> has attributed this high diffusion current to Auger recombination in the heavily doped diffused region.

The purpose of this paper is to examine these proposed explanations by further elaboration of the theory<sup>4</sup> and by a new experimental approach which separates the various components of the dark current. The results furnish considerable insight into the origin of the high-diffusion dark current in the highly doped *n*-region, and it is concluded that both this current and the field-enhanced recombination current are important in limiting the efficiency of present solar cells.

### Theoretical Discussion

The solar cell theory presented in Ref. 4 consists of the following equations (corrected for previously undetected errata) for the current density vs voltage relationship of a *p-n*

junction solar cell:

$$J = J_{1n} (e^{qV/2kT} - 1) + J_{1p} (e^{qV/2kT} - 1) - J_1 \\ = J_1 + J_{1n} - J_2 \quad (1)$$

where

$$J_{1n} = \frac{\pi q n_i (kT/q)}{E_s (\tau_p \tau_n)^{1/2}} e^{\Delta E_s / 2kT} \quad (2)$$

$$\Delta E_s = \left( \frac{h q}{2\pi (m^*)^{1/2}} \right)^{2/3} E_s^{2/3} \quad (3)$$

$$m^* = 2m_n m_p / (m_n + m_p) \quad (4)$$

$$J_{1n} = \left( \frac{q p_0 D_p}{L_p} \right) \frac{S_p \cosh(W_N/L_p) + (D_p/L_p) \sinh(W_N/L_p)}{(D_p/L_p) \cosh(W_N/L_p) + S_p \sinh(W_N/L_p)} \\ + \left( \frac{q n_0 D_n}{L_n} \right) \frac{S_n \cosh(W_p/L_n) + (D_n/L_n) \sinh(W_p/L_n)}{(D_n/L_n) \cosh(W_p/L_n) + S_n \sinh(W_p/L_n)} \\ = J_{1n} + J_{1p} \quad (5)$$

The first term on the right-hand side of Eq. (1) represents the recombination dark current density in the junction enhanced by high field bandgap narrowing; the second term represents the diffusion dark current density in the *n*- and *p*-regions of the cell; and the last term  $J_1$  represents the short-circuit current density generated by the light. The notation is as follows:  $q$  is the electron charge,  $k$  is the Boltzmann constant,  $T$  is the absolute temperature,  $n_i$  is the intrinsic carrier density, and  $\tau_p$  and  $\tau_n$  are the hole lifetime in the *n*-material and electron lifetime in the *p*-material, respectively. The electric field at the junction is denoted by  $E$ ;  $\Delta E_s$  is the energy bandgap decrease caused by the electric field;  $h$  is the Planck constant;  $m_n$  and  $m_p$  are the effective masses for electrons and holes, respectively; and  $p_0$  and  $n_0$  are the thermal equilibrium minority carrier densities in the *n*- and *p*-type materials, respectively.  $D$  is the diffusion constant,  $L$  is the diffusion length,  $S$  is the surface recombination velocity of the minority carriers, and  $W_N$  and  $W_p$  are the thicknesses of

\* Received July 28, 1977; revision received Jan. 9, 1981. Copyright American Institute of Aeronautics and Astronautics, Inc., 1981. All rights reserved.

† Director of Applied Sciences, Associate Fellow AIAA.

‡ Member of the Technical Staff, Semiconductor Technology Department.

§ Staff Scientist, Applied Sciences Laboratory.

the  $n$ - and  $p$ -type regions of the diode, respectively. Subscripts  $p$  and  $n$  refer to minority carrier holes and electrons, respectively. In the following detailed discussion of these equations, several new points of importance are highlighted.

#### Recombination Current ( $J_r$ )

The voltage dependence of the current density is not given simply by Eq. (1) with  $J_{00}$  constant because  $E$  and  $\Delta E_g$  also depend upon the potential drop across the junction. Since this potential is the difference between the applied voltage and the built-in potential, it is necessary to include these dependencies in accurately fitting  $J$ - $V$  characteristics.

#### Diffused Region Minority Carrier Lifetime ( $\tau_p$ )

The coefficient multiplying the exponential term in Eq. (2) is the well-known result of the Sah, Noyce, Shockley (SNS) theory<sup>8</sup> for dark current recombination in the junction for recombination centers near mid-gap. Equation (2) is an approximation appropriate to undamaged silicon cells. The SNS theory assumes a single recombination center of uniform density  $N_t$  throughout the junction and neutral regions. Hence,  $\tau_p$  is the hole lifetime corresponding to  $N_t$  in heavily doped  $n$ -material. However, the experimentally determined hole lifetime in the  $n$ -region will generally be much less than the  $\tau_p$  of the SNS theory; this can be attributed to either a higher recombination center density in the  $n$ -region than in the  $p$ -substrate (from high temperature diffusion) or to Auger recombination<sup>9</sup> in the highly doped  $n$ -material. For example, the hole lifetime in the  $n^+$  surface region of conventional silicon solar cells deduced from a dead layer thickness of 0.15  $\mu\text{m}$  is of the order of  $10^{-10}$  s,<sup>10</sup> whereas the value of  $\tau_p$  in Ref. 4, which produces excellent agreement between theory and experiment, is  $10^{-8}$  s.

#### Energy Band Decrease ( $\Delta E_g$ )

The derivation of Eq. (2) assumed that the thermal bandgap simply shifts to lower energy with increasing electric field by an amount equal to the optical bandgap narrowing. Values for the latter quantity were taken in Ref. 4 from the measurements of Britsyn and Smirnov<sup>11</sup> on a silicon  $p$ - $n$  junction. Although these data fit the  $E^{1/2}$  dependence of the Franz-Keldysh theory fairly well, closer examination reveals that the proportionality factor is an order of magnitude higher than the quantity in brackets in Eq. (3). Alternatively, the value of the reduced effective mass [Eq. (4)] must be nearly three orders of magnitude lower than the presently accepted value in silicon to permit agreement with theory. Hence, it is questionable whether the Franz-Keldysh effect is the physical basis for the relatively large optical bandgap shift observed by Britsyn and Smirnov<sup>11</sup> and earlier by Hamakawa et al.<sup>12</sup> Accordingly, the field-enhanced recombination will no longer be referred to as the "Franz-Keldysh effect;" however, the Britsyn and Smirnov experimental results will still be used to determine values of  $\Delta E_g$  for Eq. (2) by using an effective mass in Eq. (3) of  $6.35 \times 10^{-4}$  kg.

#### $n^+$ Region Diffusion Current ( $J_{dN}$ )

The diffusion contribution to the dark current density in the  $n$ -region ( $J_{dN}$ ) was neglected in the higher resistivity cells of Ref. 4 because the dark current from the bulk ( $J_{dP}$ ) was so much higher than  $J_{dN}$ . However, Lindholm et al.<sup>6</sup> have experimentally found an anomalously large  $J_{dN}$  in solar cells with a highly doped substrate. Thus, an examination of the magnitude of  $J_{dN}$  for all base doping levels is required. Equation (5) is generally valid; however, it is necessary to define more closely  $W_n$ , the thickness of the  $n$ -region, and to emphasize the appropriate values of  $p_n$  and  $S_p$  to be used in this equation.

#### Field-Free Region ( $W_c$ )

In the usual theoretical treatment of the  $p$ - $n$  junction, the junction region is handled as though its thickness were in-

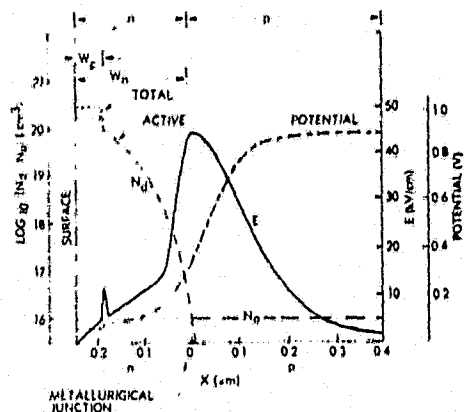


Fig. 1 Doping density, electric field, and potential in the vicinity of the metallurgical junction for a shallow junction solar cell.

finite, since the space charge extension into the respective neutral semiconductors is generally small compared to the thickness of the neutral regions. However, in shallow junction solar cells this is no longer true for the surface region. The work of Tsai<sup>13</sup> on the diffusion of phosphorous into silicon has shown that the phosphorous diffusion profile takes the form idealized in Fig. 1.

The depth of the constant portion of the profile  $W_c$  is directly proportional to the diffusion time, whereas the position of the junction with respect to  $W_c$  is proportional to the square root of time. Thus, beyond  $W_c$  the spatial variation of the doping concentration produces a space-varying potential which merges with the junction potential. This region, which in shallow junction cells may far exceed  $W_c$ , should be treated as part of the junction as in Ref. 4. Thus, the usual boundary condition

$$p = p_0 e^{qV/kT} \quad (6)$$

applies at the distance  $W_c$  from the surface<sup>8</sup> rather than at the edge of the normally calculated depletion region ( $W_n - W_{pn}$ ). Although the hole lifetime in the constant composition region may be very low (e.g.,  $10^{-10}$  s) because of Auger recombination, the condition  $W_c/L_p \ll 1$  is fulfilled, simplifying the first term on the right-hand side of Eq. (5) to

$$J_{dN} \approx q p_n D_p \left( S_p + \frac{D_p W_c / L_p^2}{D_p + W_c S_p} \right) \quad (7)$$

#### Minority Carrier Surface Recombination Velocity ( $S_p$ )

The necessity of contacting the front surface of the cell with a metallic grid establishes regions on the surface with extremely high surface recombination velocity. Such excellent sinks for minority carriers will produce a high diffusion gradient leading to a relatively high diffusion dark current. Therefore, Eq. (7) must be applied separately to the surface area contacted by metallization and to the semiconductor surface area covered with antireflection coating and the corresponding values of  $J_{dN}$  must be calculated with appropriate values of  $S_p$ .

The maximum possible surface recombination velocity of a perfect sink is kinetically limited to<sup>14</sup>

$$(S_p)_{\max} = (kT/2\pi m)^{1/2} \quad (8)$$

<sup>14</sup>See Appendix A for a more detailed discussion.



where  $m$  is the effective mass of the minority carrier. The value of  $S_p$  for metallic contacts to  $n$ -silicon can thus be as high as  $3.8 \times 10^6$  cm/s, which is about three orders of magnitude higher than the value<sup>15</sup> of  $S_p$  for silicon heavily doped with phosphorous and covered with thermally grown oxide. In practice, perfect ohmic contacts are not achieved, and the value of  $S_p$ , which may vary with different metals and processing, will be lower. Nevertheless, considering that a significant fraction (typically 5%) of the cell surface is covered with metallic contacts, inclusion of their effects in Eq. (7) could increase the value of  $J_{ph}$  by more than an order of magnitude for shallow junction solar cells.

#### Minority Carrier Density ( $p_0$ )

Determination of the value  $p_0$ , for use in Eq. (7), from the commonly employed equation for nondegenerate material of doping density  $N_d$ ,

$$p_0 = n_i^2 / n_0 \approx n_i^2 / N_d \quad (9)$$

may produce a large error for heavily doped silicon because of bandgap narrowing, Fermi degeneracy, and fractional ionization. If the high doping concentration in the region lowers the energy bandgap by  $\delta E_g$ , the value of the intrinsic carrier density is increased to  $n_i^{*2}$  where

$$n_i^{*2} = n_i^2 \exp(\delta E_g / kT) \quad (10)$$

Neither experimental nor theoretical determination of bandgap narrowing in heavily doped degenerate material is straightforward. The scanty experimental data available for heavily phosphorous-doped silicon ( $2 \times 10^{20}$  cm<sup>-3</sup>) range from  $\delta E_g = 90$  mV (Ref. 16) to  $\delta E_g = 170$  mV.<sup>6</sup> A theoretical prediction for uncompensated degenerate material with this doping density is  $\delta E_g = 182$  mV.<sup>17</sup> Compensated acceptors in the diffused region will also increase  $p_0$ .<sup>18</sup>

Fermi degeneracy and bandgap narrowing alter the form of Eq. (9), so that one must use Eq. (11), derived from Ref. 19 (notation changed slightly) and Eq. (10).

$$p_0^* = n_i^{*2} / P_0 e^{\eta} \quad (11)$$

where

$$\eta = (E_f - E_c) / kT = F_0^{-1} \{ (n_0 / 2P) \pi^{-1/2} \}$$

$$P_0 = 2(2\pi m_e kT / h^2)^{3/2}$$

$m_e$  is the effective mass of the electrons,  $F_0^{-1}$  is the Inverse Fermi function of order  $1/2$ ,  $P_0$  is the partition function for material of sufficiently low doping density so that  $m_n$  is invariant with  $N_d$ , and  $E_c$  is the conduction edge of the heavy doping narrowed bandgap.

In general the evaluation of Eq. (11) for a given value of  $N_d$  is ambiguous since, to determine  $n_0$ , several assumptions must be made: the position of the Fermi level  $E_f$  or of the donor level with respect to the conduction band edge, the shape of the band edge, the donor state degeneracy, and the effective mass of the electrons and holes. However, the problem is somewhat simplified, since Eq. (7) requires a value for  $P_0$  only in the constant composition region  $W_c$ , and there are experimental data for  $n_0$  and  $m_n$ .

An  $n^+$  layer diffused with phosphorous at 820°C should have a surface concentration near  $3 \times 10^{20}$  cm<sup>-3</sup>.<sup>11</sup> Fair and Tsai<sup>20</sup> report an "electrically active" doping density of  $1.8 \times 10^{20}$  cm<sup>-3</sup> for this surface concentration. If  $n_0$  is assumed to be this electrically active concentration, then only a reasonable value of  $m_n$  is needed to determine  $P_0$  and then  $\eta$ . The increase in the experimental values of  $m_n$  that occurs with donor density is assumed to incorporate any change in band edge shape. Extrapolation of accumulated data<sup>21</sup> to

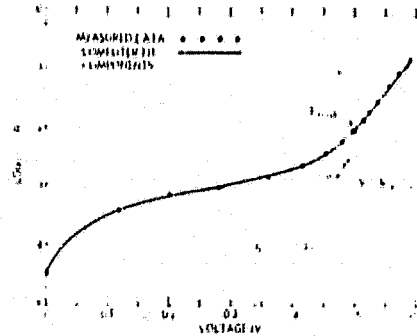


Fig. 2 Sample output of computer curve fitting program illustrating measured data, computer fit to this data, recombination and diffusion components of dark current, shunt leakage, and maximum power point.

$N_d = 3 \times 10^{20}$  cm<sup>-3</sup> gives a range for  $m_n$  of  $(1.8 \pm 0.2) m_0$ . Use of the experimental values for  $n_0$  and  $m_n$  gives a value for  $E_f$  of  $54 \pm 8$  mV above the conduction band edge. In Eq. (11), both  $n_i^{*2}$  and  $P_0$  are based on the low doping values for  $m_n$  of  $1.2 m_0$ . Validation of the assumptions is discussed in the results after  $\delta E_g$  is determined.

The denominator in Eq. (11) can be compared with  $N_d$ , which is generally used in place of  $n_0$  in Eq. (9). When evaluated for  $W_c$ ,

$$P_0 e^{\eta} \approx 2.7 \left( \begin{matrix} +1.3 \\ -0.7 \end{matrix} \right) \times 10^{20} \text{ cm}^{-3}$$

The close agreement with  $3 \times 10^{20}$  cm<sup>-3</sup> implies that, for this range of  $N_d$ , bandgap narrowing calculations, which unjustifiably use Eq. (11) with  $N_d$  instead of  $P_0 e^{\eta}$  are still likely to be within experimental error. Equation (11) is sometimes rearranged<sup>22</sup> to define an effective doping density  $[N_{eff} = P_0 \exp(\eta - \delta E_g / kT)]$  so that  $p_0 = n_i^{*2} / N_{eff}$ . The value of  $p_0^*$ , when corrected for Fermi degeneracy and bandgap narrowing from both acceptor and donor concentrations, is two to three orders of magnitude larger than the uncorrected minority carrier concentration in heavily doped silicon. The largest factor by far is from the bandgap narrowing due to donor concentration.

#### Experimental Method

The modified theory<sup>4</sup> exhibited good agreement with data obtained on solar cells with substrate resistivities of 10 and 2  $\Omega$ -cm, respectively. To test the theory critically at higher electric fields and to examine the diffusion dark current in the  $n$ -region, shallow junction solar cells with a wide range of substrate resistivities, varying grid contact areas, and differing diffused junction depths were fabricated.

The primary data consisted of the current vs voltage characteristic (I-V) under AM0 illumination from which the dark I-V characteristic was deduced by subtracting the photon generated current. A computer program provided a least-squares fit to a modification of Eq. (1) which includes the series and shunt resistances<sup>4</sup>:

$$I = I_m (e^{qV / (R_s + R_{sh})} - 1) + I_{ph} (e^{qV / (R_s + R_{sh})} - 1) \quad (12)$$

<sup>4</sup>The program utilized the full SNS formalism for the voltage dependent recombination current  $I_{rs}$ , but for most cases the results are indistinguishable from those using Eq. (12).

Table 1 Influence of substrate resistivity and contact area on the dark current and  $V_{oc}$  of shallow junction solar cells

Substrate resistivity ( $\Omega\text{-cm}$ )	Grid metal to silicon contact area (%)	Dark Diffusion Current		Open circuit voltage (mV)
		Total ( $J_{dt}$ ) experimental ( $\mu\text{A}/\text{cm}^2$ )	Bulk ( $J_{db}$ ) calculated ( $\mu\text{A}/\text{cm}^2$ )	
30	5	110	100 <sup>a</sup>	500
2	5	2.8	2 + 0.4 <sup>b</sup>	598
2	0.14	2.4	2 ± 0.4 <sup>b</sup>	601
0.12	5	1.8	0.1 <sup>c</sup>	606
0.12	0.14	0.8	0.1 <sup>c</sup>	616

<sup>a</sup> Ohmic back contact employed. <sup>b</sup> Error limits from uncertainty in effectiveness of  $n^+$  back contact. <sup>c</sup> Corrected to include heavy doping effects.

As a first approximation, a value of  $R_s$  was determined using the graphical method of Wolf and Rauschenbach,<sup>21</sup> and data points were taken from the I-V curve. A least-squares fit was made, varying the values for  $I_{ph}$ ,  $I_{01}$ , and  $R_{sh}$ . To determine a "best fit,"  $R_s$  was incremented to obtain a maximum correlation coefficient.

The set of values for  $I_{ph}$ ,  $I_{01}$ ,  $R_{sh}$ , and  $R_s$  that provided the highest correlation was then chosen for further analysis. Typical correlation coefficients were about 0.9999. The best fit value of  $R_s$  was usually within 0.02  $\Omega$  of the experimentally determined value. The "fitted"  $R_{sh}$  had little effect on determining the values of  $I_{ph}$  and  $I_{01}$ , and was typically within 20% of the value calculated from the slope of the reverse I-V characteristic. This method was judged superior to direct measurement of the unilluminated characteristic, for which the junction and base recombination rates may differ from those of the illuminated case. This method is also more rigorous than the previous experimental test,<sup>4</sup> since the dark current terms are determined from a fit over the entire I-V characteristic rather than just at the maximum power point and the open-circuit voltage. A sample output of this program is shown in Fig. 2.

The after-processing value of the bulk doping was verified to be identical with the starting material by four-point probe measurements on samples from which the junction and contacts had been removed.<sup>22</sup> The maximum electric field in the junction region (for use in determining the field-induced bandgap narrowing) was calculated by using the abrupt junction approximation and substituting for the depletion width in the  $n$ -region the junction depth minus the depth of the constant concentration portion of the profile  $W_c$ . The change in forbidden bandgap was taken from the data of Britsyn and Smirnov<sup>11</sup> for fields within their measured range and from an  $E^{1/2}$  extrapolation of these data for higher fields.<sup>11</sup> The value of  $W_c$  was determined from the data of Tsai<sup>13</sup> for the diffusion time and temperature employed in individual cell fabrication.

### Results and Discussion

Shallow junction cells were fabricated from  $p$ -type silicon with resistivities from 30 to 0.12  $\Omega\text{-cm}$  to examine solar cell

efficiency limitations. Higher substrate doping resulted in an increase in the  $J_{dt}$  term (from the higher junction field) and in a decrease in the  $J_{db}$  term (from the reduction in  $n_d$ ) as predicted by theory [Eqs. (2) and (5)]. Since the  $J_{dt}$  term in the lower resistivity range was much greater than  $J_{ph}$ ,  $J_{dt}$  [Eqs. (5) and (7)] dominated. However, it was possible to reduce  $J_{dt}$  and thus  $J_{dt}$  sufficiently, so that  $J_r$  became the dominant term in Eq. (1) at  $V_{oc}$ .

The process for lowering  $J_{dt}$  consisted of reducing the grid contact area from 5 to 0.14% of the total area. Table 1 lists the calculated values for  $J_{dt}$  (based on representative measured values of  $L_n$ ), and the experimental values of  $J_{dt}$  for various substrate resistivities and grid contact areas. In the 0.12- $\Omega\text{-cm}$ , 5% grid area case,  $J_{dt}$  is more than an order of magnitude higher than  $J_{ph}$ , which can therefore be ignored; hence,  $J_{dt} \approx J_{dt}$ . Reduction of the grid contact area by more than an order of magnitude lowers the  $J_{dt}$  value by more than a factor of 2 for the 0.12- $\Omega\text{-cm}$  cells. This is also reflected in a 10-mV gain in  $V_{oc}$ . Thus, the effect of the 5% metal contact area on  $J_{dt}$  is greater than that of the 95% oxide area. In the 2- $\Omega\text{-cm}$  case,  $J_{ph}$  dominates the  $J_{dt}$  term; however, lowering the contact area still reduces  $J_{dt}$ .

The following quantitative information can be extracted from the data of Table 1: bandgap narrowing from the heavy phosphorous doping; bandgap narrowing in the diffused region from compensating acceptors; surface recombination velocity of the metal-silicon interface  $S_m$ ; and surface recombination velocity of the oxide-silicon interface  $S_{ox}$ . These four terms can be obtained from the values of  $J_{dt}$  occurring in the 2- and 0.12- $\Omega\text{-cm}$  cells of differing contact areas. The contributions to  $J_{dt}$  from the separate surface area coverages (grid and oxide) and the  $n^+$  layer provide four independent equations (each derived from Eqs. (5), (7), (9), and (10)) but with five unknowns. The fifth unknown is  $J_{ph}$  for the 2- $\Omega\text{-cm}$  case. (In the 0.12- $\Omega\text{-cm}$  case,  $J_{ph}$  is sufficiently small so that the theoretical value may be used.) Since approximate values for two of the unknowns,  $S_m$  and  $S_{ox}$ , exist in the literature, a range of values can be established for the bandgap narrowing, from which a self-consistent range of values for  $S_m$  and  $S_{ox}$  can be deduced.

Constants used in the evaluation are  $W_c = 30 \text{ \AA}$ ;  $\tau_p \approx 10^{-10} \text{ s}$  (from Auger recombination for  $n \approx 1.8 \times 10^{20} \text{ cm}^{-3}$ );  $D_p \approx 1.3 \text{ cm}^2/\text{s}$ ; and  $n_i \approx 1.2 \times 10^{10} \text{ cm}^{-3}$ . The estimated value of  $S_{ox}$  was  $5 \times 10^3 \text{ cm/s}$  based on two properties observed for the  $\text{Ta}_2\text{O}_5$ -silicon interface<sup>24</sup>: The quantum yield of solar cells with  $\text{Ta}_2\text{O}_5$  antireflecting coatings can approach 0.9 at 300 nm, indicating a low surface recombination velocity. Also, the surface state density induced by thermally grown  $\text{Ta}_2\text{O}_5$  is higher than that in the best thermally grown silicon dioxides which have surface recombination velocities of the order of  $10^3 \text{ cm/s}$ . The literature values for an upper limit of surface recombination velocity for metal on heavily doped  $n$

<sup>22</sup> Capacitance methods of determining base doping are not as reliable for heavily doped material since the depletion width includes the diffusion profile.

<sup>24</sup> Britsyn and Smirnov determined the increase in the optical absorption coefficient as a function of wavelength and average electric field in the junction. Dependence of energy shift on average field (Fig. 2) was reported for a wavelength "in the vicinity" of 1  $\mu\text{m}$ . At the threshold wavelength of 1.12  $\mu\text{m}$ , the field induced energy shift is lower, fortuitously by an amount such that use of the maximum field at this wavelength produces the same energy shift as use of the average field at 1  $\mu\text{m}$ .

type silicon are about  $10^6$  cm/s.<sup>25</sup> In the present study, the value of the surface recombination velocity for a Cr-Si interface  $S_{Cr}$  exceeded that of  $S_{Ta}$  used on the 5% contact area cells of Table 1. With the assumption that  $S_{Cr}$  is close to the upper limit of  $10^6$  cm/s, a value of  $S_{Ta} = 5 \times 10^5$  cm/s was used for the initial value of the Si-Ta contact surface recombination velocity.

A unique feature of this analysis is the bandgap narrowing contribution to the  $J_{sc}$  term resulting from the compensating acceptors remaining in the  $n^+$  region after the diffusion of phosphorous into a substrate with a background doping of  $4 \times 10^{17}$ /cm<sup>3</sup> boron atoms. Comparison of the 2- $\Omega$ -cm with the 0.12- $\Omega$ -cm cells establishes this bandgap narrowing as  $18 \pm 5$  mV.<sup>11</sup> Correcting the data from the 0.12- $\Omega$ -cm cells for this effect establishes two equations with three unknowns. Independent, successive use of the surface recombination velocities of  $S_{Ta} = 5 \times 10^5$  cm/s and  $S_{Ta} = 5 \times 10^5$  cm/s provides upper and lower limits for heavy phosphorous concentration bandgap narrowing of  $\delta E_g = 160$  mV§§ and 143 mV, respectively. The average of the values, 152 mV, is significantly lower than the 170 mV provided by Lindholm et al.<sup>2</sup>; however, their results, on 0.1  $\Omega$ -cm material also unknowingly included the bandgap narrowing from the compensating acceptors. The two analyses coincide when an 18 mV correction for compensating acceptors is employed.

The values in this analysis for bandgap narrowing in the  $n^+$  region from donors and acceptors ( $\delta E_g = 152 \pm 9$  mV and  $\delta E_g = 18 \pm 5$  mV) yield self-consistent solutions for  $J_{sc}$  of  $1.9 \pm 0.2 \times 10^{-12}$  A/cm<sup>2</sup> (Table 1) and for Ta<sub>2</sub>O<sub>5</sub>-Si, Ta-Si, and Cr-Si interface surface recombination velocities of  $S_{Ta} = 7 \pm 2 \times 10^5$ ,  $S_{Ta} = 4 \pm 1 \times 10^5$ , and  $S_{Cr} = 7 \pm 2 \times 10^5$  cm/s, respectively. These values are not too different from the initial assumptions and depend upon a comparison of theoretical and experimental values of  $p_0^*$ . A check for self-consistency in the basic premises consists of examining the determined bandgap narrowing, the relative position of  $E_f$  and donor levels, and fractional ionization.

Bandgap narrowing of  $\approx 152$  mV from a donor concentration of  $3 \times 10^{20}$ /cm<sup>3</sup> will lower the conduction band edge by at least 76 mV, but by less than 152 mV. The Fermi level has been theoretically determined to be  $\approx 54$  mV above the band edge, and the donor level is 44 mV (Ref. 28) below the intrinsic band edge. Therefore, the donor level is between 27 and 108 mV above the lowered band edge, and  $E_f$  is from 22 mV above the donor level to 54 mV below the donor level. If all  $3 \times 10^{20}$ /cm<sup>3</sup> phosphorous atoms are electrically active and only 60% are ionized, the Fermi level would be  $\approx 8$  or  $\approx 25$  mV above the donor level depending on the donor degeneracy (2 or 4, respectively). For internal consistency of the model, 60% fractional ionization implies nearly even division of the bandgap narrowing. If this is the case, then the hole effective mass  $m_h$  and corresponding partition function may be increased, thereby reducing the value for  $\delta E_g$  by up to 5 mV.

If the lower value for  $E_f$  is used, 95% of the electrically active phosphorous in the  $W^+$  region must be ionized, and  $10^{20}$ /cm<sup>3</sup> phosphorous atoms must be nonactive (perhaps precipitated). Precipitation or other means of inactivating  $\approx 30\%$  of the phosphorous implies that bandgap narrowing must affect only the conduction band edge. The bandgap narrowing used in this analysis produced fractional ionization and  $p_0^*$  values which are consistent with the experimental results for both active and total phosphorous concentration. Better knowledge of the split in bandgap narrowing between conduction and valence band edges will provide more specific information as to the fractional ionization and concentration of the electrically active phosphorous.

§§Additional data sets were used to establish this range, which is the same as reported in Ref. 26 for heavier acceptor compensation.

§§This value agrees with the upper limit indicated by experimental work in Ref. 27.

Table 2 Dependence of junction recombination current on electric field in the junction

Diffusion time, $t$ (min)	Average electric field at $P_{max}$ $E$ (MV/m)	$E^{-1}$ (m/MV)	Recombination current at $P_{max}$ $J_r$ (mA/cm <sup>2</sup> )	Field-dependent terms of Eq. (2) exp ( $\delta E_g/2kT$ ) / $E$ (m/MV)
8	3.5	0.29	$3.4 \pm 0.2$	2.5
10	3.2	0.31	$2.9 \pm 0.7$	2.4
15	2.4	0.42	$2.0 \pm 0.5$	2.2

The value of  $p_0$  depends on data for  $n_0$  from diffusion into less heavily doped  $p$ -type silicon. If the bandgap narrowing from the acceptors were divided evenly between the bands (the worst case), the donor level would increase by  $\approx 9$  mV relative to the conduction band edge. This would lower  $p_0$  by  $\approx 10\%$  and increase  $\delta E_g = 3$  mV.

It is interesting to note that the experimental expression of Slotboom and deGraaf<sup>29</sup> for nondegenerate,  $p$ -type silicon, when extrapolated to  $3 \times 10^{20}$ /cm<sup>3</sup>, yields  $\delta E_g = 144$  mV compared to the 152 mV predicted here for degenerate  $n$ -type material. Their prediction for an acceptor concentration of  $4 \times 10^{17}$ /cm<sup>3</sup> is  $\delta E_g = 25$  mV, which is not far from our results for the contribution to band gap narrowing from compensating acceptors. Also, in comparison to the above mentioned results, surface recombination values for SiO<sub>2</sub>-Si and Al-Si interfaces of  $5 \times 10^5$  cm/s and  $5 \times 10^5$  cm/s, respectively, have been deduced from experimental results.<sup>30</sup>

Another group of cells was fabricated in 0.12- $\Omega$ -cm  $p$ -type material which was diffused for three different times to vary the junction depth and therefore the junction field. Low resistivity, 0.14% contact area cells were chosen to increase the junction field and to minimize  $J_d$  so that reasonable accuracy could be obtained for  $J_r$ . Table 2 shows the diffusion time, the average electric field in the junction at  $P_{max}$ , and its reciprocal, the experimentally determined field-enhanced junction-recombination current at  $P_{max}$ , and the combined field dependent terms in Eq. (2).

The experimentally determined values for  $J_r$  increase with increasing electric field. This trend is opposite to the  $1/E$  dependence predicted by SNS theory alone [Eq. (2) with the bandgap narrowing term removed]. The combined field-dependent term (last column of Table 2) increases with increasing field, in qualitative agreement with the behavior of  $J_r$ .

Quantitative agreement requires a value of  $\tau_p$  of several nanoseconds and a small decrease of  $\tau_p$  with junction depth. If field-induced bandgap lowering were not to occur, the range of  $\tau_p$  required to fit the data would exceed an order of magnitude and absolute values would be much too low to be consistent with Shockley-Read recombination used in the SNS theory.

Reduction of the electric field and consequently  $J_r$  improves both the open-circuit voltage and especially the fill factor in low-resistivity solar cells where  $J_d$  is no longer the limiting factor. The field-enhanced junction recombination is the thermal counterpart of the observed field-induced optical bandgap narrowing<sup>11,12</sup> and provides a logical and experimentally consistent model of the solar cell junction.

### Conclusions

A sound experimental foundation has been established for the proposed field-enhanced junction recombination.<sup>4</sup> The high surface recombination of the metallic contacts on the front surface has been identified as a major source of the diffusion dark current in the highly doped surface region. This current becomes important for shallow junction cells at substrate resistivities below about 2- $\Omega$ -cm. Bandgap lowering in the field-free  $n$ -type surface caused by high doping is an

important ingredient of this diffusion current and is necessary for self-consistent results. Heavy doping in the substrate influences  $J_{pn}$  (as well as  $J_{pp}$ ) by bandgap narrowing and  $J_p$  by increased electric fields. Incomplete ionization of donors in the highly doped  $n$ -region and a field-free region which is much thinner than the junction depth are also important in determining the diffusion dark current. Finally, methods have been developed and experimentally verified for the reduction of both the diffusion and the junction recombination dark currents in low-resistivity silicon solar cells in order to enhance the efficiency.

#### Appendix A

For shallow junction cells, the field associated with the rapid fall-off in doping concentration just beyond  $W_c$  can be large and can penetrate the  $W_c$  region as shown in Fig. 1. It must then be determined whether  $W_c$  is the appropriate choice of distance from the surface for the application of Eq. (6). The boundary condition is highly insensitive to this choice of distance, since the potential varies relatively little over  $W_c$  (see Fig. 1) despite the possible presence of a strong electric field. Although volume recombination in the high field region of  $W_c$  should formally contribute to the  $J_p$  term, recombining carriers will have surmounted the full barrier height. Thus, the dependence of the contribution to the dark current upon voltage varies as  $e^{qV/kT}$  and is indistinguishable experimentally from the  $J_{pn}$  term.

Just beyond  $W_c$ , the situation is similar except that the hole lifetime increases rapidly with distance as Auger recombination becomes less significant; the hole concentration is only slightly greater than that in the heavy-doping bandgap narrowed surface region. These facts indicate that recombination is significantly reduced in this region, and its estimated contribution to the dark current is typically only 10-20% of that from the  $W_c$  region. Thus, the distance  $W_c$  appears reasonable for the extent of the  $n^+$  region for use in Eqs. (5) and (7), at least until measurement precision and the determination of other parameters are greatly improved. If this constant composition layer were removed ( $W_c = 0$ ),  $J_{pn}$  would not be reduced because  $p_0$  [in Eq. (7)] would be higher and the resulting  $S_p$  contribution would therefore be larger than the total  $J_{pn}$  term prior to removal of  $W_c$ .

#### Acknowledgment

This paper is based upon work performed at COMSAT Laboratories under the sponsorship of the Communications Satellite Corporation.

#### References

- <sup>1</sup>Rittner, E.S., "Electron Processes in Photoconductors," *Proceedings of the Photoconductivity Conference*, edited by R.G. Breckenridge, B.R. Russel, and E.E. Hahn. John Wiley & Sons, N.Y., New York: 1956, pp. 215-268.
- <sup>2</sup>Iles, P.A. and Soclof, S.L., "Effect of Impurity Doping on Solar Cell Output," *Proceedings of the 11th IEEE Photovoltaic Specialists Conference*, May 1975, pp. 19-24.
- <sup>3</sup>Rittner, E.S., "An Improved Theory of the Silicon  $p-n$  Junction Solar Cell," International Electron Devices Meeting, Dec. 6-8, 1976.
- <sup>4</sup>Rittner, E.S., "An Improved Theory of the Silicon  $p-n$  Junction Solar Cell," *Journal of Energy*, Jan.-Feb. 1977, Vol. 1, pp. 9-17.
- <sup>5</sup>Lauwers, P., Van Meerbergen, J., Buttel, P., Merrens, R., and Van Overstraeten, R., "Influence of Band Gap Narrowing on the Performance of Silicon  $n-p$  Solar Cells," *Solid-State Electronics*, Vol. 21, 1978, pp. 747-752.
- <sup>6</sup>Linholm, F.A., Neugroschel, A., C.T., Godlewski, M.P. and Brandhorst, H.W., "A Methodology for Experimentally-Based

Determination of Gap Shrinkage and Effective Lifetimes in the Emitter and Base of  $p-n$  Junction Solar Cells," *Proceedings of the Twelfth IEEE Photovoltaic Specialists Conference*, 1976, Baton Rouge, La., pp. 1-7.

<sup>7</sup>Redfield, D., "Mechanism of Performance Limitations in Heavily Doped Silicon Devices," *Applied Physics Letters*, Vol. 33, No. 6, Sept. 1978, pp. 531-533.

<sup>8</sup>Sah, C.T., Noyce, R.N., and Shockley, W., "Carrier Generation and Recombination in  $p-n$  Junctions and  $p-n$  Junction Characteristics," *Proceedings of the Institute of Radio Engineers*, Vol. 45, Sept. 1957, pp. 1228-1243.

<sup>9</sup>Dziewior, J. and Schmid, W., "Auger Coefficients for Highly Doped and Highly Excited Silicon," *Applied Physics Letters*, Vol. 31, No. 5, Sept. 1, 1977, pp. 346-348.

<sup>10</sup>Lindmayer, J. and Allison, J.F., "The Violet Cell: An Improved Silicon Solar Cell," *COMSAT Technical Review*, Vol. 3, No. 1, Spring 1973, pp. 1-22.

<sup>11</sup>Britsyn, K.I. and Smirnov, A.A., "Change in the Width of the Forbidden Band of Silicon in the Electric Field of a  $p-n$  Junction," *Fizika Tverdogo Tela*, Vol. 8, Jan. 1966, pp. 163-165 (for translation see *Soviet Physics Solid State*, Vol. 8, July 1966, pp. 126-128).

<sup>12</sup>Hamakawa, Y., Nishino, T., and Yamaguchi, J., "Franz-Keldysh Effect in Silicon  $p-n$  Junction," *Journal of the Physical Society of Japan* (1965), Short Notes, Vol. 20, p. 1978.

<sup>13</sup>Tsai, J.C.C., "Shallow Phosphorous Diffusion Profiles in Silicon," *Proceedings of IEEE*, Vol. 57, Sept. 1969, pp. 1499-1506.

<sup>14</sup>Ghandhi, S.K., *The Theory and Practice of Microelectronics*, John Wiley & Sons Inc., New York, 1968, p. 430ff.

<sup>15</sup>Gatos, H.C., Watanabe, M., and Actor, G., "Surface Recombination Velocity and Diffusion Length of Minority Carriers in Heavily Doped Silicon Layers," NASA Conference Publication 2020, April 28-29, 1977, Cleveland, Ohio, pp. 59-68.

<sup>16</sup>Buhaman, D., "Investigation of Current-Gain Temperature Dependence in Silicon Transistors," *IEEE Transactions on Electron Devices*, Vol. ED-16, No. 1, Jan. 1969, pp. 117-124.

<sup>17</sup>Lanyon, H.P.D., and Tuft, R.A., "Band Gap Narrowing in Moderately to Heavily Doped Silicon," *IEEE Transactions on Electron Devices*, Vol. ED-26, No. 7, July 1979, pp. 1014-1018.

<sup>18</sup>Van Overstraeten, R.J., De Man H.J., and Mertens, R.P., "Transport Equations in Heavily Doped Silicon," *IEEE Transactions on Electron Devices*, Vol. ED-20, No. 3, 290-298, 1973.

<sup>19</sup>Hutner, R.A., Rittner, E.S., and DuPre, F.K., "Fermi Levels in Semiconductors," *Phillips Research Reports*, Vol. 5, June 1950, pp. 188-204.

<sup>20</sup>Fair, R.B., and Tsai, J.C.C., "A Quantitative Model for the Diffusion of Phosphorous in Silicon and the Emitter Dip Effect," *Journal of the Electrochemical Society (Solid-State Science and Technology)*, July 1977, pp. 1107-1118.

<sup>21</sup>Barber, H.D., "Effective Mass and Intrinsic Concentration in Silicon," *Solid State Electronics*, Vol. 10, No. 11, Nov. 1967, pp. 1039-1051.

<sup>22</sup>Dunbar, P.M. and Hauser, J.R., "A Theoretical Analysis of the Current-Voltage Characteristics of Solar Cells," Annual Report on NASA Grant NGR 34-002-195, NASA Lewis Research Center, Aug. 1976, Chap. 5.

<sup>23</sup>Wolf, M. and Rauschenback, H., "Series Resistance Effects on Solar Cell Measurements," *Advances in Energy Conversion*, Vol. 3, April-June 1963, pp. 455-479.

<sup>24</sup>Revesz, A.G. and Allison, J.F., "Electronic Properties of the Silicon Thermally Grown Tantalum Oxide Interface," *IEEE Transactions on Electron Devices*, ED-23, No. 5, May 1976, pp. 527-529.

<sup>25</sup>Huassell, E.L., "Recombination Beneath Ohmic Contacts and Oxide Covered Regions," *Solid-State Electronics*, Vol. 22, No. 1, Jan. 1979, pp. 89-93.

<sup>26</sup>Das, G., Phillips, A., and Dunke, W.P., "Emitter Compensation Effect," *Technical Digest IEDM*, Dec. 3-5, 1979, pp. 514-517.

<sup>27</sup>Possin, G.E., Adler, M.S., and Baliga, B.J., "Measurements of Heavy Doping in Processed Silicon Devices," *Technical Digest IEDM*, Dec. 3-5, 1979, pp. 518-521.

<sup>28</sup>See for example Neuberger, M., and Welles, S.J., "Silicon," October 1969, DDC Number AD 698342 prepared by Hughes Aircraft I.P.C.

<sup>29</sup>Slotboom, J.W. and DeGraaff, H.C., "Measurements of Bandgap Narrowing in Si Bipolar Transistors," *Solid State Electronics*, Vol. 19, No. 10, 1976, pp. 857-862.

<sup>30</sup>DeGraaff, H.C., Slotboom, J.W., and Schmitz, A., "The Emitter Efficiency of Bipolar Transistors, Theory and Experiments," *Solid State Electronics*, Vol. 20, No. 6, 1977, pp. 515-521.

<sup>31</sup>This fact alone is adequate for Dunbar and Hauser<sup>22</sup> to conclude that with heavy doping most of the dark current from the diffused region originates near the surface.

ORIGINAL PAGE IS  
OF POOR QUALITY

820034/P23

APPENDIX B. BACKGROUND TO THE CONTRACT

The following sections are from the contract proposal and provide the framework of the problem as viewed at that time (5/79). In retrospect, the framework is intact but it appears that special structures are necessary to overcome the limitations found in the surface recombination velocities of the oxide-silicon interfaces  $S_{OX}$  and the  $pp^+$  layer  $S_{pp^+}$ .

The equation, page, and figure numbers refer to the appendix only, not the major portion of the report. The reference numbers have been modified to fit those of the report.



2. THEORETICAL MODEL

Figure 2-1 gives the solar cell structure used in the following analysis and proposed work. The basic cell should have a shallow junction ( $W_N < 0.2 \mu\text{m}$ , or at least  $W_N \ll L_p/D_p$ ) to assure the high blue response necessary to produce the  $I_{sc} = 45 \text{ mA/cm}^2$  goal set forth in the RFP. The separate influences of the metallic grid contacts and the oxide AR coating are indicated by the surface recombination velocities  $S_a$  and  $S_{ox}$ . The contributions of the back contact and  $P^+$  layers are lumped together and represented by an effective surface recombination velocity  $S_{pp^+}$ .

The equations following Figure 2-1 are expressions for the current balance in an illuminated solar cell. The  $J_r$  term represents the current contribution from generation or recombination in the junction region;  $J_\ell$  is the contribution from photon generated minority carriers; and  $J_d$  is the current from the  $N^+$  and  $P$  bulk regions, from the oxide and contacts on the  $N^+$  layer, and from the  $P^+$  layer and contacts. The individual contributions to  $J_d$  from the  $N$  and  $P$  regions are expressed in the approximate forms pertinent to the conditions necessary to fulfill the contract, for example, long diffusion length, thin  $N$  region, perfect  $P^+$  back contact, and low oxide surface recombination velocity. The stated assumptions reflect these conditions plus one limitation, the high value for  $S_m$ .

Figure 2-2a indicates the doping profiles of a typical 1.0- $\Omega$ -cm  $N^+ - P - P^+$  solar cell. The dashed line indicates the effective doping level  $N_D^*$  that results from band gap narrowing  $\delta E_g$  [1], [6], [8] represented by equations (2-10)-(2-15). The effective values  $n_1^*$ ,  $n_0^*$ , and  $p_0^*$  must be used in equations (2-3), (2-5), (2-7), and (2-8) to obtain realistic values of  $J_d$  and  $J_r$ .

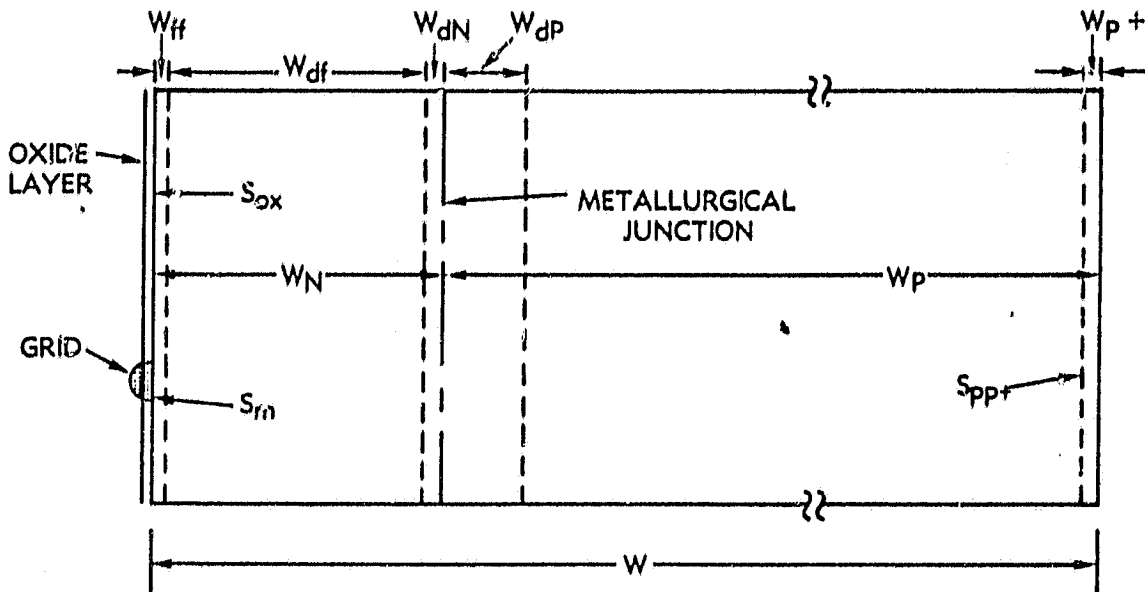


Figure 2-1. Solar Cell Structure and Terms

$$J = J_r + J_d - J_\ell \quad (2-1)$$

$$J_r = J_{ro} (e^{qV/2kT} - 1) \quad (2-2)$$

$$J_{ro} \approx qn_i (kT/q) (\pi/2) \sqrt{\tau_p \tau_n E} \quad (2-3)$$

$$J_d = (J_{dp} + J_{dN}) (e^{qV/kT} - 1) \quad (2-4)$$

$$J_{dp} \approx q(n_o D_n) (W_p) / (L_n)^2 \quad (2-5)$$

(assumes low  $S_{pp+}$ ,  $W_p \approx W_p - W_{dp}$ , and  $L_n \gg W_p$ ).

$$J_{dN} = J_{dNox} + \left[ 1 - (A_{grid}) / (A_{total}) \right] J_{dNm} \quad (2-6)$$

$$J_{dNox} \approx qP_o (S_{ox} + W_N / \tau_p) \quad (2-7)$$

(assumes that  $W_N \ll L_p$ ,  $W_N \approx W_N - W_{dN}$ , and  $S_{ox} \ll W_N / \tau_p$ ).

$$J_{dNm} \approx qD_p P_o S_m (D_p + W_N S_m) \quad (2-8)$$

(assumes that  $S_m \gg W_N / \tau_p$ ).

$$n_o P_o = n_i^2 \quad (2-9)$$

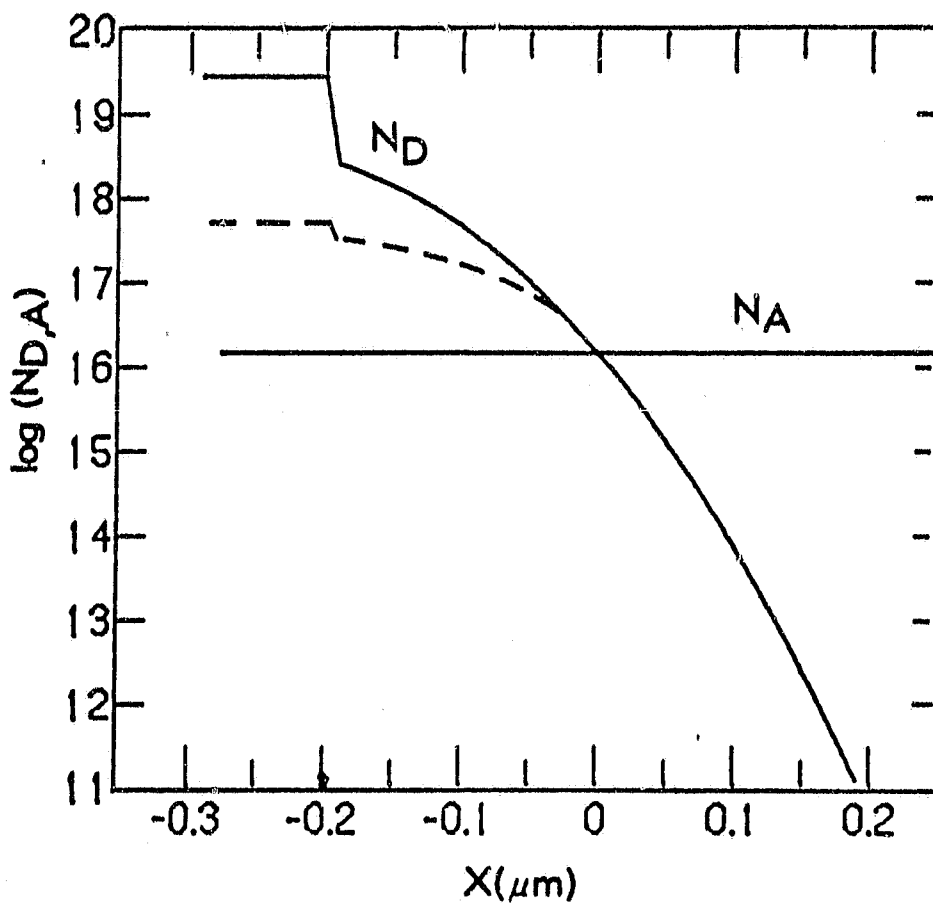
ORIGINAL PAGE IS  
OF POOR QUALITY

Figure 2-2a. Donor and Acceptor Doping Profiles in 1.0- $\Omega$ -cm Silicon Showing the Effects of Band Gap Narrowing



$$E_g(\text{mV}) = 9[\ln(N/N_0) + \sqrt{|\ln(N/N_0)|^2 + 0.5}] \quad (2-10)$$

$$\delta E_g(\text{mV}) = 22.5 (N^-/10^{18})^{1/2} \quad (2-11)$$

$$\Delta E_g(\text{mV}) = [hqE/2\pi\sqrt{m^*}] \quad (2-12)$$

where

$N$  = impurity concentration

$N_0 = 10^{17}/\text{cm}^3$

$N^-$  = ionized impurity concentration

$m^*$  = effective mass necessary to fit the data of Britsyn and Smirnov.

$$n_i^* = n_i (e^{\delta E_g q/kT}) \quad (2-13)$$

$$p_o^* = n_i^{*2}/N_A = n_i^2/N_A^* \quad (2-14)$$

$$n_o^* = n_i^{*2}/N_D = n_i^2/N_D^* \quad (2-15)$$

Figure 2-2b gives the electric field strength ( $E$ ) throughout the  $N^+$  and depletion region. Curves showing the influence of heavy doping (HD) only as well as that of electric field induced band narrowing (FI) only are overlaid to indicate the changes in electric field in the flat  $N^+$  region in Figure 2-2a.

Based on the extreme gradient in donor doping concentration  $N_D$  Figure 2-2a and the intense fields in Figure 2-2b, equations (2-7) and (2-8) must be modified. A simple but effective model [1] has been proposed in which a field-free region ( $W_{ff}$ ), where  $E < 2 \text{ kV/cm}$  and a drift-field region ( $W_{df}$ ), where  $E > 2 \text{ kV/cm}$ , are defined. All photogenerated carriers in  $W_{df}$  are collected and this region is considered to have a

negligible contribution to  $J_d$ , since the minority carrier lifetime in  $W_{df}$  is much greater than that in  $W_{ff}$ . Therefore,  $W_{ff}$  is substituted for  $W_N$  in the above equations, yielding:

$$J'_{dNox} \approx q p_O^* (S_{ox} + W_{ff}/\tau_p) \quad (2-16)$$

$$J'_{dNm} \approx q D_p p_O^* s_m / (D_p + W_{ff} S_m) \quad (2-17)$$

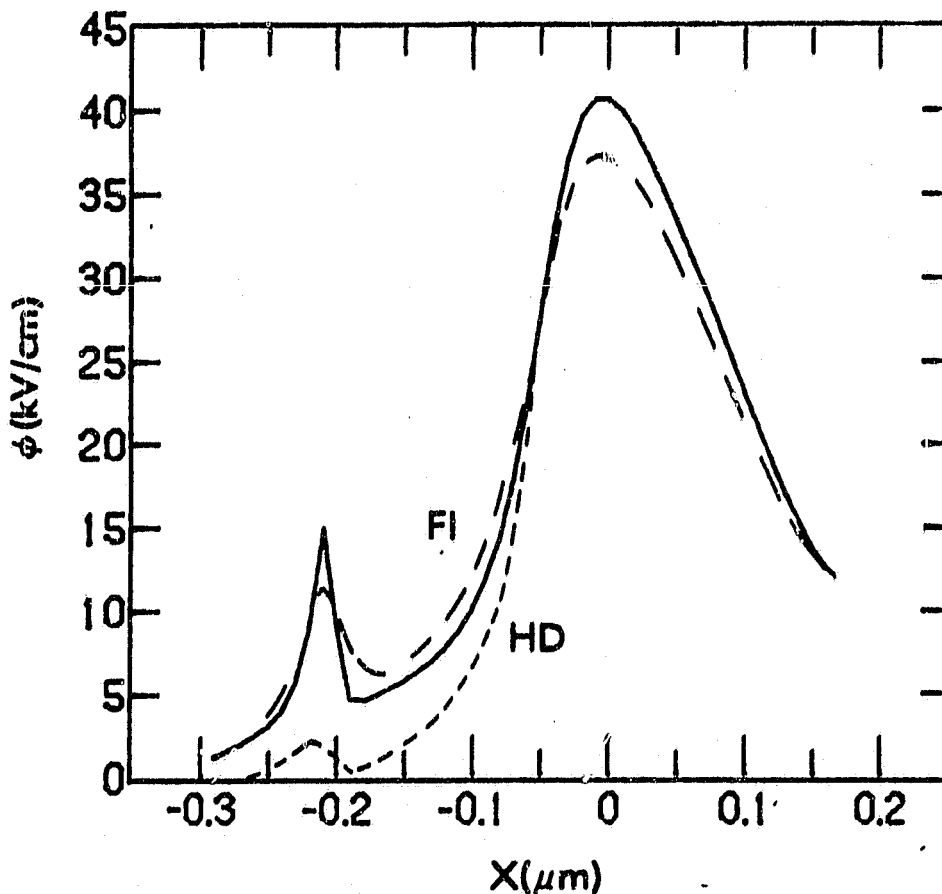


Figure 2-2b. Electric Field in Junction and  $N^+$  Regions  
Produced by Doping Profiles of Figure 2-2a

## 5. SOLAR CELL OUTPUT LIMITATIONS

Three cases are examined to indicate present experimental dark current values and those required to achieve a 700-mV cell. Table 5-1 contains these calculations and the inherent assumptions. The first case assumes that  $J_{ro} = 0$  and that the best experimental value measured for  $J_{do}$  of  $8 \times 10^{-13}$  A/cm<sup>2</sup> is obtained. These values permit a maximum  $V_{oc}$  of 636 mV. The second case assumes that  $J_{do} = 0$  and that the best experimental value for  $J_{ro}$  of  $3 \times 10^{-8}$  A/cm<sup>2</sup> is obtained. These values allow a maximum  $V_{oc}$  of 731 mV and indicate that  $J_{ro}$  is not the voltage limiting factor.

The third case is used to compute the necessary values of  $J_{do}$  and  $J_{ro}$  to obtain 700 mV if  $J_r$  and  $J_d$  are equal at this voltage. The required value of  $J_{do} = 3.3 \times 10^{-14}$  A/cm<sup>2</sup> is significantly lower than the value of  $J_{dp} = 8 \times 10^{-14}$  A/cm<sup>2</sup> expected from a 0.025-cm thick 0.1- $\Omega$ -cm cell with a perfect  $p^+$  back contact. This value of  $J_{dp}$  includes the band narrowing provided by equations (2-12) and (2-13). Equation (2-5) shows that reduction of the cell thickness will allow  $J_{dp}$  to be reduced to the necessary value, assuming that  $J_{dn}$  is negligible. It will be difficult to obtain  $J_{dn} \ll J_{dp}$ . However, if  $J_{dp}$  can be reduced by one-half by increasing  $L_n$  and/or by decreasing  $W_p$ , then the condition  $J_{dn} \approx J_{dp}$  might be easier to achieve and would also yield  $V_{oc} = 700$  mV.

Table 5-2 gives the values of  $J_r$  and  $J_d$  at several voltages based on the values of  $J_{do}$  and  $J_{ro}$  from case 3. At  $P_{max}$  (~600 mV),  $J_r$  dominates; therefore, the diode quality factor will be ~2 and the fill factor will only be ~0.76. It is necessary to reduce  $J_r$  by an order of magnitude to provide a fill factor above 0.8. Reduction of  $J_r$  by simply increasing the junction depth, as in Figure 3-4, will increase  $J_{dn}$  and lower  $J_d$ . Therefore, less straightforward methods must be used.

Table 5-1. Limiting Cases for Shallow Junction  
Solar Cells

Case 1
<p>Assume that <math>J_r = 0</math>, <math>J_l = 45 \text{ mA/cm}^2</math>  Use the best experimental value for <math>J_{do}</math>  (<math>8 \times 10^{-13} \text{ mA/cm}^2</math>)  Equation (2-4) gives <math>V_{oc} = 25.7 \text{ mV } \ln(0.045/8 \times 10^{-13})</math>  <math>V_{oc} = 636 \text{ mV}</math></p>
Case 2
<p>Assume that <math>J_d = 0</math>, <math>J_l = 45 \text{ mA/cm}^2</math>  Use the good experimental value for <math>J_{ro}</math>  (<math>3 \times 10^{-8} \text{ A/cm}^2</math>)  Equation (2-2) gives <math>V_{oc} = 5.14 \text{ mV } \ln(0.045/3 \times 10^{-8})</math>  <math>V_{oc} = 731 \text{ mV}</math></p>
Case 3
<p>Assume that <math>J_r = J_d</math> at 700 mV, <math>J_l = 45 \text{ mA/cm}^2</math>  What values of <math>J_{do}</math> and <math>J_{ro}</math> will give <math>V_{oc} = 700 \text{ mV}</math>?  <math>700 \text{ mV} = 25.7 \ln(0.045/2J_{do}) = 51.4 \ln(0.045/2J_{ro})</math>  <math>J_{do} = 3.3 \times 10^{-14} \text{ A/cm}^2</math>  <math>J_{ro} = 2.7 \times 10^{-8} \text{ A/cm}^2</math></p>

Table 5-2. Relative Values of  $J_r$  and  $J_d$   
as a Function of Voltage

V (mV)	$J_d$ (mA)	$J_r$ (mA)	$J_r/J_d$
700	22	22	1
600	0.46	3.2	6.9
500	0.009	0.45	20

Another goal of the contract is to obtain  $J_{sc} = 45 \text{ mA/cm}^2$  at AM0. This current density can be collected only if NR cell surfaces and/or sawtooth cover-slides are employed. The use of an etched surface would not only increase  $J_l = J_{sc}$ , but also  $J_{dn}$  and  $J_r$ . The consequent reduction of  $V_{oc}$  and FF could only be overcome with a major effort. Multilayer AR coatings and sawtooth cover-slides may be used to increase  $J_l$  without altering  $J_{dn}$  and  $J_r$ . This latter approach is simpler but does not offer as great a potential (see Figure 1-1) as the etched surface combined with the sawtooth cover-slide.

6. TECHNICAL APPROACHES

This section discusses organized approaches to the problem of increased  $V_{oc}$ . The  $J_d$  term will be examined first since  $J_d$  must be lowered by more than an order of magnitude to attain a  $V_{oc}$  of 700 mV. Figure 6-1 indicates the three major contributions to  $J_d$  that must be reduced and the various means for achieving this goal. Means for reducing  $J_{dp}$  are indicated in equation (2-5). Success of the program depends on achieving a low value of  $S_{pp+}$  relative to  $D_n/L_n$  as assumed in this equation. COMSAT is presently working on a contract to provide a perfect  $P^+$  back contact to a range of base resistivities from 1-1000  $\Omega$ -cm. The extension to lower resistivities should be reasonable since  $D_n/L_n$  is larger for more heavily doped material. A recent process of inducing an accumulation or depletion layer by use of charged oxides [11] is quite promising; however, the behavior in a radiation environment must be closely examined.

Reduction of the  $J_{dn}$  bulk term [equations (2-6), (2-16)], and (2-17)] is parallel to that of the  $J_{dp}$  term. However, it is more important that  $W_{ff}$  be reduced than  $W_N$  for shallow junction cells. One major difference between  $J_{dp}$  and  $J_{dn}$  is that the  $N^+$  region is generally introduced into a P-type substrate. Therefore, band narrowing from heavy substrate doping will add to the band narrowing introduced by the heavy doping necessary to form the  $N^+$  layer [1], [7]. Use of epitaxial or out-diffusion techniques are means of avoiding or decreasing the compensating acceptor concentration, thereby reducing the band narrowing by 15-25 mV for 0.1  $\Omega$ -cm base material.

Reduction of  $S_p$  has been standard practice at COMSAT since the Violet cell was introduced with its oxidized  $Ta_2O_5$  AR coating. The resulting low value of  $S_{ox}$  and relatively low value of  $S_m$  (Cr-Ta-Si) permit the shallow junction structure necessary

ORIGINAL PAGE IS  
OF POOR QUALITY

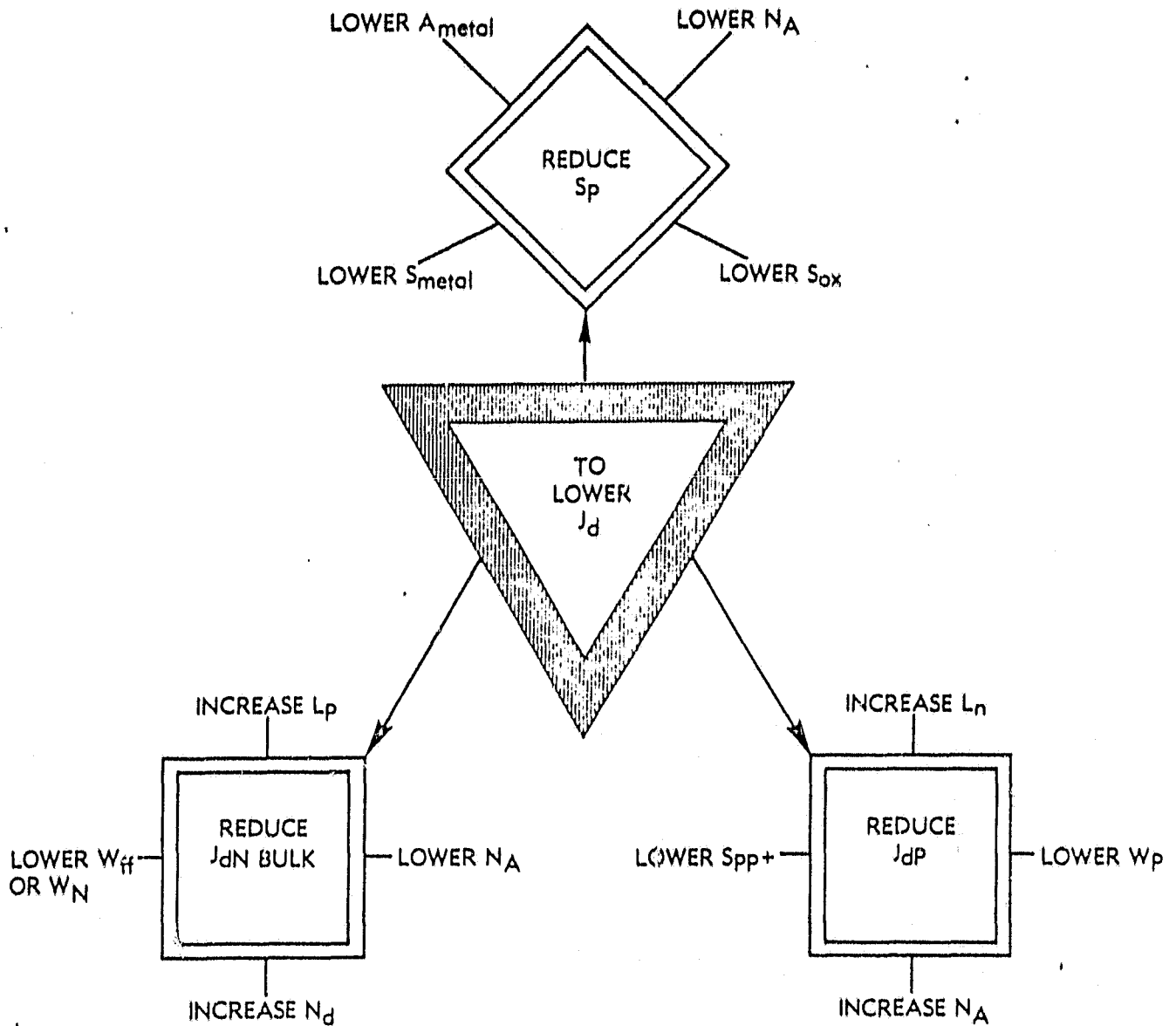


Figure 6-1. Methods for Lowering  $J_r$

ORIGINAL PAGE IS  
OF POOR QUALITY

for good blue response. A patent issued to COMSAT in 1976 [12] provided a practical means of reducing metal contact area for low-resistivity solar cells.

Methods of lowering  $J_r$ , displayed in Figure 6-2, are based on equations (2-3), (2-12), and (2-13). The most important item in each case is the reduction of the electric field in the junction region. Epitaxial growth techniques can be used in all three methods. Ion implantation may be useful for tailoring doping profiles in the junction and surface regions.

The use of less heavily doped material in the junction region has two benefits. The electric field is lowered (by increasing the depletion layer thickness), and the band narrowing from heavy doping is also reduced. This latter effect, for  $J_r$ , has not yet been proven and may not be as important as it would be for  $J_d$ . The reduced importance could result from the dependence of  $J_r$  on  $n_i^*$  rather than  $n_i^{*2}$ ; but for a diffused junction heavy doping exists from both  $N^+$  and P layers increasing  $J_r$  two to three times more than an undoped region.

Junction profiles must be established which reduce the maximum electric field in the junction and yet guarantee collection of carriers from the cell surface, even after irradiation. Deep  $N^+$  layers are particularly susceptible to this problem because of the high radiation damage coefficient. Junction depths in excess of 2  $\mu\text{m}$  may reduce  $J_r$  but would increase the radiation sensitivity. Some of these approaches have already been exploited; variations and combinations are proposed for this contract.



ORIGINAL PAGE IS  
OF POOR QUALITY

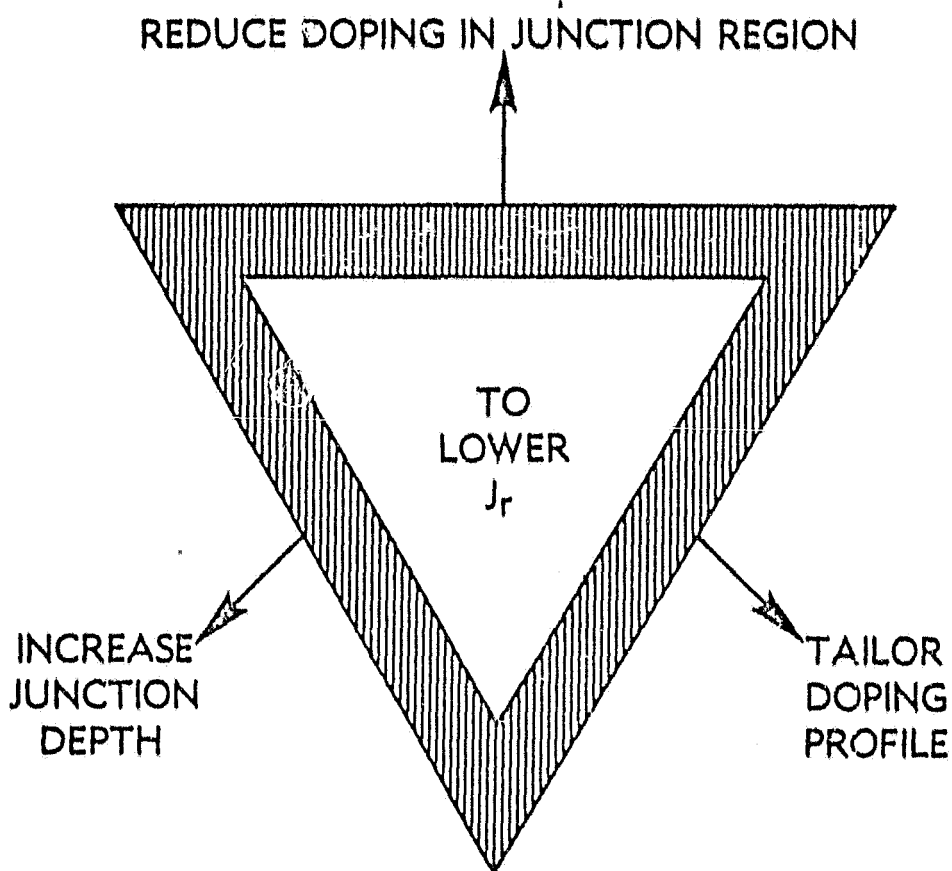


Figure 6-2. Methods of Reducing  $J_r$

## APPENDIX C. GETTERING PROCESSES IN SILICON

The large body of diffusion length data, accumulated during this contract, has provided an opportunity to test some models of gettering, or the process of attracting impurities to a sink. Neither the impurities themselves nor their sources are identified, but are important in reducing bulk diffusion lengths in silicon. It is possible that the source of these impurities is characteristic of fabrication (the lab, the solvents and the processing) rather than the material itself. If this is the case, the observations made here may not pertain to other facilities and operations. The material used in this work was generally 0.1- $\Omega$ -cm Wacker Float Zone Refined silicon. However, some use was made of 1- $\Omega$ -cm material and no difference was noted in the gettering results.

It is hoped that this appendix will be useful to those people interested in maintaining or obtaining long lifetime in silicon material. More detailed studies (e.g., with DLTS) would be important in confirming these models.

### C.1 BORON GETTERING

An exhaustive study of boron doped  $p^+$  back layers was not carried out; however, some interesting effects on the minority carrier diffusion length ( $L_n$ ) of these cells were observed in comparison to aluminum  $p^+$  contacts. Table C-1 indicates an influence of temperature on gamma current. It is difficult to separate the effects of diffusion length and  $p^+$  layer on the gamma current unless the  $p^+$  layer is stripped off and an ohmic contact is subsequently added. However, when this procedure is carried

Table C-1. Fabrication Steps for Boron Diffused Cells and the Resultant Gamma Currents  $I_\gamma$

Cell No.	PreOx 1050°C/ 30 min.	1st Diffusion				2nd Diffusion <sup>a</sup>			I <sub>γ</sub> (μA)
		Front N250C	Back. 0317D	Temp/Time	Si Etch <sup>b</sup>	Front N250C	Back	Temp/Time	
1403 1-4 5-8	yes yes		yes yes	950°C/30min. 900°C/10min.	No No	yes yes		850°C/ 40min.c 350°C/-40min.c	5.5 5.4
1411 1,2 3,4 6,7 8,9	no no no no	yes yes yes yes	yes yes	830°C/70hr. 830°C/70hr. 830°C/70hr. 880°C/70hr.	9 min. 9 min. 5.5 min. 5.5 min.	yes yes yes yes	Al 0317D Al 0317D	820°C/15min. 820°C/15min. 820°C/15min. 820°C/15min.	5.8 4.5 6.4 3.0
1423 3-9 1,2	yes yes		yes yes	950°C/30min. 950°C/30min.	No No	yes yes		820°C/15min.c 820°C/15min.c	6.0 ± 0.3 6.9
1431 1,2,3	no		yes	950°C/17hr.	No	yes		820°C/15min.c	7.1 ± 0.1
1433 1,2	yes		yes	950°C/17hr.	No	yes		320°C/15min.c	5.4 ± 0.1

<sup>a</sup>Gamma currents corrected for decay of <sup>60</sup>Co source.

<sup>b</sup>100:1 : 350:1 HF Rate = 5000 Å/min.

<sup>c</sup>Subsequently annealed at 450°C/16 hr.

out on Al backed cells, the variations in gamma current appear to depend more on  $L_n$  than on the  $p^+$  layer. This dependence implies a gettering effect from the Al which might also be expected from boron.

Table C-1 lists the gamma currents resulting from various fabrication processes utilizing a boron spin-on source (Emul-sitone 0317D). An essential step in these processes is the long (16 hr.), low-temperature (450°C) anneal. The boron doped glass does not anneal silicon as rapidly as does the molten aluminum. In fact, other data (Sections 3.3.2, C.3, and C.4) indicate that high temperature (950°C) diffusion steps actually lower  $L_n$ . The anneal step, therefore, removes the damage resulting from the diffusion (perhaps stress related) and further getters impurities from the bulk. Comparison of the four groups in set 1411 indicates that:

- a. long term diffusion with 0317D removes some defects not gettered by a short diffusion,
- b. aluminum getters very quickly, and
- c. aluminum getters right through a deep boron layer.

This set was not annealed, so that the influence of the diffusion itself could be observed. The indifference of  $I_\gamma$  to the nature of the boron  $p^+$  layer is seen in the cells of 1403 which have different diffusion conditions and, therefore, different  $p^+$  layer thicknesses (1500Å vs 3800Å).

The variation ( $\pm 5$  percent) of  $I_\gamma$  in cells processed identically within a given set is less than that between cells processed identically but in different sets (the extreme values of sets 1403 and 1423-3+8 barely overlap). It would appear that variations in processing or conditions in the laboratory from set

ORIGINAL PAGE IS  
OF POOR QUALITY

to set are greater than variations within the material or the conditions during a given fabrication step. For this reason, whenever possible, process changes are incorporated so that comparisons may be made within a set rather than between sets. The data of set 1423 emphasize the benefit of aluminum alloyed through a boron  $p^+$  layer and show that the low temperature, lengthy annealing of the boron diffused cell is not as effective as the addition of Al on the back during the short diffusion for the  $n^+$  layer.

Normally the boron source is applied to the wafer with oxide present on the front face to guard against contamination. In order to simplify the process, some cells were fabricated without the protective oxide. Although two of three cells in this case suffered front surface contamination, the set (1431) had some of the best diffusion lengths obtained during this contract. The differences between set 1431 and the other sets in Table C-1 are the lack of a high temperature step ( $1050^\circ\text{C}/30\text{ min}$ ) and the lack of a thick surface oxide during the boron diffusion step. The relative importance of these two differences, in determining the diffusion length of boron diffused silicon, is unknown. However, since the nature of the boron doped  $p^+$  layer (extreme thickness in set 1433) did not appear to influence  $I_\gamma$ , and because it was found that Al can more quickly and reproducibly getter bulk silicon, boron investigations were dropped.

## C.2 ALUMINUM GETTERING

The previous sections and tables indicate that aluminum is an excellent getter (probably the best). A probable reason

ORIGINAL PAGE IS  
OF POOR QUALITY

for this has to do with the facts that silicon dissolves in Al and that it is liquid at a low temperature. As the silicon goes into solution, it generates vacancies which diffuse through the silicon wafer and thereby enhances the migration of impurities within the wafer. The Si-Al eutectic alloy provides an active sink for impurities which are thus prevented from building up on the silicon surface and rediffusing back into the wafer. The liquid state (or mixture of liquid phase and solid phase) allows ready migration of contaminants to the outside surface where they are incorporated into the growing crust of oxides. The possibility of stress relief by the liquid and low stress during cooling (as a result of a relatively malleable alloy if the maximum alloy temperature is kept reasonably low) may also be important.

In contrast to the Al alloy process, a glass or oxide on the silicon surface (even if molten) may bind impurities close to the Si-glass interface where impurity-oxides are first formed. In addition, the glass is probably a net sink for vacancies rather than a net source as postulated for aluminum. A vacancy sink provides a gradient which will increase the concentration of some impurities about the sink and/or draw impurities out of the sink. This can be seen by envisioning the mobility of some impurities as increasing with vacancy concentration. These impurities will move rapidly until they reach the low vacancy area of the sink where they slow down. If the vacancy sink contains impurities, they are likely to migrate out along the vacancy gradient.

An alternative to the metallic aluminum or glass sources used to form  $p^+$  layers is an aluminum paste which can be silk-screened onto the back of the silicon wafers. An aluminum paste, as used commercially for  $p^+$  back contacts, is an excellent getter for three reasons. First, it generally provides more Al

for the Si to dissolve into than an evaporated Al layer. Second, it has a high concentration of oxides and/or frit which slows the migration of silicon through the melt and thereby provides a more continuous source of vacancies (and probably a higher net vacancy capability). Third, the oxides and frit provide binding points for the gettered impurities thereby lowering the concentration of mobile impurities which can diffuse back out of the Al-Si alloy. A potential problem is purity, both in the material and the application process.

High purity aluminum is desired for an alloy source so that it will not contain impurities that could contaminate the silicon. However, thicknesses in excess of 0.5  $\mu\text{m}$  have been found necessary for optimum lifetime and this thickness of pure aluminum is found to "ball up" during the high temperature alloy cycle. Evaporation of Al from a resistance-heated crucible provides layers with a pale gold finish which is stable but non-contaminating. Following the vacancy generation model and the Si-Al phase diagram, it is apparent that at higher temperatures more silicon will enter a given thickness of aluminum than at lower temperatures; thereby, within limits, increasing the vacancy population and the gettering capabilities. This effect may be seen in Table 2-1. At lower temperatures, thicker layers of aluminum and longer alloy times would be required for the same gettering capability.

### C.3 PHOSPHORUS AND ARSENIC GETTERING

It has been known for a long time that phosphorus is a good getter. It has been proposed [C1] that phosphorus diffuses by vacancy interaction and if the heavily doped surface region is

an active source of vacancies then a gettering mechanism like that of Al could be expected. A major difference in timing would be predicted, however. The aluminum alloy process would generate the highest concentration of vacancies in the beginning, decaying to a relatively low equilibrium concentration, whereas the P diffusion process would probably show an increase in vacancy generation with time as the heavily doped "dead layer" is created on the surface. Evidence to support this model comes from  $\text{PH}_3$  diffusion runs (1395,6,7,8) where gamma currents decrease with decreasing diffusion time (10, 7, and 5 min.) at  $840^\circ\text{C}$  and (30, 15 min.) at  $810^\circ\text{C}$ . Since all cells in these runs had the same aluminum alloy cycle (at  $880^\circ\text{C}$ ) prior to the phosphine diffusion step, no interference from the Al getter source would be expected.

Most of the cells fabricated under this contract were diffused with Emulsitone N250C emitter dopant, which contains both phosphorus and arsenic. Excellent diffusion lengths were obtained with this material, although the best values of  $I_\gamma$  were obtained when the diffusion time exceeded that required for good shallow junction cells.

In an effort to optimize the emitter, variations in the composition of the standard N250C were tried. However, variations that were observed in diffusion length indicated the complexity of the bulk gettering problem. Sets 1448 and 1449 in Table C-2 are 1  $\Omega$ -cm, 10 mil cells that have been diffused with lower concentrations of P and/or As than that of N250C. The low phosphorus, regular arsenic mixture (LoP/RA) has a phosphorus concentration of only 1/40 that of N250C. The low phosphorus, low arsenic mixture (LoP/LoA) has both P and As reduced to 1/40 of that in N250C. Since the surface concentration is lower for these mixtures a higher-temperature, longer, diffusion is



ORIGINAL PAGE IS  
OF POOR QUALITY

Table C-2. Gamma Currents of 1  $\Omega$ -cm Cells  
That Have Been Fabricated with Different  
Emitter Dopants and Schedules

Set No.	Cell No.	$I_{\gamma}(\mu A)^a$	Treatment
1448	1	7.9	LoP/RA 16 hrs. 900°C
	2	7.9	
	8	8.3	LoP/LoA 16 hrs. 900°C
	9	8.5	
	4	8.5	LoP/LoA 16 hrs. 900°C + LoP/RA 3 hrs. 900°C
	5	8.4	
	6	7.9	LoP/LoA 16 hrs. 900°C + 2xAs 3 hrs 900°C
	7	7.8	
1449	1	8.7	LoP/RA 16 hrs. 850°C +
	2	8.4	
	3	8.5	LoP/RA 3 hrs 850°C
	5	8.4	LoP/LoA 16 hrs. 850°C +
	6	8.2	
	7	8.2	LoP/RA 3 hrs. 850°C
1454	3	8.1	2xAs <sup>b</sup> 6 hrs. 900°C
	5,6	6.5	2xAs 16 hrs. 900°C
1422	1,2	5.0	As <sup>b</sup> 1050°C/7 min. + N250/820°
	5,7,8	1.7	As 1050°C/7 min.

<sup>a</sup> $I_{\gamma}$  data corrected for decay of gamma cell.

<sup>b</sup>The arsenic source should provide a surface doping concentration of  $2 \times 10^{20}/\text{cm}^3$ . The 2xAs source has twice the As concentration in the spin-on dopant.

required to obtain appropriate junction depths. The  $I_{\gamma}$  data in Table C-2 indicates that in the 900°C range, the LoP/LoA mixture (which has the same ratio of P to As as N250C) is superior to the LoP/RA mixture (1448-8,9 vs 1,2). This is not totally unexpected since the relative concentration of P and As in N250C has been optimized for low stress in the silicon diffused layer. However at 850°C (set 1449), the difference is much less and may be reversed (statistics are not sufficient to assure this last comment). In the lower temperature range, the gettering rate may be the limiting factor in determining diffusion lengths and introduction of defects by stress may be inconsequential ( $I_{\gamma}$  for both groups of set 1449 is high). If stress from the diffused layer is a problem at the higher temperatures, then a prior diffusion is seen to block it in the case of the LoP/RA mixture (1448-4,5) but not in the case of a high concentration arsenic diffusion source (2xAs in 1448-6,7). Arsenic spin-on dopants are observed to severely damage bulk lifetime if diffused at high temperatures (set 1422). The damage cannot be completely healed by a subsequent low temperature diffusion with N250C and Al. At lower temperatures (950°C) the As diffusion does little damage and little gettering or a balanced amount of both. Experiments were not carried out directly comparing the effects of P and As at the same temperatures. The trends for P indicate that  $I_{\gamma}$  increases to about 850°C and then decreases with increasing diffusion temperature. The arsenic diffused cell data also show  $I_{\gamma}$  decreasing as diffusion temperature increases and the trend lines of the two diffusion sources could well overlap or even join. However, it is unknown if and where the As diffused cells will display the peak in  $I_{\gamma}$  as observed in P diffused cells.

#### C.4 OTHER PROCESS DEPENDENT INFLUENCES ON $I_{\gamma}$

A strong indication of the gettering ability of the N250C formulation is displayed in Figure C-1. The SIMS data shows the profile of As, B, and P(+SiH)\* for a standard 820°, 15 min. diffusion. The B is strongly concentrated at the surface by the diffusion, whereas in Figure C-2, which is a high temperature (1050°C) oxidation step, no such buildup is observed. In fact, a drop in B concentration may be observed near the surface from out-diffusion into the oxide. This is gettering into the oxide rather than into a diffused region. These results are discussed further in Section 4.3, but an issue here is the values of  $I_{\gamma}$  for such treatments. Attempts at high temperature (> 1000°C) gettering (with wet oxygen or TCE) prior to standard low temperature diffusion resulted in cells with values of  $I_{\gamma}$  which were always worse than those from comparable untreated cells. We feel, therefore, that high temperature processing introduces defects and/or impurities which cannot be completely gettered by the steps that we normally use. In addition, the gettering ability (at least for some impurities) of the oxides is less than that of P or As.

We have seen how high temperature conditions can strongly influence getter rates and ultimate diffusion length. Unexpected results have also been observed at low temperatures (set 1401):

a. for cells with emitters from an N250C diffusion, but with no aluminum on the back, an overnight anneal (450°C) is found to improve  $I_{\gamma}$ ;

\*The resolution for these runs does not separate  $^{30}\text{Si}$  +  $^1\text{H}$  from  $^{31}\text{P}$ .

ORIGINAL PAGE IS  
OF POOR QUALITY

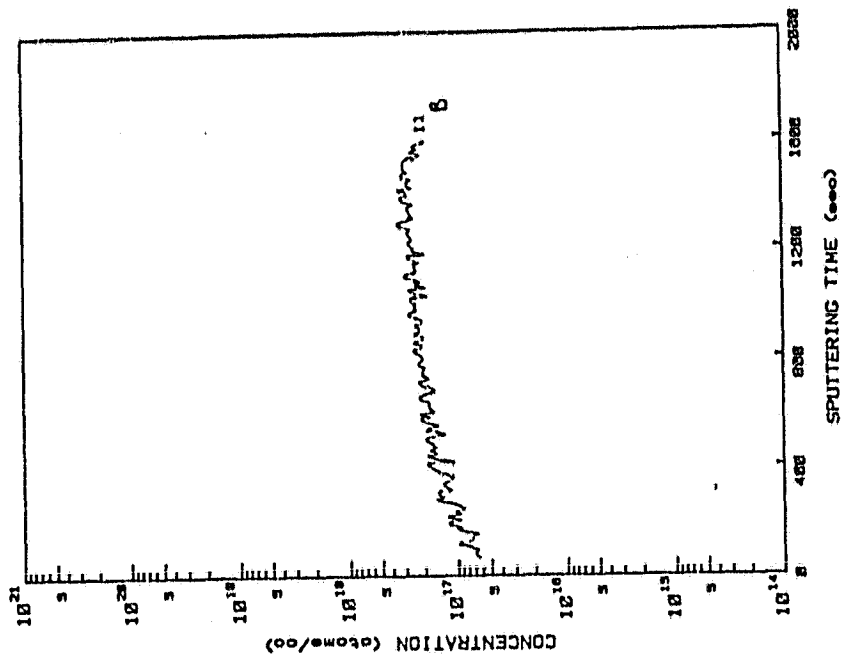


Figure C-2. Boron Concentration in a  
0.1  $\Omega$ -cm Wafer, Thermally Oxidized,  
1050°C for 4 Hours, and Then  
Etched in Hf

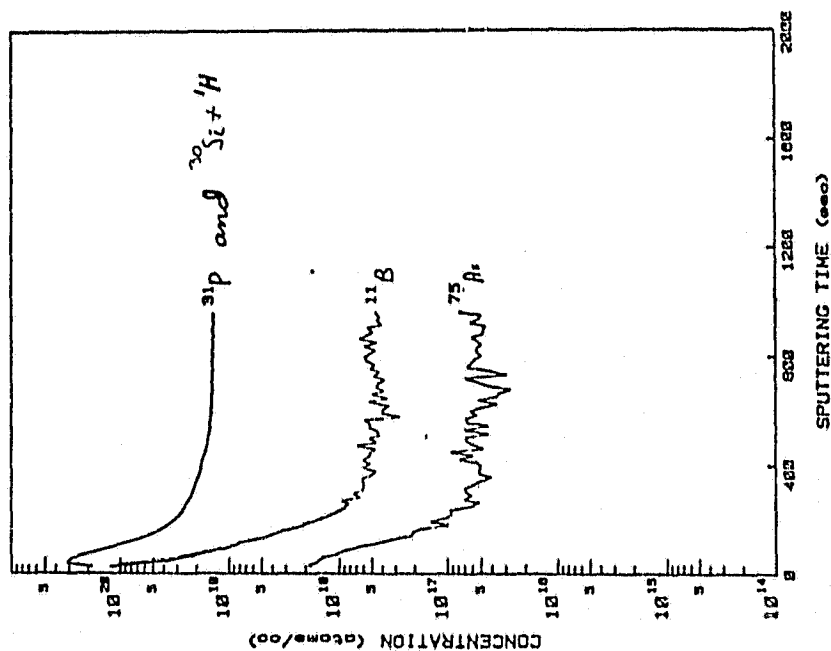


Figure C-1. Profiles of P, As and  
Boron After 15 Minute Diffusion  
(820°C) with N250C

b. however, subsequent oxidation of tantalum (525°C for 10 min) on the surface (to create the Ta<sub>2</sub>O<sub>5</sub> anti-reflective coating [C2]) reduces I<sub>γ</sub>;

c. addition of a 1-μm layer of Al and heating to 325°C reduces I<sub>γ</sub> for cells coated with Ta<sub>2</sub>O<sub>5</sub> but raises I<sub>γ</sub> for cells coated with tantalum metal.

The possible implications are:

a. N250C continues to getter at low temperatures and/or the bare back surface acts as a getter;

b. material drawn to the surface by the gettering action of N250C can be rapidly redistributed when Ta is oxidized on it or a contaminant in the Ta very rapidly diffuses into the bulk; and

c. low temperature heating of Al on the back of the cell serves to draw contaminants from the oxidized surface into the bulk (on its way to the Al) and draws contaminants from the bulk (that are not replaced from the surface if the Ta metal still binds them there).

The first implication could indicate that the overnight anneal required to give acceptable results on boron doped cells might provide gettering to the emitter rather than to the p<sup>+</sup> layer. A study of annealing in boron diffused wafers prior to application of the emitter could be interesting.

The second implication has support from studies of tantalum thermal oxidation, where it has been observed [C3] that silicon diffuses into the Ta or Ta<sub>2</sub>O<sub>5</sub> during the process. As silicon dissolves into the Ta layer gettered contaminants bound to the silicon surface could diffuse into the metal and also back into the emitter and bulk of the wafer. As the oxidation

proceeds (from the front surface), contaminants could be rejected from the oxide and concentrated in the metal and ultimately forced into the silicon.

The third implication is a low-temperature version of the Al gettering process. As silicon dissolves into the Al metal, a flood of vacancies are released into the bulk creating a vacancy gradient through the silicon. Vacancy assisted diffusion could draw impurities from the front surface and the emitter into the bulk of the wafer. The process is slow at low temperatures (325°C) and the number of vacancies generated too low for the complete gettering expected at high temperatures, so that many of the contaminants remain trapped in the bulk after the process is terminated. If the contaminants are embedded in Ta near the surface, rather than trapped at the silicon interface, they are less likely to be drawn back into the silicon by the vacancy gradient.

## C.5 SUMMARY

The dependence of diffusion length on process parameters is quite complicated. The following empirical observations and interpretations point to, but do not confirm, a self-consistent theory of gettering by vacancies.

a. Surface treatment, both front and back, has an effect on diffusion length.

b. Sequence of treatments can alter the final diffusion length (impurities gettered in one operation can be released in another).

c. Certain treatments (such as high temperature) create defects which cannot be totally removed by simple gettering processes.

d. Gettering can proceed at temperatures as low as 325°C (with Al metal).

e. Optimum gettering results appear in the range of 850°-900°C (at least in 0.1  $\Omega$ -cm p-type silicon).

f. Vacancy concentration and concentration gradient seem to be the main factors in the gettering process.

g. Precipitation or trapping of gettered impurities is important for gettering to be most effective.

h. Concentration of phosphorus, quantity of aluminum, and temperature, all influence the amount of vacancies available for gettering and probably influence the impurity trapping capability.

Results reported here may not pertain to all laboratories, since we have observed variations in diffusion lengths from day to day in identically processed wafers from the same ingot. Variations between laboratories would be larger than daily variations in a single lab.

#### REFERENCES FOR APPENDIX C

- [C-1] D. L. Kendall and R. Carpio, "A Defect Model for Phosphorous Diffusion in Silicon and For the Dead Layer of n/p Solar Cells," Conference Proceedings of IEEE Sectional Meeting, Monterey, New Mexico, September 1977.
- [C-2] A. G. Revesz, J. F. Allison, T. D. Kirkendall, and J. H. Reynolds, "Oxidation of Tantalum Film on Silicon," Thin Solid Films, (October 1974), Vol. 23, No. 3, pp. S63-S66.
- [C-3] A. G. Revesz and T. D. Kirkendall, "Film-Substrate Interaction in Si/Ta and Si/Ta<sub>2</sub>O<sub>5</sub> Structures," Journal of the Electrochemical Society, October 1976, Vol. 123, No. 10, pp. 1514-1519.



#### **APPENDIX D. DIFFUSION LENGTH MEASUREMENT AND DARK CURRENT DETERMINATION OF IRRADIATED SOLAR CELLS**

This appendix describes the use (and results) of irradiation to determine the relative contributions of base and emitter to the dark current of a solar cell. Two low resistivity (0.1 and 0.2  $\Omega$ -cm) solar cells were sequentially irradiated and measured to provide a data base for determining the sources of dark current for the irradiated and unirradiated cells. The results prove that in 0.1  $\Omega$ -cm cells, as fabricated under this contract, the emitter strongly dominates the dark current. Even for such cells with  $V_{oc} > 650$  mV (1 sun intensity), this conclusion should still be valid.

D-1. DIFFUSION LENGTH MEASUREMENT

COMSAT Labs has long used the  $^{60}\text{Co}$  gamma cell to generate a uniform concentration of carriers within the bulk of a solar cell and thus to provide the basis for determining a range of minority carrier diffusion lengths for most cells [1],[2]. In an earlier paper on the subject [1], the relationship between current collected from the solar cell while in the gamma cell ( $I_\gamma$ ) and the solar cell diffusion length  $L$  was established for two back surface conditions. These conditions were: an ohmic back contact, with the surface recombination velocity,  $S = \infty$ , and a perfectly reflecting back contact, with  $S = 0$ . The relationships were described as:

$$I_\gamma = I_\infty \frac{\cosh (W/L) - 1}{\sinh (W/L)} \quad \text{for } S = \infty \quad (\text{D-1})$$

and

$$I_\gamma = I_\infty \frac{\cosh (2W/L) - 1}{\sinh (2W/L)} \quad \text{for } S = 0 \quad (\text{D-2})$$

where  $W$  is the cell thickness,

$$I_\infty = \frac{L}{K}$$

and  $K$  is a proportionality constant that depends on the geometry of the source and on the type, energy, and flux of the ionizing radiation.\*  $K$  is determined by calibrating the gamma cell with a

\* $K \approx 16$  for the period of this contract.

ORIGINAL PAGE IS  
OF POOR QUALITY

solar cell of known  $W$ ,  $L$ , and  $S$ . An interesting feature of equations (1) and (2) is the dependence on  $W$ . The basis of this relationship is made more physical if a trigonometric identity\* is made so that equations (D-1) and (D-2) become

$$I_Y = \frac{L}{K} \tanh \frac{W}{2L} \quad \text{for } S = \infty \quad (\text{D-1}')$$

and

$$I_Y = \frac{L}{K} \tanh \frac{W}{L} \quad \text{for } S = 0 \quad (\text{D-2}')$$

The form of equation (D-2') is similar to that for the dark current equations of a diode of thickness  $W$  with a perfectly reflecting back contact [see equation (D-4) below]. The  $W/2$  in equation (D-1') now indicates that the front junction only collects current from the front half of the cell and the carriers in the back half of the cell all migrate to the ohmic back contact. As the cell diffusion length gets small,  $I_Y$  in both equations (D-1') and (D-2') approaches  $I_\infty$  (see Figure D-1), and no ambiguity can exist in the determination of  $L$  if  $K$  is known. However, for large values of  $L$ , the determination of  $L$  depends upon the value of  $S$  which is generally not well known. Therefore, a range of values for  $L$  are generally given for a measured  $I_Y$  and these extreme values are usually sufficient for most analysis since the relative values of  $L$  between nearly identical cells are often of greatest interest. When  $L$  exceeds  $W$ , the effect of cell thickness may be dominant in  $I_Y$ , and the value of  $L$

\*Use  $\cosh (2W/L) = 1 + 2 \sinh^2 (W/L)$  and  $\sinh (2W/L) = 2 \sinh (W/L) \cosh (W/L)$ .

ORIGINAL PAGE IS  
OF POOR QUALITY

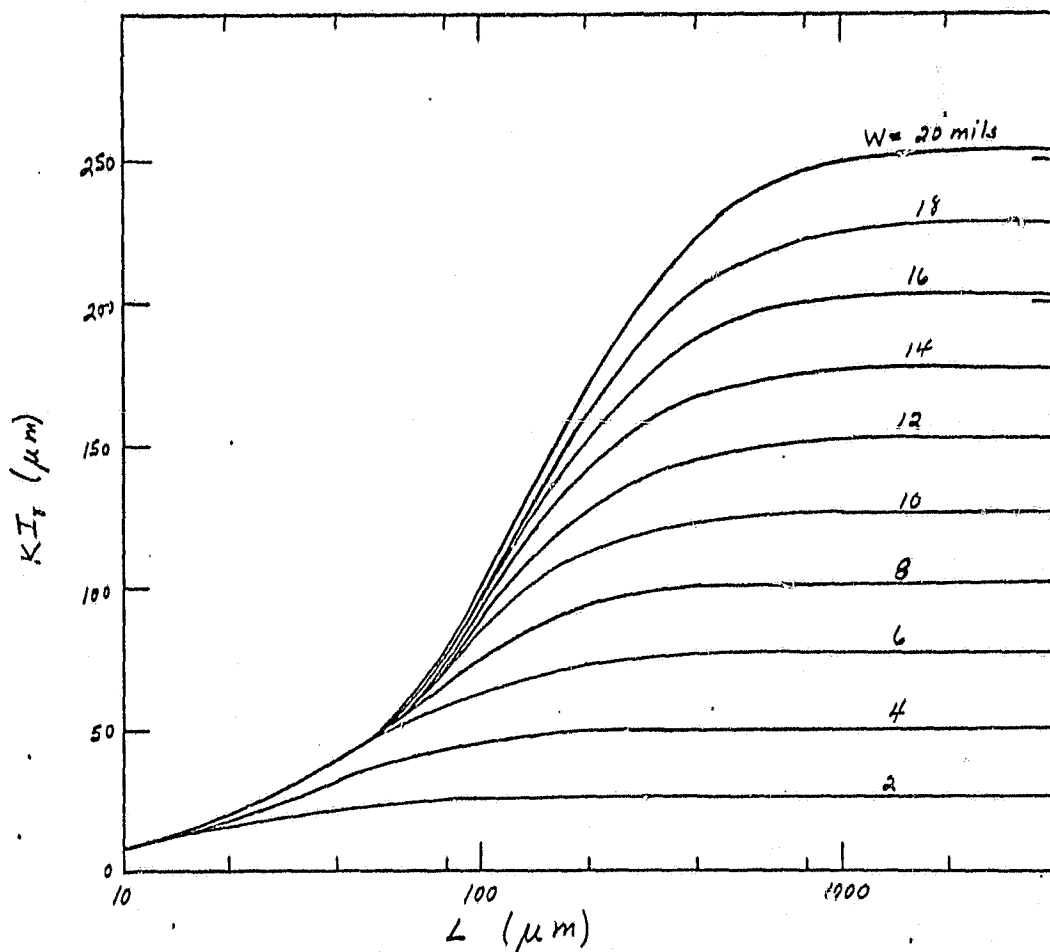


Figure D-1. Normalized Gamma-Cell Current vs Solar Cell Diffusion Length for  $S = \infty$  and Different Cell Thicknesses  $W$   
(for  $S = 0$  use the curves corresponding to  $2W$ )

ORIGINAL PAGE IS  
OF POOR QUALITY

determined from the  $S = \infty$  case often goes to infinity since most present cells do not have ohmic back contacts.

## D-2. DARK CURRENT DETERMINATION

The dark current density,  $J_b$ , from the bulk of a solar cell can be expressed as:

$$J_b = \frac{A}{L} \coth \frac{W}{L} \quad \text{for } S = \infty \quad (D-3)$$

and

$$J_b = \frac{A}{L} \tanh \frac{W}{L} \quad \text{for } S = 0 \quad (D-4)$$

where

$$A = \frac{qn_i^2 D}{N_A} \quad (D-5)$$

and the usual definitions hold. The total dark current  $I$  from a cell consists of components from the bulk  $I_b$ , the junction  $I_r$ , and the emitter  $I_e$ .

$$I = (I_e + I_b) e^{qV/KT} + I_r e^{qV/2KT} \quad (D-6)$$

$I_0$  ( $I$  at  $V = 0$ ) can be easily determined from the illuminated cell  $I$ - $V$  characteristics and equation (D-7),

$$V_{oc} = \frac{KT}{q} \ln \frac{I_{sc}}{I_0} \quad (D-7)$$

ORIGINAL PAGE IS  
OF POOR QUALITY

if we can assume that the  $I_r$  term is negligible at  $V_{oc}$ . Since  $I_r$  is not zero,  $I_o$ , as determined from equation (D-7), is an upper limit  $I_{om}$  which is explicitly written as

$$I_{om} = I_{sc} e^{-qV_{oc}/KT} \quad (D-8)$$

The above equations provide a means of determining  $I_{om}$  and separating  $I_e$  and  $I_b$ , since  $I_{om} \geq I_e + I_b$ . By measuring  $I_r$ ,  $V_{oc}$ , and  $I_{sc}$  of a solar cell after various levels of irradiation,  $I_{om}$  and a range for  $L$  can be determined. With two different irradiation levels and with the assumption that  $I_e$  does not change with irradiation, simultaneous equations can be set up to solve for  $I_e$  and  $I_b$ .

$$I_{om1} = I_{e1} + \frac{A}{L_1} \coth \frac{W}{L_1} \quad (D-9a)$$

$$I_{om2} = I_{e2} + \frac{A}{L_2} \coth \frac{W}{L_2} \quad (D-9b)$$

$$I_{e1} = I_{e2} \quad (D-9c)$$

We have assumed  $S = \infty$  [equation (D-3)] for equations (D-9), but  $S = 0$  [equation (D-4)] can also be used, if applicable.

### D-3. EXPERIMENTAL RESULTS

Two cells (one 0.1  $\Omega$ -cm and the other 0.2  $\Omega$ -cm) were measured, irradiated, and remeasured to provide six data sets per cell. Equation (D-9) was modified to the form

$$(I_{omi} - PER_i \cdot I_{omi}) = \frac{A}{L_i} \coth \frac{W}{L_i} \quad (D-10)$$

where  $PER_i = I_{ei}/I_{omi}$ . The values of  $PER_i$  ( $PER_i \leq 1$ ) were varied until  $I_{ei}$  was nearly constant for all levels of irradiation. For simplicity,  $A$  was determined by providing a value of  $PER_6 [= PER_6 = PER(6)]$  and then was substituted in the other equations to give  $PER_i$  from which  $I_{ei}$  and  $I_{bi}$  were determined.

Figure D-2 is an example of the results from such an analysis of the 0.2  $\Omega$ -cm cell assuming  $S = 0$ . The table included in the figure provides all the data and results used in the analysis. Variations of the parameter  $K$  [see equations (D-1') and (D-2')] have only a small effect on the values of  $I_e$  obtained. Changing from the  $S = 0$  to the  $S = \infty$  form of the equations has a great impact (see Figure D-2a vs D-2b). In Figure D-2b, the value of  $L$  at 630 mV is given at 1000  $\mu$ m. In reality, the value of  $IG \cdot K$  at this point ( $IG = I_\gamma = 6.5 \mu$ A and  $K = 16$ ) exceeds the possible value for 250- $\mu$ m cells when assuming an ohmic contact (Figure D-1). The proper value of  $K$  is close to 16; only if  $K$  were decreased or  $W$  were increased, would it be possible to question the nonohmic nature of the back contact. With the extreme assumptions of  $S = 0$  and  $S = \infty$ , Figures D-2a and D-2b show the contribution of  $I_e$  at 630 mV to vary from 50 + 100 percent of the total dark current.

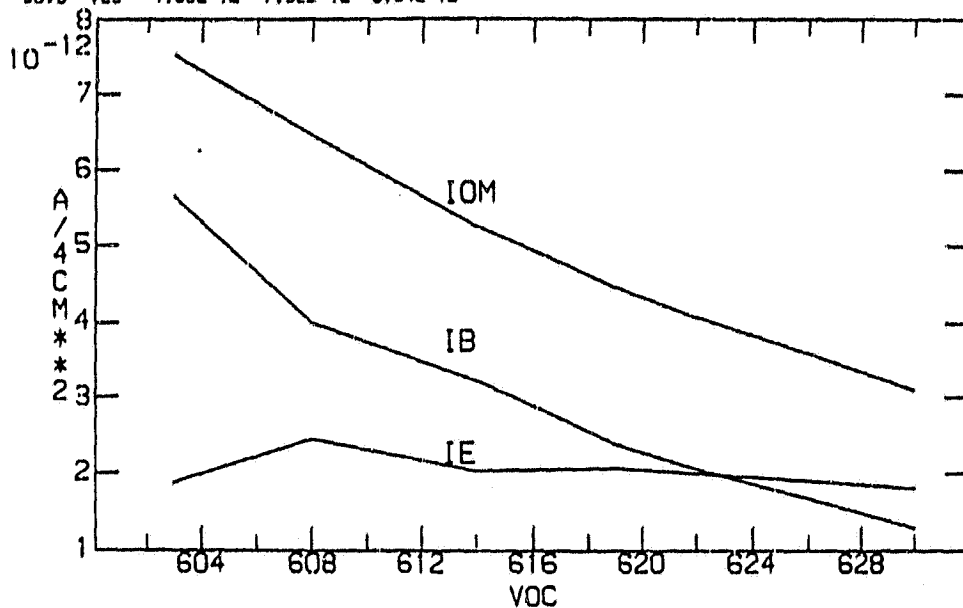
A similar analysis was performed on the 0.1  $\Omega$ -cm cell at both extremes:  $S = 0$  (Figure D-3a) and  $S = \infty$  (Figure D-3b). The contribution of  $I_e$ , at  $V_{oc} = 635$  mV, varies from 72 percent to 99 percent of  $I_{om}$  in this 0.1  $\Omega$ -cm case. The fact that realistic values of  $L$  are possible for  $K = 16$  and  $S = \infty$  implies that the back contact is ohmic or at least much closer to being ohmic than that of the 0.2  $\Omega$ -cm cell.

VOC	IL	IG	L	PER	IE	IOM	IB	K	A
630	.145	0	156	.585	1.81E-12	3.89E-12	1.20E-12	16	2.17E-10
622	.130	6.4	184	.403	2E-12	4.85E-12	2.05E-12		
610	.136	5.6	98.5	.466	2.87E-12	4.45E-12	2.38E-12		
614	.132	4.2	67.5	.389	2.84E-12	5.25E-12	3.21E-12		
608	.128	3.4	54.5	.381	2.46E-12	6.44E-12	3.89E-12		
603	.123	2.4	38.5	.25	1.88E-12	7.52E-12	5.64E-12		

ORIGINAL PAGE IS  
OF POOR QUALITY

PERG = .25  
W = 250

a)



VOC	IL	IG	L	PER	IE	IOM	IB	K	A
630	.145	9	1880	.748	2.31E-12	3.89E-12	7.78E-13	16	1.91E-10
622	.130	6.4	150	.663	2.69E-12	4.85E-12	1.36E-12		
610	.136	5.6	110	.603	2.68E-12	4.45E-12	1.77E-12		
614	.132	4.2	71	.488	2.57E-12	5.25E-12	2.69E-12		
608	.128	3.4	55	.462	2.97E-12	6.44E-12	3.47E-12		
603	.123	2.4	39	.35	2.63E-12	7.52E-12	4.89E-12		

PERG = .35  
W = 250

b)

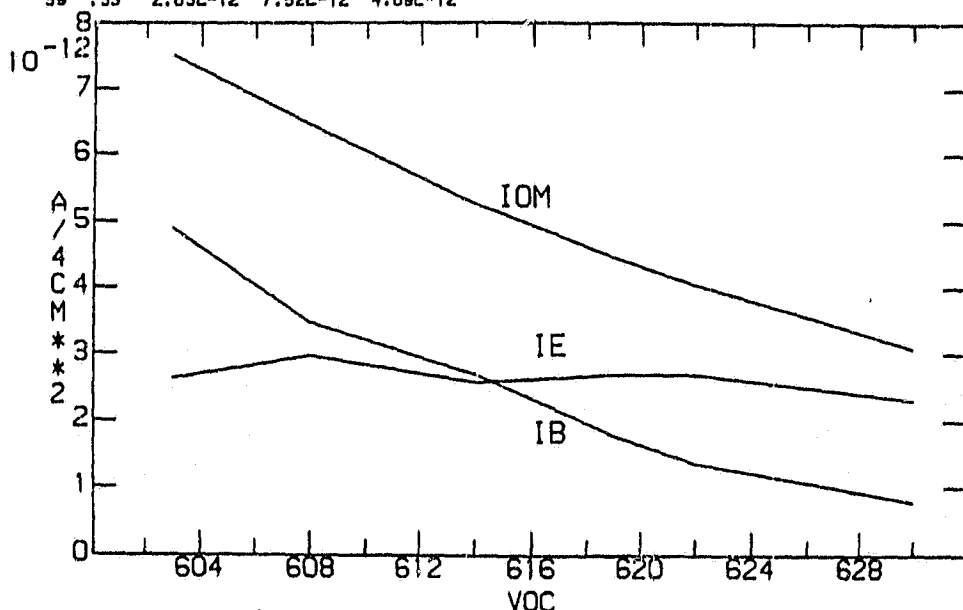


Figure D-2. Dark Current Components as a Function of Open Circuit Voltage at Various Levels of Irradiation  
Electrical Characteristics of 0.2  $\Omega$ -cm cells:  
a)  $S = 0$ ; b)  $S = \infty$

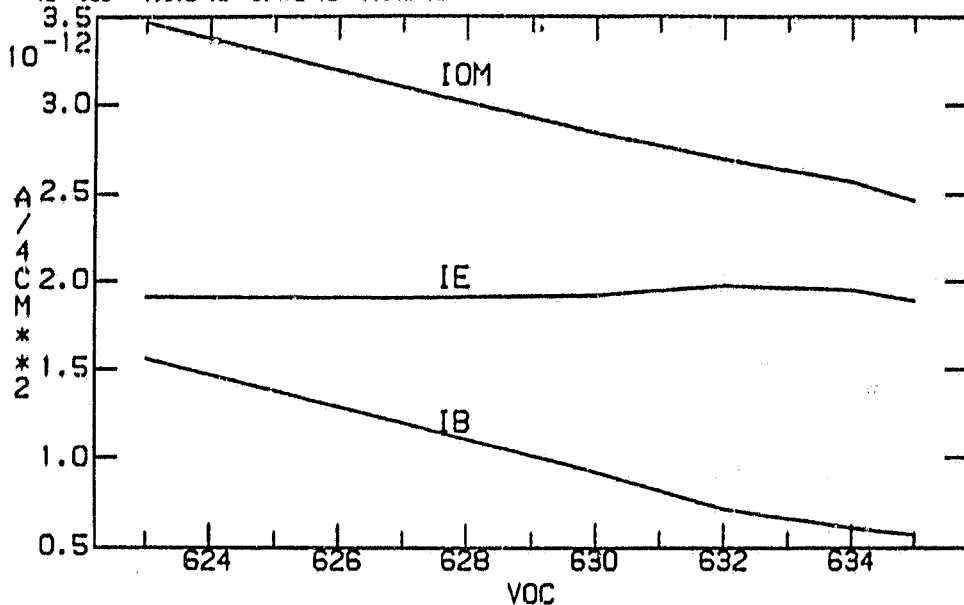


VOC	IL	IG	L	PER	IE	IOM	IB	K	A
635	.14	6.5	118	.768	1.09E-12	2.46E-12	5.71E-13	16	6.57E-11
634	.14	6.3	104	.762	1.05E-12	2.55E-12	6.00E-13		
632	.136	5.5	90	.733	1.07E-12	2.68E-12	7.16E-13		
630	.133	4.4	71	.676	1.02E-12	2.84E-12	9.2E-13		
627	.129	3.4	55	.614	1.0E-12	3.09E-12	1.10E-12		
623	.124	2.6	42	.55	1.01E-12	3.47E-12	1.56E-12		

ORIGINAL PAGE IS  
OF POOR QUALITY

PERG n .55  
W \* 200

a)



VOC	IL	IG	L	PER	IE	IOM	IB	K	A
635	.14	6.5	650	.911	2.24E-12	2.46E-12	2.10E-13	16	4.30E-11
634	.14	6.3	345	.908	2.32E-12	2.55E-12	2.35E-13		
632	.136	5.5	139	.87	2.33E-12	2.68E-12	3.40E-13		
630	.133	4.4	83	.812	2.3E-12	2.84E-12	5.35E-13		
627	.129	3.4	57	.751	2.32E-12	3.09E-12	7.69E-13		
623	.124	2.6	42	.7	2.43E-12	3.47E-12	1.04E-12		

PERG n .7  
W \* 200

b)

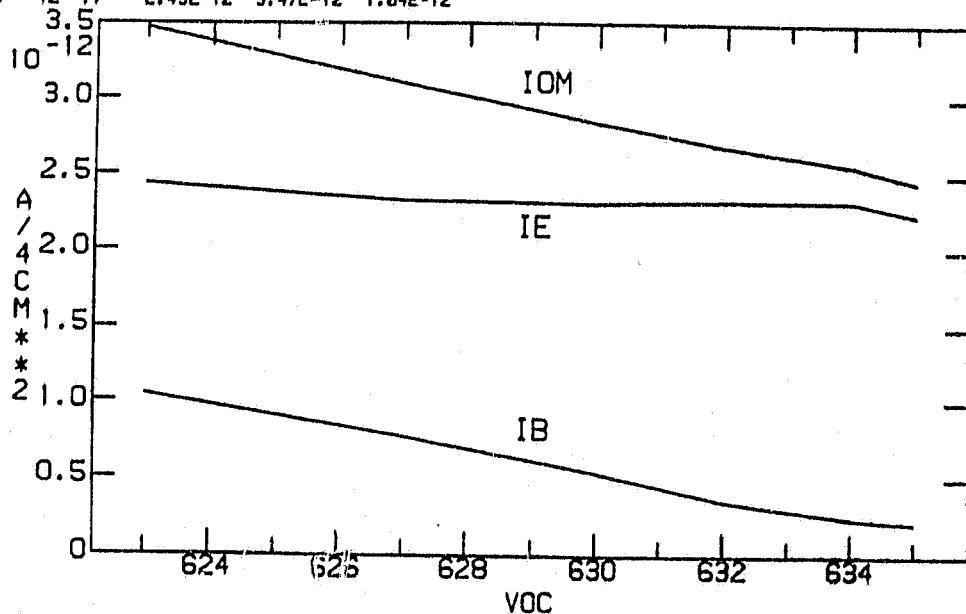


Figure D-3. Dark Current Components as a Function of Open Circuit Voltage at Various Levels of Irradiation  
Electrical Characteristics of 0.1  $\Omega$ -cm cells:  
a)  $S = 0$ ; b)  $S = \infty$

#### D-4. ANALYSIS AND DISCUSSION OF RESULTS

The extreme values of  $I_e/I_{om}$  in the unirradiated cells are 0.51 and 1.0 for the 0.2  $\Omega$ -cm cell and 0.72 and 0.99 for the 0.1  $\Omega$ -cm cell. The lower extremes are based on assumptions of  $S = 0$  which is impossible for the heavily doped base and aluminum alloyed back configuration of these cells. This configuration results in contacts closer to the  $S = \infty$  condition, but in the 0.2  $\Omega$ -cm case, actual ohmic contacts are seen to be unlikely. As a result, the limits of  $I_e/I_{om}$  are more likely to be 0.7 - 0.9 for 0.2  $\Omega$ -cm cell and 0.8 - 0.95 for the 0.1  $\Omega$ -cm cell.

Using the same baseline as above, we can provide a probable value for A [see equation (D-3)] =  $(4.8 \pm 0.2) \times 10^{-15}$  Amps/cm in the 0.2  $\Omega$ -cm cell and  $(1.6 \pm 0.3) \times 10^{-15}$  Amps/cm in the 0.1  $\Omega$ -cm cell.\*

Conductivity ( $\sigma = 1/\rho$ ) is proportional to the majority carrier concentration  $N_A$  and mobility ( $\mu$ ) of a material; therefore we expect that  $\sigma_{0.1}/\sigma_{0.2} = 2 = (N_A\mu)_{0.1}/(N_A\mu)_{0.2}$ . Since  $\mu_{0.2} \approx 1.2\mu_{0.1}$ ,  $N_{A0.1} \approx 2.4 \times N_{A0.2}$ . Values found for  $N_A$  in the 0.1  $\Omega$ -cm cell (from the literature [3], capacitance profile measurements, and SIMS data) all fall within  $N_{A0.1} = 3 \pm 1 \times 10^{17}/\text{cm}^3$ . For the 0.2  $\Omega$ -cm cell,  $N_{A0.2} = 1.3 \pm 0.3 \times 10^{17}/\text{cm}^3$ . The values [3] needed for evaluating A in equation (D-5) are:

$\rho$ ( $\Omega$ -cm)	0.1		0.2
$N_A$ ( $\text{cm}^{-3}$ )	$3 \times 10^{17}$		$1.3 \times 10^{17}$
$D$ ( $\text{cm}^2/\text{s}$ )	9.1		11.7
$n_i^2$ ( $\text{cm}^{-6}$ )	--	$1.5 \times 10^{20}$	--
$q$ (Coulomb)	--	$1.6 \times 10^{-19}$	--

\*Units of A in the figures are (amps/4  $\text{cm}^2$ )  $\mu\text{m}$ .

The calculated values for A become:

$$A_{0.2} = 2.2 \times 10^{-15} \text{ A/cm}$$

$$A_{0.1} = 0.73 \times 10^{-15} \text{ A/cm}$$

and

$$A_{0.2}/A_{0.1} = 3.4$$

The measured values of A are more than twice the calculated values, but the ratios are close (3.2 vs 3.4). Bandgap narrowing would raise  $n_i$  but more in the 0.1  $\Omega$ -cm cell, therefore does not appear to be the answer. Likewise, fractional ionization of the acceptors, which would reduce  $N_A$  to the hole concentration, will increase  $A_{0.1}$  more than  $A_{0.2}$ . No experimental errors or approximations could lower the experimental values of A to the calculated value. However, a change in  $n_i^2$  from  $1.5 \times 10^{20}$  to  $3.3 \times 10^{20}/\text{cm}^6$  would completely reconcile the data to theory. Since the published values of  $n_i^2$  vary between  $1.5$  and  $4 \times 10^{20} \text{ cm}^{-6}$ , this change does not appear to be too unrealistic. However, a more likely explanation is the presence of a junction recombination contribution,  $I_r$ , to the dark current,  $I_0$ , which would lower the value of  $I_b + I_0$  [as seen in equation (D-6)] and therefore A. Support for the contribution of  $I_r$  to the dark current is found in the cell fill factors which drop with irradiation from 0.80 to 0.76 in the 0.1  $\Omega$ -cm case and from 0.79 to 0.77 in the 0.2  $\Omega$ -cm case.

The greatest source of uncertainty in the solar cell parameters is the effective recombination velocity at the back surface. This uncertainty creates a large uncertainty in the value of L when L is comparable to, or larger than, the cell thickness. Uncertainty in L has a direct impact in determined results for  $I_b$ . But, for the low resistivity cells reported

here, this uncertainty in  $S$  and  $L$  has only a small impact on  $I_e$ , which is the dominant component of the dark current for both cells. To provide a  $0.1 \Omega\text{-cm}$  cell [4] with  $V_{OC} = 654 \text{ mV}$ ,  $I_0$  must decrease by a factor of two. To achieve this decrease in the extreme (and impossible) case (Figure D-3a) of  $S = 0$ ,  $I_e$  could be reduced by a factor of 3.3 while  $I_b$  is unchanged. With this reduction in  $I_e$ ,  $I_b$  would exceed  $I_e$  by about 20 percent. However, in the more likely situation ( $S$  very high, Figure 3-b),  $I_e$  so strongly dominates  $I_0$  that reducing  $I_e$  by two will likewise reduce  $I_0$  by two and  $I_e$  will still be an order of magnitude greater than  $I_b$ . These data have been analyzed in a different manner in Reference 5, but with essentially identical results.

#### D-5. SUMMARY

Two low-resistivity cells ( $0.1$  and  $0.2 \Omega\text{-cm}$ ) have been studied at different levels of gamma irradiation. By assuming that the dark current contribution from the emitter  $I_e$  is constant, the illuminated  $I$ - $V$  characteristics and gamma cell current were utilized to generate internally self-consistent values of  $I_e$ ,  $I_b$ , and  $I_0$  at the different irradiation levels. The experimental results agree very well with theory if  $n_i^2 = 4.3 \times 10^{20}/\text{cm}^6$  is used in the theoretical calculation. Since this value for  $n_i^2$  is higher than published values, a non-negligible  $I_r$  term is postulated. Analysis of these values points to the dominance of  $I_e$  in both cells and even at  $653 \text{ mV}$ , the  $I_e$  term will be significantly larger than the  $I_b$  term for the  $0.1 \Omega\text{-cm}$  cell.

D-6. REFERENCES

- [1] J. H. Reynolds and A. Meulenber, Jr., "Measurement of Diffusion Length in Solar Cells," Journal of Applied Physics, Vol. 45, No. 6, June 1974, p. 2582.
- [2] J. H. Reynolds and A. Meulenber, "Diffusion Length Measurements in Thin Silicon Solar Cells," CL-31-75, April 1975.
- [3] M. Neuberger and S. J. Welles, Silicon Electronic Properties Information Center DS-162, October 1969.
- [4] R. A. Arndt et al., "Advances in High Output Voltage Silicon Solar Cells," Proceedings of the 15th IEEE Photovoltaic Specialists Conference, Kissimmee, Florida, May 1981.
- [5] A. Meulenber, Jr. and R. A. Arndt, "Limitations on Solar Cell Open-Circuit Voltage and Efficiency," COMSAT Technical Review, Vol. 14, Spring 1983 (to be published).

REFERENCES

- [1] E. S. Rittner, A. Meulenberg, and J. F. Allison, "Dependence of Efficiency of Shallow Junction Silicon Solar Cells on Substrate Doping," Journal of Energy, Vol. 5, No. 1, (Jan.-Feb. 1981), p. 9-14. (Included as Appendix A). See also: E. S. Rittner, "An Improved Theory for the Si p-n Junction Solar Cell," Journal of Energy, Vol. 1, No. 1 (Jan.-Feb. 1977), pp. 9-17.
- [2] E. S. Rittner, "Use of p-n Junctions for Solar Energy Conversion," Physical Review, Vol. 96, No. 6, 1708-1709, December 15, 1954.
- [3] A. Meulenberg and E. S. Rittner, "Limiting Processes in shallow Junction Solar Cells," presented at the Third Solar Cell High Efficiency and Radiation Damage Meeting, June 13, 1979. (Based on material in Appendix B.)
- [4] Workshop on Heavy Doping Effects in Silicon Devices, May 6-9 1981, University of Florida, Gainesville, Florida. (No proceedings available.)
- [5] J. R. Hauser, "Minority Carrier Transport in Heavily Diffused Semiconductor Devices," Final Report on NSF Grant GK-1615, September 1969, North Carolina State University, Raleigh, N.C.

- [6] H. P. D. Lanyon and R. A. Tuft, "Bandgap Narrowing in Heavily Doped Silicon," International Electron Devices Meeting, December 4-6, 1978, Technical Digest, pp. 316-319.
- [7] R. J. Van Overstraeten, H. J. DeMan, and R. P. Mertens, "Transport Equations in Heavy Doped Silicon," IEEE Transactions on Electron Devices, Vol. ED-20, No. 3, 1973, p. 290.
- [8] J. W. Slotboom and H. C. DeGraaff, "Measurements of Bandgap Narrowing in Si Bipolar Transistors," Solid State Electronics, Vol. 19, 1976, pp. 857-862.
- [9] J. A. Minnucci and K. W. Matthei, "Study Program to Improve the Open-Circuit Voltage of Low Resistivity Single Crystal Silicon Solar Cells," NASA Report NAS CR-159833, February 7, 1980.
- [10] F. A. Lindholm, et al., "Design Considerations for Silicon HLE Solar Cells," 13th IEEE Photovoltaic Specialists Conference, June 5-8, 1978, Washington, D.C., Proc., pp. 1300-1305.
- [11] M. A. Green, et. al., "The MINP Solar Cell--A New High Voltage, High Efficiency Silicon Solar Cell," 15th IEEE Photovoltaic Specialists Conference, Kissimmee, Florida, May 12-15, 1981, pp. 1405-1408.

- [12] J. Lindmayer and J. F. Allison, "Dotted Contact Fine Geometry Solar Cell," United States Patent 3,982,964, September 28, 1976.
- [13] A. Meulenberg, "The Sawtooth Cover-Slide: A New Means of Coupling Light into Solar Cells," Journal of Energy (May-June 1977), Vol 1, No. 3, pp. 151-154.
- [14] M. P. Godlewski, C. R. Baraona, and H. W. Brandhorst, "Low-High Junction Theory Applied to Solar Cells," IEEE Photovoltaic Specialists Conference, Palo Alto, California, November 13-15, 1973, Proc., p. 40.
- [15] J. Dzierwior and W. Schmid, "Auger Coefficients for Highly Doped and Highly Excited Silicon," Applied Physics Letters Vol. 31, No. 5, September 1, 1977, pp. 346-348.
- [16] J. H. Reynolds, and A. Meulenberg, "Measurement of Diffusion Length in Solar Cells," Journal of Applied Physics, (June 1974), pp. 2582-2592.
- [17] J. F. Allison, R. A. Arndt, and A. Meulenberg, "Thin n-i-p Radiation-Resistant Solar Cell Feasibility Study," Final Report, Contract NAS 3-21280.
- [18] R. T. Young, et al., "Pulsed Laser Techniques for Solar Cell Processing," IEEE Transactions on Electron Devices, Vol. ED-27, No. 4, April 1980, pp. 808-815.



- [19] N. G. Tarr, D. J. Pulfrey, and P. A. Iles, "Induced Back Surface Field and MISIM Solar Cells on pSi Substrates," Fifteenth IEEE Photovoltaic Specialists Conference, May 12-15, 1981, Kissimmee, Florida, pp. 1409-1411.
- [20] M. P. Godlewski, T. M. Klucher, G. A. Mazaris, and V. G. Weizer, "Open-Circuit Voltage Improvements in Low Resistivity Solar Cells," Fourteenth IEEE Photovoltaic Specialists Conference, January 7-10, 1980 San Diego, CA, Proc., pp. 166-171.
- [21] R. C. Y. Fang and J. R. Hauser, "A Theoretical Analysis of the Current-Voltage Characteristics of Solar Cells," Annual Report on NASA Grant NGR 34-002-195, September 1977.
- [22] J. Snel, "The Doped Si/SiO<sub>2</sub> Interface," Solid State Electronics, Vol. 24, February 1981, pp. 135-139.
- [23] A. G. Revesz and J. H. Allison, "Electronic Properties of the Silicon-Thermally Grown Tantalum Oxide Interface," IEEE Transactions on Electron Devices, Vol. ED-23, No. 5, May 1976, pp. 527-529.
- [24] I. Weinberg, "Application of the MOS C-V Technique to Determine Impurity Concentrations and Surface Parameters on the Diffused Face of Silicon Cells," Proc. Eleventh IEEE Photovoltaic Specialists Conference, May 6-8, 1975, Scottsdale, Arizona, pp. 78-82.

- [25] J. Geist, E. Liang, and A. R. Schaefer, "Complete Collection of Minority Carriers from the Inversion Layer in Induced Junction Diodes," Journal of Applied Physics, Vol. 52, No. 7, July 1981, pp. 4879-4881.
- [26] T. M. Buck and R. L. Meek, "Crystallographic Damage to Silicon by Typical Slicing, Lapping, and Polishing Operations," NBS Special Publications 337, Silicon Device Proc., NTIS COM-71-00182.
- [27] J. G. Haynos, J. F. Allison, R. A. Arndt, and A. Meulenberg, "The COMSAT Non-Reflective Silicon Solar Cell: A second Generation Improved Cell," International Conference on Photovoltaic Power Generation, September 1974, Proc., pp. 487-500.
- [28] V. G. Wiezer and J. D. Broder, "On the Cause of the Flat Spot Phenomenon Observed in Silicon Solar Cells at Low Temperatures and Low Intensities," 15th IEEE Photovoltaic Specialists Conference, Kissimmee, Florida, May 12-15, 1981, pp. 235-236.
- [29] H. P. Maruska, et al., "On the Stability of  $\text{SnO}_2/\text{n-Si}$  Solar Cells," 15th IEEE Photovoltaic Specialists Conference, Kissimmee, Florida, May 12-15, 1981, pp. 1412-1417.
- [30] S. M. Sze, Physics of Semiconductor Devices, New York, Wiley-Interscience, 1969, p. 366.

ORIGINAL PAGE IS  
OF POOR QUALITY

- [31] A. Meulenberg, Jr. and R. A. Arndt, "Limitations on Solar Cell Open-Circuit Voltage and Efficiency," COMSAT Technical Review, Vol. 14, Spring 1983 (to be published).